

Dissertation zur Erlangung des Doktorgrades
der Fakultät für Chemie und Pharmazie
der Ludwig-Maximilians-Universität München

Multinary Nitridoaluminates and Their Application as LED Phosphor Materials

Philipp Alexander Hubert Pust

aus

München, Deutschland

2014

Erklärung

Diese Dissertation wurde im Sinne der von § 7 der Promotionsordnung vom 28. November 2011 von Herrn Prof. Dr. W. Schnick betreut.

Eidesstattliche Versicherung

Diese Dissertation wurde eigenständig und ohne unerlaubte Hilfe erarbeitet.

München, den

.....
(Philipp Pust)

Dissertation eingereicht am

1. Gutachter Prof. Dr. W. Schnick

2. Gutachter Prof. Dr. O. Oeckler

Mündliche Prüfung am 22.12.2014

Für meine Eltern

Acknowledgement

Besonderer Dank gilt Herrn Prof. Dr. Wolfgang Schnick für die Möglichkeit meine Doktorarbeit über ein so interessantes und innovatives Thema anfertigen zu können. Die große Freiheit bei der Umsetzung neuer Ideen, die unzähligen gestalterischen Möglichkeiten, sowie die hervorragenden Arbeitsbedingungen waren die beste Voraussetzung für diese Arbeit. Auch für die Gelegenheit Ergebnisse in wissenschaftlichen Fachzeitschriften, bzw. auf (inter)nationalen Tagungen darzustellen sowie der Möglichkeit zur aktiven Beteiligung an Projekten wie der Philips-Kooperation oder der DFG-Forschergruppe „FOR 1600: Chemistry and Technology of the Ammonothermal Synthesis of Nitrides“ gebührt großer Dank. Der hohe Grad an Abwechslungsreichtum regte stets zu neuen Ideen an. Ferner waren die vielen Gespräche über alle möglichen Dinge stets sehr informativ und haben mich immer wieder zu neuen Anregungen beflügelt.

Großer Dank gilt auch Herrn Prof. Dr. Oliver Oeckler für die Übernahme des Korreferats und seine große Hilfsbereitschaft bei jeglichen Fragen chemischer, kristallographischer oder auch kunlinarischer Natur.

Frau Prof. Dr. Christina Scheu, sowie den Herrn Prof. Dr. Konstantin Karaghiosoff, Prof. Dr. Hans-Christian Böttcher und Prof. Dr. Thomas M. Klapötke danke ich für die Bereitschaft, als weitere Prüfer zur Verfügung zu stehen.

Auch möchte ich mich ganz herzlich bei allen Beteiligten des Kooperationsprojekts mit Philips Lumileds bedanken. Hierbei möchte ich besonders Dr. Peter J. Schmidt, Volker Weiler und Cora Hecht hervorheben, die mir durch zahlreiche Synthesen, Lumineszenzmessungen und spannende Diskussionen den langen Weg durch die Doktorarbeit erleichtert haben. Ich freue mich sehr, dass ich durch diese enge Zusammenarbeit einen tiefen Einblick in moderne Beleuchtungstechnologie gewinnen konnte, und vor allem auch, dass durch unsere gemeinsame Forschung nachhaltige Ergebnisse geschaffen werden konnten.

Bei Frau Prof. Dr. Christina Scheu sowie bei Frau. Dr. Angela Wochnik möchte ich mich für die Durchführung der TEM-Untersuchungen, sowie der Auswertung der Daten sehr bedanken.

Frau Olga Lorenz, Herrn Thomas Miller und Herrn Wolfgang Wünschheim danke ich für die stete Hilfe bei allerlei organisatorischen, computertechnischen und sicherheitsrelevanten Fragen. Dadurch war es möglich, sich ganz seinen Ideen und seiner Forschung hinzugeben und auch trotz der Umstellung des Betriebssystems, nahezu lückenlos weiterarbeiten zu können.

Ferner Danke ich auch Dr. Constantin Hoch und Dr. Peter Mayer für die zahlreichen Einkristalluntersuchungen und auch für den intensiven Beistand bei diversen Problemdatensätzen.

Herrn Christian Minke bin ich großen Dank schuldig für die zahlreichen Stunden am REM, die unzähligen EDX-Messungen und die aufgenommenen Bilder. Auch denke ich gerne an die lustigen Abende beim Griechen und die Besuche auf der Weinmesse.

Großer Dank gilt auch den beiden Doktoren Martin Zeuner und Sandro Pagano, die bei mir schon während meiner Praktikantenzeit die Begeisterung für Festkörperchemie und die Welt der Leuchtstoffe geweckt haben.

Ganz besonderer Dank gilt auch meinen Laborkollegen aus D2.107 und später D2.074 für die schöne und beinahe schon zu schnell vergangene Zeit. Herrn Sebastian Schmiechen, Herrn Christian Ziegler, Herrn Stephan Werner, Herrn Martin Mangstl, Herrn Dr. Markus Seibald und Frau Nicole Braml. Vielen Dank für die immer lustigen Events an zahlreichen Abenden und auch den intensiven „Ratsch“ um der Arbeit zu entgehen.

Natürlich gilt auch großer Dank meinen Praktikanten Sascha Harm, Andreas Locher, Daniela Zitnanska, Elen Baumann, Claudia Göbel, Henrik Eickhoff und Ann-Kathrin Henß. Ohne den ständigen Ehrgeiz zur Forschung und die tatkräftige Unterstützung beim Synthetisieren und Auswerten wäre all das kaum möglich gewesen.

Ich möchte mich auch bei allen weiteren Kollegen der Arbeitskreise Schnick, Oeckler, Hoch, Schmedt auf der Günne, Johrendt und Lotsch ganz herzlich für die tolle Zeit bedanken.

Allergrößter Dank gilt aber meinen Eltern, sowie meiner Freundin Pamina, ohne eure Hilfe und Unterstützung wäre all dies nicht möglich gewesen.

“Ich beschäftige mich nicht mit dem, was getan worden ist.

Mich interessiert, was getan werden muss.”

(Marie Curie)

Table of Contents

1	Introduction.....	1
2	Ammonothermal Reactions	10
2.1	Preface.....	10
2.2	Ammonothermal Synthesis and Crystal Structure of BaAl₂(NH₂)₈·2NH₃	12
2.2.1	Introduction	13
2.2.2	Results and Discussion	13
2.2.3	Conclusions	16
2.2.4	Experimental Section.....	17
2.2.4.1	Synthesis.....	17
2.2.4.2	Single-Crystal Preparation.....	17
2.2.4.3	Single-Crystal X-ray Diffraction	18
2.2.5	References	18
3	Nitridoaluminates - New Host Lattices for Phosphor Materials.....	20
3.1	Ca[LiAlN₂]: A Quaternary Nitridoaluminate	20
3.1.1	Introduction	21
3.1.2	Results and Discussion	21
3.1.2.1	Crystal Structure.....	21
3.1.2.2	Lattice-Energy Calculations (MAPLE).....	25
3.1.3	Conclusion	26
3.1.4	Experimental Section.....	26
3.1.4.1	Synthesis.....	26
3.1.4.2	Single-Crystal X-ray Diffraction.....	27
3.1.4.3	Powder X-ray Diffraction.....	27
3.1.4.4	Electron Microscopy	27
3.1.5	References	28
3.2	Group (III) Nitrides M[Mg₂Al₂N₄] (M = Ca,Sr,Ba,Eu) and Ba[Mg₂Ga₂N₄] - Structural Relation and Nontypical Luminescence Properties of Eu²⁺ Doped Samples.....	30
3.2.1	Introduction	31
3.2.2	Experimental Section.....	32
3.2.2.1	Synthesis.....	32
3.2.2.2	Electron Microscopy	33
3.2.2.3	Single-Crystal X-ray Diffraction.....	33
3.2.2.4	Powder X-ray Diffraction.....	34
3.2.2.5	UV/Vis Spectroscopy	34
3.2.2.6	Luminescence	34

3.2.3	Results and Discussion	35
3.2.3.1	Synthesis and Chemical Analysis.....	35
3.2.3.2	Single-Crystal Structure Analysis	36
3.2.3.3	Luminescence	39
3.2.4	Conclusions	43
3.2.5	References	44
3.3	Ca[LiAl₃N₄]:Eu²⁺ - A Narrow Band Red-Emitting Nitridolithoaluminate.....	46
3.3.1	Introduction	47
3.3.2	Experimental Section.....	48
3.3.2.1	Synthesis.....	48
3.3.2.2	Single-Crystal X-ray Diffraction.....	48
3.3.2.3	Electron Microscopy	48
3.3.2.4	EDX Spectroscopy	49
3.3.2.5	Electron Energy-Loss Spectroscopy (EELS)	49
3.3.2.6	Luminescence	49
3.3.3	Results and Discussion	49
3.3.3.1	Synthesis and Chemical Analysis.....	49
3.3.3.2	Single-Crystal Structure Analysis	50
3.3.3.3	Lattice-Energy Calculations	53
3.3.3.4	EELS.....	53
3.3.3.5	Luminescence	54
3.3.4	Conclusion	55
3.3.5	References	56
3.4	Narrow-Band Red-Emitting Sr[LiAl₃N₄]:Eu²⁺ as a Next-Generation LED-Phosphor Material.....	59
3.4.1	Article	60
3.4.2	Methods	69
3.4.3	References	71
3.5	Investigations of the Electronic Structure and Bandgap of the Next-Generation LED-Phosphor Sr[LiAl₃N₄]:Eu²⁺ - Experiment and Calculations	74
3.5.1	Communication	74
3.5.2	Experimental Section.....	81
3.5.3	References	83
3.6	Ca_{18.75}Li_{10.5}Al₃₉N₅₅:Eu²⁺ - Supertetrahedron Phosphors for Solid-State Lighting	85
3.6.1	Introduction	86
3.6.2	Experimental Section.....	87
3.6.2.1	Synthesis.....	87

3.6.2.2	Single-Crystal X-ray Diffraction.....	87
3.6.2.3	Powder X-ray Diffraction.....	87
3.6.2.4	Electron Microscopy	87
3.6.2.5	EDX Spectroscopy	88
3.6.2.6	Electron Energy-Loss Spectroscopy (EELS)	88
3.6.2.7	Luminescence	88
3.6.3	Results and Discussion	88
3.6.3.1	Synthesis and Chemical Analysis.....	88
3.6.3.2	Crystal Structure.....	89
3.6.3.3	Powder X-ray Diffraction.....	91
3.6.3.4	Luminescence	92
3.6.3.5	EELS.....	94
3.6.4	Conclusion.....	94
3.6.5	References	95
3.7	Narrow Red Emitters for Brighter White Light.....	97
3.7.1	Comment	97
3.7.2	References	99
4	Conclusion and Outlook.....	101
5	Summary	105
6	Appendix.....	109
6.1	Supporting Information for Chapter 3.1	109
6.2	Supporting Information for Chapter 3.2	110
6.3	Supporting Information for Chapter 3.4.....	116
6.4	Supporting Information for Chapter 3.6.....	122
7	Publications	124
7.1	List of Publications Included in This Thesis.....	124
7.2	Patent Applications	128
7.3	Other Publications	128
7.4	Conference Contributions	129
7.5	CSD Numbers.....	131

1 Introduction

In the last century the lighting industry was one of the most stable, slowly but steadily growing business sectors in the world. Well established lighting technologies like incandescent light bulbs were supplemented by the more energy efficient compact fluorescent lamps (CFL). All of these products were mounted on standardized sockets, like E27, allowing easy substitution of different products. However, all these devices have their advantages and disadvantages. The color rendering index (CRI) of classical light bulbs reaches a maximum value of 100, correlating with daylight. But the major disadvantage of incandescent lamps is that only 5-10% of the consumed electrical energy is converted to visible light. The residual energy is dissipated as heat by the glowing tungsten filament.^[1]

Commercial fluorescent tubes and CFLs on the other hand show increased energy efficiency. However, with typical CRI values as low as 70-80, the emitted light significantly lacks in color rendition. Furthermore, the functional principle of these lamps requires an UV light source, typically containing the toxic heavy metal mercury. The produced UV radiation is absorbed by solid-state phosphor materials and re-emitted in the visible spectral region.

An evaluation of the Central Association of the Electronic Industry showed that 55 million incandescent light bulbs were sold in 2011. This number correlates with a total market share of about 95%.^[2] However, facing a potentially disastrous anthropogenic climate change necessitates new appreciation of natural resources and reduced squandering of electrical energy.

With the introduction of regulations to gradually ban low efficiency light sources like incandescent bulbs, the European Commission set the course towards sustainability in lighting. By replacing incandescent lamps with CFLs, the annual consumption of electrical energy can be reduced by 15%. For the entire European Union these savings accumulate to approximately 40 TWh of electrical energy and about 15 million tons of CO₂ per year.^[3] However, the transition to CFLs as an alternative light source proved to be very difficult. The fact that CFLs contain Hg impedes widespread household use due to mainly two reasons. Firstly, damaged CFLs can release highly toxic Hg vapor and secondly CFLs disposal is highly problematic. Furthermore, the color rendition of fluorescent lamps is rather low. This leads to illuminated objects as well as persons looking very pale. Here, phosphor-converted light-emitting diodes (pc-LEDs) emerged as an advanced alternative to CFLs (see Figure 1). Meanwhile, industry and science all over the world agree that LEDs will be the lighting technology of the future. Up to now, pc-LEDs are unrivaled in efficiency and environmental

acceptability during the whole production period and life cycle. In this context, a current survey by McKinsey predicts that the global market share of pc-LEDs in general lighting will be about 45% in 2016 and almost 70% in 2020, with a market volume of around 64 billion €. ^[4]



Figure 1. Left: 12 W Philips LED master bulb, corresponds to a 60 W incandescent lamp; Middle: 9 W Philips Retrofit light bulb, corresponds to a 60 W incandescent lamp; Right: Classic incandescent lamp (60 W). All devices are mounted on E27 sockets, enabling easy exchange.

Oleg Lossev was one of the discoverers of electroluminescence, demonstrating the effect by glowing SiC crystals under applied current. ^[5] Based on this work the first commercial LED emitting in the visible spectral region was developed by *Holonyak* et al. as early as 1962, using GaAsP as semiconducting red-emitting material. ^[6] From there on, a multitude of different semiconductors (e.g. InGaP, GaAlAs) were investigated and enabled access to all colors of the visible spectrum. This development led the way to the common LED, mainly applied in indicator lights. ^[6] The emission of these semiconductor based LEDs is caused by electron-hole-transitions between different layers (p- and n-doped) of semiconducting materials. Here, the color of the emitted light correlates with the band gap energy of the semiconductor material used. However, these LEDs were no attractive candidates for general lighting purposes. The efficiencies of early LEDs were low and because of limited current densities also their brightness. Furthermore, the development of an efficient blue LED proved to be very difficult because hardly any applicable large band gap semiconductors were accessible at that time. The application of GaN as a direct band gap semiconductor was seriously considered in the late 1950s, ^[7] but the synthesis of high quality GaN single crystals and also the n- and p-type doping of the material were not possible, yet. In the 1970s, new

crystal growth techniques like MOVPE (Metalorganic Vapour Phase Epitaxy) were developed,^[8] and *Isamu Akasaki* began his work on adapting this method on GaN crystal growth. Together with *Hiroshi Amano* high quality device-grade GaN was obtained for the first time in 1986.^[9] They also obtained first evidences for successful p-doping with Mg and Zn and increased emission intensity after treating the samples with an electron beam.^[10] The effect of this treatment was investigated and described by *Shuji Nakamura*.^[11,12] Acceptors such as Mg or Zn form complexes with hydrogen during synthesis and thus become passive. The electron beam dissociates these complexes and the acceptors become active. Furthermore, *Nakamura* could show that a simple thermal annealing also leads to the activation of Mg acceptors. Another critical step toward the development of efficient LEDs was the growth and p-doping of alloys (AlGaN, InGaN) which are necessary to produce heterojunctions. Here, the recombination processes occur more efficiently. These were realized by *Akasaki's* and *Nakamura's* research groups.^[13,14] In 1994, *Nakamura* achieved a quantum efficiency of 2.7% with a blue-emitting double heterojunction InGaN/AlGaN LED.^[15] These investigations were the fundamental steps for energy efficient lighting, pioneering solid-state lighting solutions for general illumination.^[16] In 2014, the Nobel Prize in Physics was awarded to *Isamu Akasaki, Hiroshi Amano, and Shuji Nakamura* for “*the invention of efficient blue light-emitting diodes which has enabled bright and energy-saving white light sources*”.

Lighting applications require white light covering the entire visible spectrum from blue to red. This is hardly achievable with direct emitting LEDs due to the monochromatic light emission of each single emitter. Based on the results brought by *Akasaki, Amano, and Nakamura*, pc-LEDs have been developed. The functional principle of such pc-LEDs is comparable to the principle of fluorescent lamps developed by Germer in 1926.^[17] Ultraviolet (UV) to blue light emitted by a primary light source is used to stimulate the emission of downconversion phosphor materials. Additive mixing of the primary light emission and the emission of the luminescent materials can produce white light with high quality by covering at least major parts of the sensitivity region of the human eye. Commercially available LED products usually contain a blue-emitting primary LED combined either with a broadband yellow emitting compound (1-pc-LED) or with green and orange emitting phosphor materials (2-pc-LED) (see Figure 2).^[18,19]

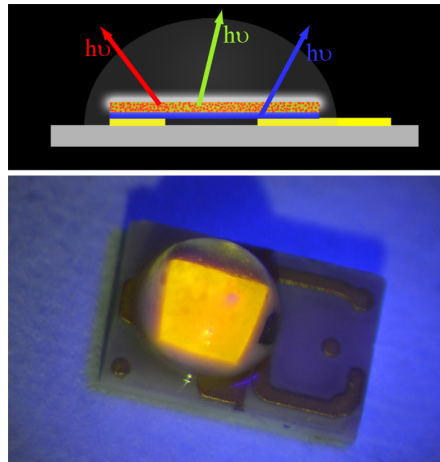


Figure 2. Top: Scheme of a 2-pc-LED with a green and an orange phosphor material placed on a blue emitting InGaN semiconductor LED. LED board (gray), contacts (yellow). Bottom: Picture of a LUXEON® Rebel white LED under UV irradiation.^[20]

The conversion of light in such a luminophoric material is based on excitation and emission processes of rare earth ions (activator ions, e.g. Eu^{2+} , Eu^{3+} , Ce^{3+}) incorporated in the crystal structures of the host compounds. During the excitation process (irradiation with UV to blue light) of Eu^{2+} or Ce^{3+} one electron is transferred from the 4f state to the 5d (excited) state. A part of the absorbed energy is re-emitted in form of visible light during the parity allowed relaxation process (e.g. $4f^6(^7F)5d^1 \rightarrow 4f^7(^8S_{7/2})$ transition in Eu^{2+}), the residual energy is afforded in nonradiative processes. Figure 3 shows a scheme of the influencing factors on the emission processes of Eu^{2+} and Ce^{3+} . The relative position of the excited state potential depends on the coordination sphere around the activator ion and the possibility of distortion of the coordination sphere.^[21] The energy difference between ground and excited state is strongly influenced by the chemical bonding type between the activator ion and the surrounding ligands (nephelauxetic effect). Here, covalent bonding increases the effect and results in a red-shifted emission. Another manipulating effect is the crystal field splitting of the 5d energy levels, directly depending on the strength of the ligand field around the activator site. The energetic difference between the centroid of the excitation band and emission band is called Stokes shift. Eu^{2+} and Ce^{3+} show broadband emission due to the overlap of several energy levels, the resulting large number of allowed transitions and the strong influence of the vibrating activator coordination spheres on the emission. In contrast to this, Eu^{3+} shows a well defined line emission of parity forbidden f-f transitions. Strong shielding effects of unoccupied 5d states hinder influencing effects from the host lattice. In this context, Eu^{3+} based luminescent materials can be discussed as important red-emitting components in white-emitting pc-LEDs. However, as mentioned before, the f-f transition in Eu^{3+} is parity forbidden resulting in an emission intensity several magnitudes smaller than

compared to Eu^{2+} . In modern high-power LEDs the blue light output of the primary LED is usually greater than $100 \text{ W}\cdot\text{cm}^{-2}$. These high pump rates would cause a saturation of the Eu^{3+} excited states because of the relatively long decay time of the f-f transition of Eu^{3+} in the order of ms.^[18]

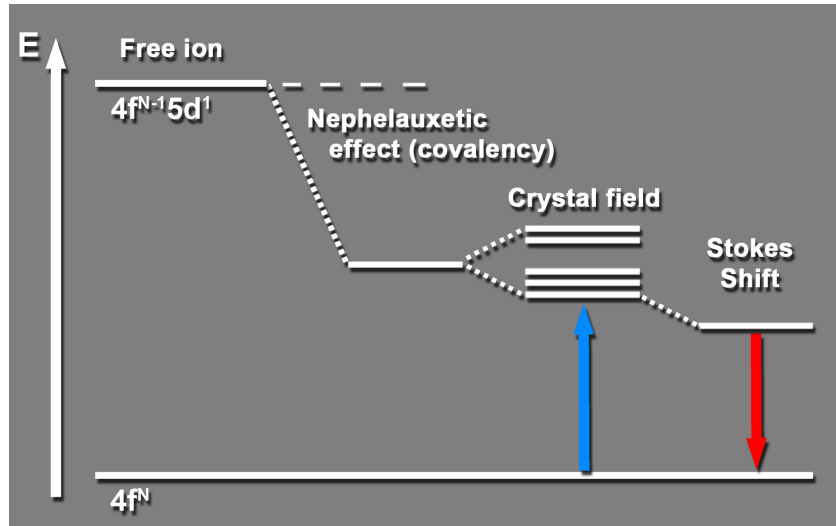


Figure 3. Scheme of excitation and emission processes in Eu^{2+} or Ce^{3+} considering influencing effects like the crystal field around the activator site and the nephelauxetic effect.^[20]

Due to intense parity allowed (for Ce^{3+} also spin allowed) transitions and short decay times of the excited states, Eu^{2+} and Ce^{3+} are predominantly used as doping agents for pc-LEDs.

In addition to short decay times and intense transitions, a potential phosphor material faces several more requirements for application in modern high-luminance pc-LEDs. High chemical and thermal stability are essential during the manufacturing process and for product lifetime. Furthermore, high quantum efficiencies close to 100% are important for a nearly non-dissipative light conversion. Typically, modern blue-emitting high-power LEDs are operated at currents of about 350 mA, and due to ohmic resistance heating the chip surfaces reach temperatures of up to $150 \text{ }^\circ\text{C}$. At these operating conditions thermal quenching can significantly reduce the quantum efficiency of a phosphor material. The causes for thermal quenching often are strong electron-phonon coupling. This effects, that the absorption of photons, which lift the activator's electrons in the excited states, does not result in re-emission but in an energy transfer to the host lattice (lattice vibrations). Highly-condensed rigid host lattices are beneficial to reduce phonon activation and therefore, thermal quenching.^[22]

Over the last years, (oxo)nitridosilicates emerged as superior host lattices for rare-earth doping and thus, for efficient phosphor materials.^[23] Similar to classical oxosilicates, the fundamental building units of (oxo)nitridosilicates are Si atoms in tetrahedral coordination by four N or O atoms, respectively.^[24] These polyhedra can be either isolated (0D) in the crystal

structure or connected by common corners or even edges forming 1D chains, 2D layers or 3D networks. Furthermore, compared to classical (oxo)silicates Si-N distances are large enough to enable three- and even fourfold ammonium-type $N^{[4]}$ coordination like in the nitridosilicates $MYbSi_4N_7$ ($M = \text{Eu}, \text{Sr}, \text{Ba}$) (see Figure 4).^[24]

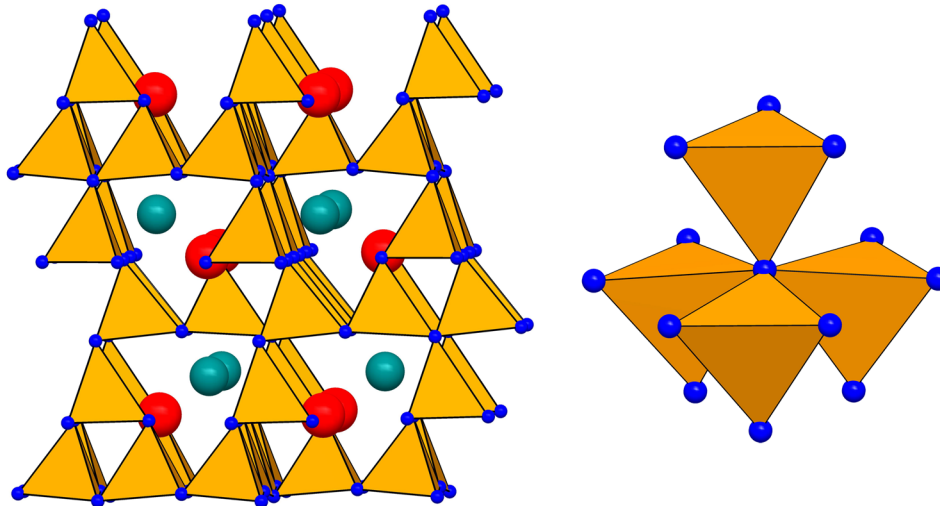


Figure 4. Crystal structure of $MYbSi_4N_7$ ($M = \text{Eu}, \text{Sr}, \text{Ba}$). Left: Sheets of highly condensed *dreier* rings along $[100]$. Right: $[N(\text{SiN}_3)_4]$ building block with $N^{[4]}$. $[\text{SiN}_4]$ tetrahedra orange, metal ions red and green and nitrogen blue.^[23,25-27]

Liebau classified oxosilicates in dependence of the connectivity of the respective tetrahedra.^[28] This nomenclature is also largely valid for nitride analogues. The degree of condensation κ (here: atomic ratio Si : N/O) of these materials can in principle be derived from the stoichiometric formula (e.g. $\kappa = 4/7$ for $MYbSi_4N_7$).

Almost no nitrogen containing silicate occurs in nature. Since oxygen is omnipresent in natural environments and due to the fact that a Si-O bond is energetically favored compared to Si-N bonds, hardly any (oxo)nitridosilicates have been found in nature.^[29] A famous exception of this is the mineral *sinoite*, $\text{Si}_2\text{N}_2\text{O}$, which was one component of the meteorite *Neuschwanstein*.^[30] However, in laboratory conditions these materials can be synthesized under reducing atmosphere in pure nitrogen or forming gas (N_2/H_2) at high temperatures. Thereby a number of novel materials have been synthesized and characterized recently.^[23] In the compound class of (oxo)nitridosilicates several important LED-phosphor materials have been found after doping with rare-earth ions. The group of $M_2\text{Si}_5\text{N}_8:\text{Eu}^{2+}$ ($M = \text{Ca}, \text{Sr}, \text{Ba}$) show intense orange to red emission and $(\text{Sr}, \text{Ba})_2\text{Si}_5\text{N}_8:\text{Eu}^{2+}$ ($\lambda_{\text{em}} = 590\text{-}625 \text{ nm}$; $\text{FWHM} \sim 2050\text{-}2600 \text{ cm}^{-1}$) is currently used as a red-emitting component in illumination-grade pc-LEDs.^[31] Furthermore, this material can also be applied in amber full-conversion pc-LEDs, employed for example as turn signal lights in the automotive sector. The (oxo)nitridosilicates $\text{Sr}_{1-x}\text{Ba}_x\text{Si}_2\text{O}_2\text{N}_2:\text{Eu}^{2+}$ emerged as important phosphors with a tunable

emission from blue to yellow depending on the x value. An LED application of these materials is currently in discussion.^[32]

The compound class of (oxo-)nitridosilicates can also be extended by partial substitution of Si by Al. Partial substitution yields the group of nitridoalumosilicates, total substitution leads to nitridoaluminates. Only very few compounds are known in the latter field, which is probably due to mainly unreactive Al reactants and the thermodynamically very stable binary nitride AlN. According to reports from literature, alkaline-earth nitridoaluminates tend to form less condensed structures compared to AlN, containing chains of AlN₄ tetrahedra like in $M_3Al_2N_4$ ($M = \text{Sr, Ba}$) or layers of AlN₄ polyhedra as in $Ca_3Al_2N_4$.^[33-35] On the other hand, a highly condensed crystal structure is found in alkaline nitridoaluminate Li_3AlN_2 forming a fluorite-type superstructure with LiN_4 and AlN_4 tetrahedra.^[36] Luminescence of Eu^{2+} doped nitridoaluminates has not been reported so far, although the principal requirements for phosphor materials should be met.

This thesis is focused on a current challenge for the LED industry of further improving the CRI of illumination-grade light sources without comprising energy efficiency. The CRI value of a white pc-LED critically depends on the spectral peak position and width of the red-emitting component.^[18] Currently available materials greatly limit the maximum achievable luminous efficacy because of rather broad emission bands. This causes significant losses in light output with increasing CRI values. In this context, the development of a narrow-band red-emitting phosphor material is of major interest. Such a phosphor would exhibit strongly reduced emission of infrared radiation, which is beyond human visual perception. At least in theory, Eu^{2+} doped nitridoaluminates could be potential candidates for red emission.

The first focus in this thesis is the expansion of the compound class of nitridoaluminates as well as finding synthesis routes to possible new Al precursor materials. Doping experiments on novel nitridoaluminates revealed that several compounds in this class show intense emission in the red spectral region under irradiation with blue light. Therefore, detailed investigations on the luminescence properties of these materials have been performed. The investigations carried out in the preparation of this thesis help to deeply understand the dependency between the host lattice structure and the observed luminescence. Additionally, a number of different parameters influencing the luminescence process (e.g. band gap) have been considered critically. The results should help to develop such highly desired narrow-band red-emitting phosphor materials.

References

- [1] C. Feldmann, *Z. Anorg. Allg. Chem.* **2012**, 638, 2169.
- [2] <http://www.greenpeace-magazin.de/magazin/archiv/6-11/gluehlampen/>, visited on 19th August **2014**.
- [3] http://ec.europa.eu/energy/lumen/professional/index_de.htm; follow link “FAQ für Fachleute”, visited on 12th August **2014**.
- [4] McKinsey & Company, Lighting the way: Perspectives on the global lighting market; www.mckinsey.com/~media/mckinsey/dotcom/client_service/automotive%20and%20assembly/lighting_the_way_perspectives_on_global_lighting_market_2012.ashx, visited on 16th October **2014**.
- [5] N. Zheludev, *Nat. Photon.* **2007**, 1, 189.
- [6] C. Ronda, *Luminescence*, Wiley-VCH Verlag, Weinheim, Germany, **2008**.
- [7] H. G. Grimmeiss, H. Koelmans, *Z. Naturforsch.* **1959**, 14a, 264; **1960**, 15, 799.
- [8] H. M. Manasevit, F. M. Erdman, W. I. Simpson, *J. Electrochem. Soc.* **1971**, 118, 1864.
- [9] H. Amano, N. Sawaki, I. Akasaki, Y. Toyoda, *Appl. Phys. Lett.* **1986**, 48, 353.
- [10] H. Amano, I. Akasaki, T. Kozawa, K. Hiramatsu, N. Sawaki, K. Ikeda, Y. Ishii, *J. Lumin.* **1988**, 40-41, 121.
- [11] S. Nakamura, N. Iwasa, M. Senoh, T. Mukai, *Jpn. J. Appl. Phys.* **1992**, 31, 1258.
- [12] S. Nakamura, T. Mukai, M. Senoh, N. Iwasa, *Jpn. J. Appl. Phys.* **1992**, 31, L139.
- [13] H. Murakami, T. Asahi, H. Amano, K. Hiramatsu, N. Sawaki, I. Akasaki, *J. Crystal Growth* **1991**, 115, 648.
- [14] S. Nakamura, T. Mukai, *Jpn. J. Appl. Phys.* **1992**, 31, L1457.
- [15] S. Nakamura, T. Mukai, M. Senoh, *Appl. Phys. Lett.* **1994**, 64, 1687.
- [16] S. Nakamura, G. Fasol, *The blue laser diode*, Springer, Berlin, Germany, **1997**.
- [17] E. Germer, F. Meyer, H. J. Spanner, *US 2182732 A*, **1939**.
- [18] M. Krames, G. O. Mueller, R. B. Mueller-Mach, H. Bechtel, P. J. Schmidt, *PCT Int. Appl.*, WO 2010131133, A1, **2010**.
- [19] R. Mueller-Mach, G. O. Mueller, M. R. Krames, T. Trottier, *IEEE J. Select. Top. Quant. Electron.* **2002**, 8, 339.
- [20] S. Schmiechen, P. Pust, W. Schnick, *Nachr. Chem.* **2014**, 62, 847.
- [21] G. Blasse, B. Grabmaier, *Luminescent Materials*, Springer, Berlin, Germany, **1994**.
- [22] G. Blasse, A. Brill, *Philips Tech. Rev.* **1970**, 31, 314.
- [23] M. Zeuner, S. Pagano, W. Schnick, *Angew. Chem.* **2011**, 123, 7898.

- [24] W. Schnick, H. Huppertz, *Chem. Eur. J.* **1997**, *3*, 679.
- [25] H. Huppertz, W. Schnick, *Z. Anorg. Allg. Chem.* **1997**, *623*, 212.
- [26] H. Huppertz, W. Schnick, *Chem. Eur. J.* **1997**, *3*, 249.
- [27] H. Huppertz, W. Schnick, *Acta Crystallogr., Sect. C: Cryst. Struct. Commun.* **1997**, *53*, 1751.
- [28] F. Liebau, *Structural Chemistry of Silicates*, Springer, Berlin, Germany, **1985**.
- [29] W. Schnick, *Angew. Chem.* **1993**, *105*, 846.
- [30] A. Bischoff, T. Grund, T. Jording, B. Heying, R.-D. Hoffmann, U. Ch. Rodewald, R. Pöttgen, *Z. Naturforsch.* **2005**, *60b*, 1231.
- [31] M. Zeuner, F. Hintze, W. Schnick, *Chem. Mater.* **2009**, *21*, 336.
- [32] M. Seibald, T. Rosenthal, O. Oeckler, W. Schnick, *Crit. Rev. Solid State Mater. Sci.* **2014**, *39*, 215.
- [33] W. Blase, G. Cordier, M. Ludwig, R. Kniep, *Z. Naturforsch. B: Chem. Sci.* **1994**, *49*, 501.
- [34] M. Ludwig, J. Jaeger, R. Niewa, R. Kniep, *Inorg. Chem.* **2000**, *39*, 5909.
- [35] M. Ludwig, R. Niewa, R. Kniep, *Z. Naturforsch. B: Chem. Sci.* **1999**, *54*, 461.
- [36] R. Juza, F. Hund, *Z. Anorg. Allg. Chem.* **1948**, *257*, 13.

2 Ammonothermal Reactions

2.1 Preface

In the last couple of years, main group nitrides have moved into the focus of numerous investigations. Especially compounds of group III (Al, Ga, In) and group IV (Si, Ge) elements show intriguing material properties. Typical syntheses are hereby based on pyrolysis of molecular precursors, solid-state reactions at rather high temperatures or the use of salts or metals acting as fluxing agents. Usually, these routes enable access only to single crystals in μm scale of the ternary or multinary compounds. Ammonothermal reactions could be an attractive alternative for growing larger single crystals. The huge potential of solvothermal syntheses in general, for example for hydrothermal processing of quartz, is well known for a long time. A similar technique could be applicable for synthesis of nitrides employing supercritical ammonia, which can act as solvent as well as nitrogen source. The solubility of a mainly ionic solid depends on the dielectric constant ϵ of the solvent. A compound is only soluble, when the energy of solvation is higher than the lattice energy of the solid. Furthermore, there is a strong dependence of the dielectric behaviour on the temperature of the solvent. ϵ decreases with elevated temperature, which is mainly caused by the decreasing density of the solvent at increased temperatures. For NH_3 ϵ is 22 at -77.7°C , which is a rather small value compared to H_2O ($\epsilon = 81.7$ at 0°C). Therefore, NH_3 is less suitable as a solvent for inorganic compounds except ϵ could be increased. This is possible under elevated pressures since the density of ammonia is increased.^[1,2] Therefore, the interdisciplinary DFG-*Forschergruppe* "FOR 1600: Chemistry and Technology of the Ammonothermal Synthesis of Nitrides"^[3] designed special autoclaves for reaction conditions up to 600°C and 3000 bar, which are not accessible with any commercially available system. Beyond this *Forschergruppe* ammonothermal processing finds only limited application, although the academic background has been generated in Germany decades ago by *H. Jacobs et al.*^[1] The scope of this research project is to re-establish ammonothermal synthesis, focusing on synthesis and crystal growth of novel multinary nitrides including the elements Al, Ga, Mg, Li, Si or Ge. Hitherto, nitrides, also including alkaline and alkaline earth or rare earth metals as well as intermediates, obtained during synthesis should be structurally characterized. In the following chapter the synthesis and characterization of $\text{BaAl}_2(\text{NH}_2)_8 \cdot 2\text{NH}_3$ is described, which is handled as a potential precursor material for further thermal treatment to obtain novel Ba containing nitridoaluminates.

References

- [1] H. Jacobs, D. Schmidt, *Current topics in materials science* **1982**, 8, 381.
- [2] W. C. Fernelius, W. C. Johnson, *J. Chem. Educ.* **1928**, 5, 664.
- [3] A project description can be taken from: <http://gepris.dfg.de/gepris/projekt/182356696>, visited on 17th October **2014**.

2.2 Ammonothermal Synthesis and Crystal Structure of $\text{BaAl}_2(\text{NH}_2)_8 \cdot 2\text{NH}_3$

published in: *Z. Anorg. Allg. Chem.* **2013**, *639*, 1185-1187

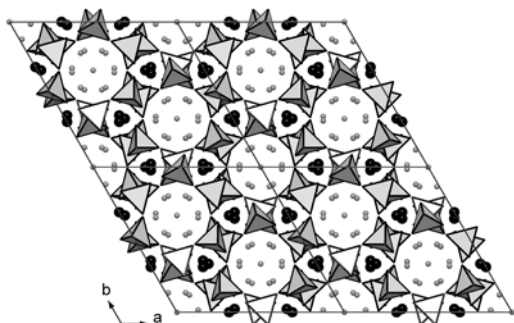
authors: Philipp Pust, Sebastian Schmiechen, Frauke Hintze and Wolfgang Schnick

DOI: 10.1002/zaac.201300088

Copyright © 2013 Wiley-VCH Verlag GmbH & Co. KGaA, Weinheim

<http://onlinelibrary.wiley.com/doi/10.1002/zaac.201300088/abstract>

Abstract. $\text{BaAl}_2(\text{NH}_2)_8 \cdot 2\text{NH}_3$ was synthesized starting from an intermetallic phase with nominal composition Al_2Ba under ammonothermal conditions in a stainless-steel autoclave at 823 K and 245 MPa. Single crystals were grown on aluminum substrates and prepared under



low-temperature conditions. The crystal structure ($R\bar{3}c$ (no. 167), $a = 15.7370(17)$, $c = 28.804(6)$ Å, $Z = 1$, 1829 reflections, 65 parameters, $wR_2 = 0.07$) was solved on the basis of single-crystal X-ray diffraction data. $\text{BaAl}_2(\text{NH}_2)_8 \cdot 2\text{NH}_3$ contains isolated $\text{Al}(\text{NH}_2)_4$ tetrahedra forming two different types of channels along [001].

2.2.1 Introduction

Synthesis of ternary or multinary nitride materials can be carried out with a broad range of synthetic approaches. Due to the high kinetic stability of nitrogen (N_2) regular high-temperature routes starting from metals and nitrogen require typically rather high temperatures above 1000 °C. Unfortunately, such reactions lead frequently to non phase-pure products.^[1,2] We have recently reported on another approach for nitrides starting from binary amides and imides as precursor compounds to form nitridosilicates.^[3,4] In such amides or imides the proximity of nitrogen and the corresponding metal ions on an atomic level facilitates a significant reduction of synthesis temperature. Employment of thermally less stable ternary amides could lead to further reduction of temperatures and may enable access to kinetically controlled nitridic products. This method could be of interest, especially in the nitridoaluminate system with respect to the thermodynamically very stable binary compound AlN.

Rouxel et al. were the first to report on ternary alkaline-earth aluminum amides.^[5-7] The syntheses were performed in liquid ammonia in sealed glass tubes starting from an alkaline-earth electride solution and an excess of metallic aluminum. A stoichiometric formula $\text{M}^{\text{II}}\text{Al}_2(\text{NH}_2)_8$ ($\text{M}^{\text{II}} = \text{Sr}, \text{Ba}$) was derived from elemental analysis and IR spectroscopy as well as thermal decomposition measurements have been performed. The compounds showed a rapid decomposition after being extracted from ammonia atmosphere and thus it was not possible to determine the crystal structure.^[5-7]

Another method to access ternary aluminum amides has been demonstrated by *Peters* et al. employing ammonothermal conditions.^[8] To increase the solubility of aluminum in supercritical NH_3 ammonobasic mineralizers like K or $\text{K}(\text{NH}_2)_2$ are useful. Formation of intermediate $\text{KAl}(\text{NH}_2)_2$ and subsequent thermal decomposition induces the generation of AlN.

We adapted this technique to our needs and performed the ammonothermal synthesis of an alkaline-earth aluminum amide employing stainless-steel autoclaves. Crystal structure determination was achieved by low-temperature single-crystal preparation and measurement.

2.2.2 Results and Discussion

$\text{BaAl}_2(\text{NH}_2)_8 \cdot 2\text{NH}_3$ was synthesized starting from an intermetallic phase with nominal composition Al_2Ba and dry ammonia in a stainless-steel autoclave at 823 K and 245 MPa under supercritical conditions. Colorless crystals, which exhibited a high sensitivity towards

hydrolysis and thermal decomposition under ambient conditions, were grown on an aluminum substrate and isolated under low-temperature conditions (213 K).

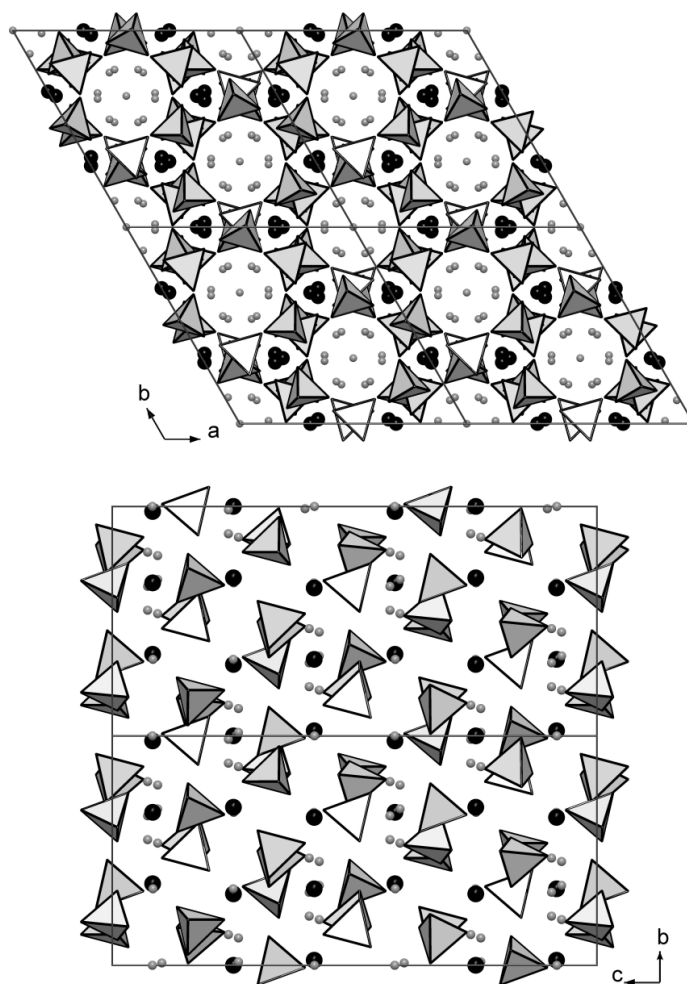
Table 1. Crystallographic data of $\text{BaAl}_2(\text{NH}_2)_8 \cdot 2\text{NH}_3$.

Formula	$\text{BaAl}_2(\text{NH}_2)_8 \cdot 2\text{NH}_3$
Crystal system	trigonal
Space group	$R\bar{3}c$ (no. 167)
Lattice parameters /Å	$a = b = 15.7370(17)$ $c = 28.804(6)$
Cell volume /Å ³	6177.7(16)
Formula units /cell	18
$\rho_{\text{calcd.}} / \text{g} \cdot \text{cm}^{-3}$	1.673
μ / mm^{-1}	3.004
T /K	200(2)
F(000)	3036
Diffractometer	Kappa CCD
Radiation, monochromator	Mo-K α ($\lambda = 0.71073$ Å), graphite
Absorption correction	multi-scan ^[12]
Max. / min. transmission	0.4322 / 0.2100
θ range /°	3.2 - 29.6
Index ranges	$-21 \leq h \leq 21$ $-21 \leq k \leq 21$ $-37 \leq l \leq 39$
Independent reflections	1829 ($R_{\text{int}} = 0.0685$)
Refined parameters	65
Goodness of fit	1.021
R_1 (all data); $R_1 (F^2 > 2\sigma(F^2))$	0.0280, 0.0246
wR_2 (all data); $wR_2 (F^2 > 2\sigma(F^2))$	0.0700, 0.0674
Max. / min. residual electron density /e·Å ⁻³	0.84 / -1.51

The crystal structure of $\text{BaAl}_2(\text{NH}_2)_8 \cdot 2\text{NH}_3$ was solved from single-crystal diffraction data and refined in trigonal space group $R\bar{3}c$ (no. 167) with $a = 15.7370(17)$ and $c = 28.804(6)$ Å. The crystallographic data of $\text{BaAl}_2(\text{NH}_2)_8 \cdot 2\text{NH}_3$ are summarized in Table 1, atomic coordinates and isotropic displacement parameters are listed in Table 2.

Table 2. Atomic coordinates and isotropic displacement parameters / \AA^2 of $\text{BaAl}_2(\text{NH}_2)_8 \cdot 2\text{NH}_3$, standard deviations in parentheses.

Atom	x	y	z	U_{eq}
Ba1	0.35543(1)	$\frac{1}{3}$	0.8333	0.02367(9)
Al1	0.35806(6)	0.15825(5)	0.00234(2)	0.02902(17)
N1	0.24822(18)	0.07955(19)	-0.03310(9)	0.0404(5)
N2	0.3991(2)	0.28800(17)	-0.01122(8)	0.0407(6)
N3	0.3232(2)	0.13391(17)	0.06434(7)	0.0377(5)
N4	0.45903(18)	0.13427(18)	-0.01033(8)	0.0368(5)
N5	0.5474(6)	0.3481(10)	0.0731(4)	0.070(3)
N6	0	0	-0.0832(4)	0.143(5)

**Figure 1.** Crystal structure of $\text{BaAl}_2(\text{NH}_2)_8 \cdot 2\text{NH}_3$. $\text{Al}(\text{NH}_2)_4$ tetrahedra gray, Ba^{2+} black, ammonia nitrogen atoms bright gray. Hydrogen atoms of the amide groups and of the ammonia molecules are not displayed. Top: Viewing direction along $[001]$, bottom: Viewing direction along $[100]$.

The crystal structure of $\text{BaAl}_2(\text{NH}_2)_8 \cdot 2\text{NH}_3$ is built up of isolated $\text{Al}(\text{NH}_2)_4$ tetrahedra forming two different types of channels along [001] (see Figure 1). Ba^{2+} -ions are located in the smaller voids, whereas the bigger channels are occupied by ammonia molecules. Volume calculations with PLATON^[9] delivered a pore volume of 1242.5 \AA^3 in the larger tubes, leading to sufficient space to enclose two NH_3 molecules per unit cell.

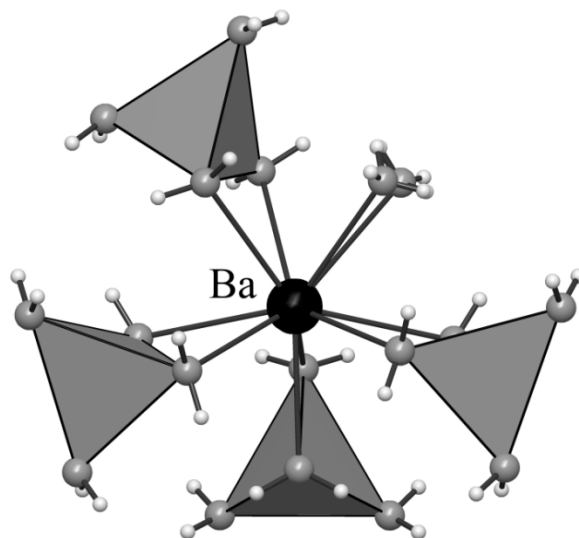


Figure 2. Coordination of Ba^{2+} in $\text{BaAl}_2(\text{NH}_2)_8 \cdot 2\text{NH}_3$. $\text{Al}(\text{NH}_2)_4$ tetrahedra gray, Ba^{2+} black, N bright gray, H white.

The shortest distance between ammonia molecules and surrounding amide groups ($2.885(13) \text{ \AA}$) is too large to form stabilizing hydrogen bonds, resulting in high mobility of the enclosed molecules and large isotropic displacement parameters. Therefore hydrogen atoms bound to ammonia nitrogen N6 were disregarded in the crystal structure refinement assuming severe rotational disorder in the NH_3 molecules.

$\text{Al}(\text{NH}_2)_4$ tetrahedra show interatomic distances (Al–N) of 1.85 \AA , which correspond with Al–N distances in nitridoaluminates like LiCaAlN_2 (Al–N: $1.92\text{--}1.96 \text{ \AA}$)^[10] or $\text{Ba}_3\text{Al}_2\text{N}_4$ (Al–N: $1.91\text{--}1.98 \text{ \AA}$).^[2]

Ba^{2+} -ions are aligned in the smaller tubes along [001] (see Figure 1). The Ba^{2+} -site is coordinated by eight amide groups and one ammonia molecule with Ba–N distances ranging from 2.93 to 2.98 \AA (see Figure 2). Similar values can also be observed in $\text{Ba}(\text{NH}_2)_2$ (Ba–N: $2.79\text{--}3.17 \text{ \AA}$).^[11]

2.2.3 Conclusions

In this contribution it was possible to elucidate the crystal structure of $\text{BaAl}_2(\text{NH}_2)_8 \cdot 2\text{NH}_3$ and to confirm the assumed stoichiometric formula given by Rouxel et al.^[6] The structure shows

tube like pores with a calculated volume of 1242.5 \AA^3 leaving space for incorporation of two NH_3 molecules per unit cell. $\text{BaAl}_2(\text{NH}_2)_8 \cdot 2\text{NH}_3$ may be a suitable precursor material for nitridoaluminate synthesis since constituting atoms are already arranged on an atomic level and a ternary compound in the system Ba-Al-N may be formed by thermal treatment and evolution of NH_3 .

2.2.4 Experimental Section

2.2.4.1 Synthesis

All manipulations were performed with rigorous exclusion of oxygen and moisture in flame-dried Schlenk-type glassware on a Schlenk line interfaced to a vacuum (10^{-4} mbar) line or in an argon-filled glove box (Unilab, MBraun, Garching, $\text{O}_2 < 1$ ppm, $\text{H}_2\text{O} < 1$ ppm). Ammonia was purified using a cleaning cartridge (Micro Torr MC400-702FV, SAES Pure Gas Inc., San Luis Obispo, CA, USA).

The synthesis of $\text{BaAl}_2(\text{NH}_2)_8 \cdot 2\text{NH}_3$ was performed in specially designed autoclaves made from Inconel stainless steel (no. 2.4668), sustaining a maximum pressure of 300 MPa and a maximum temperature of 873 K (development and design of the autoclaves was performed by the workgroup of *Prof. Dr.-Ing. E. Schlücker* and *Dr.-Ing. Dipl.-Wirt.-Ing. N. Alt* within the *DFG-Forschergruppe FOR1600* “Chemie und Technologie der Ammonothermal-Synthese von Nitriden”). 191.3 mg (1.00 mmol) of an intermetallic phase with nominal composition Al_2Ba , synthesized from the elements at 1423 K, were placed into the autoclave together with aluminum substrates. Substrates were cut from an aluminum foil and surface-ground with a rasp. A volume of ammonia (44 mL) was condensed onto the compounds at 200 K, reaching a filling degree of 45 Vol.-% inside the autoclave. The autoclave was positioned vertically in a tube furnace. The autoclave lid protruded from the furnace resulting in a measured temperature gradient of 100 K from bottom to top. Within 3 h temperature was raised to 823 K, maintained for 700 h, gaining a measured pressure of 245 MPa, and quenched down to room temperature by switching of the furnace.

2.2.4.2 Single-Crystal Preparation

For the crystal preparation, we adapted the technique described by Stalke et al.^[13] to our needs. After reaction the ammonia within the autoclave was recondensed at 200 K, the aluminum substrate was extracted and directly put into perfluoroether (Galden), which was cooled by an ethanol/dry-ice freezing mixture and a stream of cooled nitrogen to 213 K. Colorless, block-shaped single crystals grown on the aluminum substrate were isolated under

a microscope, collected on the tip of a glass fiber, immediately submerged in liquid nitrogen and transferred to the diffractometer.

2.2.4.3 Single-Crystal X-ray Diffraction

Single-crystal diffraction data were collected with a Nonius Kappa CCD diffractometer (Mo- $K\alpha$ radiation, graphite monochromator) at 200 K. A spherical absorption correction using the program SADABS^[12] was applied. The crystal structure was solved by using direct methods with SHELXS.^[14] The refinement of the structure was carried out by the method of least-squares using SHELXL.^[14] The atomic ratio Ba:Al was confirmed by energy-dispersive X-ray spectroscopy (EDX) using a JSM-6500F scanning micro-scope (Jeol) equipped with an EDX detector 7418 (Oxford Instruments). An atomic ratio Ba:Al = 1:1.9 was measured by EDX analysis and agrees with the composition of $\text{BaAl}_2(\text{NH}_2)_8 \cdot 2\text{NH}_3$. As a result of the high sensitivity at ambient temperature of the compound the nitrogen ratio was not determinable. Hydrogen positions of the $\text{Al}(\text{NH}_2)_4$ tetrahedra could be determined by difference Fourier syntheses and were refined isotropically using restraints for nitrogen-hydrogen distances, all other atoms were refined anisotropically.

Further details of the crystal structure investigations can be obtained from the Fachinformationszentrum Karlsruhe, 76344 Eggenstein-Leopoldshafen, Germany (Fax: +49-7247-808-666; E-Mail: crysdata@fiz-karlsruhe.de) on quoting the depository number CSD-425323.

2.2.5 References

- [1] M. Ludwig, J. Jaeger, R. Niewa, R. Kniep, *Inorg. Chem.* **2000**, *39*, 5909.
- [2] M. Ludwig, R. Niewa, R. Kniep, *Z. Naturforsch. B: Chem. Sci.* **1999**, *54*, 461.
- [3] M. Zeuner, F. Hintze, W. Schnick, *Chem. Mater.* **2009**, *21*, 336.
- [4] M. Zeuner, S. Pagano, W. Schnick, *Angew. Chem. Int. Ed.* **2011**, *50*, 7754.
- [5] P. Palvadeau, A.-M. Trélohan, J. Rouxel, *Compt. Rend.* **1969**, *269C*, 126.
- [6] J. Rouxel, P. Palvadeau, *Compt. Rend.* **1971**, *272C*, 63.
- [7] P. Palvadeau, M. Drew, G. Charlesworth, J. Rouxel, *C. R. Seances Acad. Sci. (Ser. C)* **1972**, 275.
- [8] D. Peters, *J. Cryst. Growth* **1990**, *104*, 411.
- [9] A. L. Spek, PLATON - A Multipurpose Crystallographic Tool, v1.07, Utrecht University, Utrecht, Netherlands, **2003**.
- [10] P. Pust, S. Pagano, W. Schnick, *Eur. J. Inorg. Chem.* **2013**, 1157.
- [11] H. Jacobs, C. Hadenfeldt, *Z. Anorg. Allg. Chem.* **1975**, *418*, 132.

- [12] G. M. Sheldrick, SADABS, v2, Multi-Scan Absorption Correction, University of Göttingen, Germany, **2001**.
- [13] T. Kottke, D. Stalke, *J. Appl. Crystallogr.* **1993**, 26, 615.
- [14] G. M. Sheldrick, *Acta Crystallogr., Sect. A: Found. Crystallogr.* **2008**, 64, 112.

3 Nitridoaluminates - New Host Lattices for Phosphor Materials

3.1 Ca[LiAlN₂]: A Quarternary Nitridoaluminate

published in: *Eur. J. Inorg. Chem.* **2013**, 1157-1160

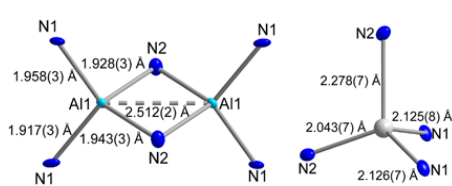
authors: Philipp Pust, Sandro Pagano and Wolfgang Schnick

DOI: 10.1002/ejic.201201283

Copyright © 2013 Wiley-VCH Verlag GmbH & Co. KGaA, Weinheim

<http://onlinelibrary.wiley.com/doi/10.1002/ejic.201201283/abstract>

Abstract. Ca[LiAlN₂] was synthesized from LiAlH₄, LiN₃, calcium, and lithium metal as fluxing agent in welded-shut tantalum crucibles at 900 °C. The compound crystallizes in the form of transparent colorless platelets that undergo hydrolysis in air and under moisture. The crystal structure [*P*2₁/*c* (no. 14), *a* = 5.7587(12) Å, *b* = 6.8773(14) Å, *c* = 5.7960(12) Å, β = 90.28(3)°, *Z* = 4] was solved from single-crystal X-ray diffraction data and was confirmed with Rietveld refinement methods and lattice-energy calculations (Madelung part of lattice energy, MAPLE). Ca[LiAlN₂] forms layers of edge- and vertex-sharing AlN₄ tetrahedra



isotypic with LiCaGaN₂. Li⁺ ions are positioned in tetrahedral voids within the [Al₂N₂N_{4/2}] layers resulting in a highly condensed structure of Al- and Li-centered polyhedra.

3.1.1 Introduction

Owing to their great structural variety and superior material properties like luminescence, nonlinear optical properties, or lithium-ion conductivity, ternary and multinary p-block nitrides have attracted significant attention over the past decade.^[1] Formally, these nitrides can be derived from the respective oxidic materials by substituting O by N. This exchange also enhances the structural variety, since nitrogen is able to connect up to four tetrahedral centers (N^[4]), like in the nitridosilicates MYbSi₄N₇ (M = Sr, Ba).^[1,2]

Only a few examples of nitridoaluminates containing alkaline-earth metal or lithium ions are known and have been fully characterized.^[3-5] The compound α -Ca₃Al₂N₄^[6] has been synthesized directly from the metals by reaction with nitrogen at temperatures above 1000 °C forming layers of edge- and vertex-sharing AlN₄ tetrahedra also known from the isotypic nitridogallate Ca₃Ga₂N₄ that forms GaN₄ tetrahedra.^[7] The crystal structure of Ca₆Al₂N₆^[8] is made up of isolated [Al₂N₆]¹²⁻ dimers analogous with [Si₂N₆]¹⁰⁻ groups known from nitridosilicates (e.g., Li₄Ca₃Si₂N₆).^[9] The lithium-containing compound Li₃AlN₂ has already been published by *Juza et al.*^[10] It can be derived from a fluorite type of structure with Li and Al occupying the tetrahedral voids in an ordered way, thereby resulting in a framework of vertex-sharing AlN₄ tetrahedra.

Here we report on the preparation and characterization of Ca[LiAlN₂], a quaternary lithionitridoaluminate that was synthesized starting from a hydride as precursor by means of a lithium flux route at moderate temperatures.

3.1.2 Results and Discussion

3.1.2.1 Crystal Structure

Ca[LiAlN₂] was solved and refined in the monoclinic space group *P*2₁/*c* (no. 14) with $a = 5.7587(12)$ Å, $b = 6.8773(14)$ Å, $c = 5.7960(12)$ Å, $\beta = 90.28(3)^\circ$. The crystallographic data of Ca[LiAlN₂] are summarized in Table 1, the atomic coordinates and the isotropic displacement parameters are given in Table 2.

An anisotropic refinement was possible for all atoms. As a result of the low ratio reflection/parameter < 10:1 the anisotropic refinement has not been carried out for the Li⁺ site. Ca[LiAlN₂] represents the first quaternary nitridoaluminate with tetrahedral AlN₄ units. The structure is isotypic to the nitridogallate LiCaGaN₂.^[11] Table 3 contains a list of known ternary nitridoaluminates exclusively built up of tetrahedral AlN₄ units. All these compounds are assembled by [Si₂N₆]¹⁰⁻-analogous [Al₂N₆]¹²⁻ dimers or show chains and layers, respectively.^[6,8,12]

Table 1. Crystallographic data of single crystal structure determination of Ca[LiAlN₂].

	Ca[LiAlN ₂]
Crystal system	monoclinic
Space group	<i>P</i> 2 ₁ / <i>c</i> (no. 14)
<i>a</i> [Å]	5.7587(12)
<i>b</i> [Å]	6.8773(14)
<i>c</i> [Å]	5.7960(12)
β [°]	90.28(3)
Cell volume [Å ³]	229.54(8)
Formula units per unit cell	4
Density [g·cm ⁻³]	2.952
μ [mm ⁻¹]	2.719
T [K]	294(3)
Diffractometer	STOE IPDS I
Radiation [Å]	Mo-K α ($\lambda = 0.71073$ Å)
F(000)	200
Profile range	$3.54 \leq \theta \leq 27.48$
Index ranges	$-7 \leq h \leq 7$ $-8 \leq k \leq 8$ $-7 \leq l \leq 7$
Independent reflections	529 [$R_{\text{int}} = 0.0414$]
Refined parameters	42
Goodness of fit	0.975
R_1 (all data); $R_1 (F^2 > 2\sigma(F^2))$	0.0510, 0.0362
wR_2 (all data); $wR_2 (F^2 > 2\sigma(F^2))$	0.0971, 0.0908
$\Delta\rho_{\text{max}}, \Delta\rho_{\text{min}}$ (e Å ⁻³)	0.638, -0.696

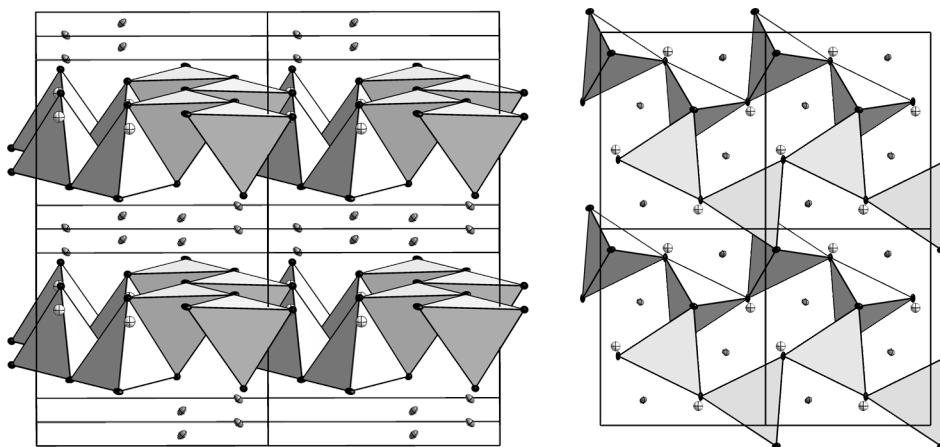


Figure 1. Crystal structure of Ca[LiAlN₂]. AlN₄ tetrahedra, bright gray; N atoms, black; Ca²⁺ ions, dark gray; and Li⁺ ions, dashed white; ellipsoids are drawn with a probability factor of 70 %. Left: viewing direction along [001]; right: viewing direction along [100].

Layers in β -Ca₃Al₂N₄ are isotypic to layers in α -Ca₃Ga₂N₄ and consist of edge- and vertex-sharing AlN₄ or GaN₄ tetrahedra.^[6,7] Ca[LiAlN₂] comprises the same arrangement of tetrahedra (see Figure 1). This layered topology is also comparable to the layers in the nitridosilicates SrSiN₂ and BaSiN₂.^[13] Distorted *sechser* rings widen from Ca[LiAlN₂] to SrSiN₂ and finally form regular hexagons in BaSiN₂ (see Figure 2).

Table 2. Atomic coordinates and isotropic displacement parameters (\AA^2) of Ca[LiAlN₂], standard deviations in parentheses.

Atom	<i>x</i>	<i>y</i>	<i>z</i>	$U_{iso}/U_{eq}^{[a]}$
Ca1	0.02678(13)	0.37193(11)	0.24055(11)	0.0046(3)
Al1	-0.37973(19)	0.13947(15)	0.07341(16)	0.0025(3)
N1	0.2674(6)	0.6471(4)	0.1073(5)	0.0041(6)
N2	0.2879(5)	0.1060(4)	0.0648(5)	0.0048(6)
Li1	0.3687(12)	0.0980(10)	0.4082(11)	0.0089(12)

[a] U_{eq} is defined as 1/3 of the trace of the orthogonalized U_{ij} tensors; U_{eq} for Li.

Li⁺ ions are centered in tetrahedral voids within the [Al₂N₂N_{4/2}] layers of Ca[LiAlN₂]. By inclusion of LiN₄ polyhedra [Li–N 2.043(3)–2.278(7) \AA], highly condensed layers of XN₄ tetrahedra (X = Al, Li) with N^[3] atoms are obtained [Al–N 1.917(3)–1.958(3) \AA]. Typically, those highly condensed layers occur frequently in products from high-temperature syntheses

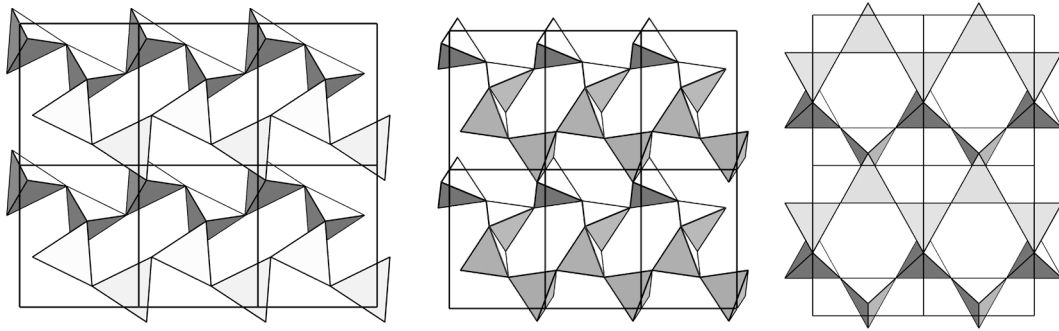


Figure 2. Illustration of layers in the structures Ca[LiAlN₂], LiCaGaN₂, β -Ca₃Al₂N₄, α -Ca₃Ga₂N₄ (left); SrSiN₂ (middle); and BaSiN₂ (right).^[6,7,11,13]

(>1300 °C) of nitridosilicates or oxonitridosilicates.^[14–17] According to *Liebau*^[18] the compound can be classified as a calcium lithionitridoaluminate since the Li⁺-centered polyhedra also take part in the tetrahedral assembly.

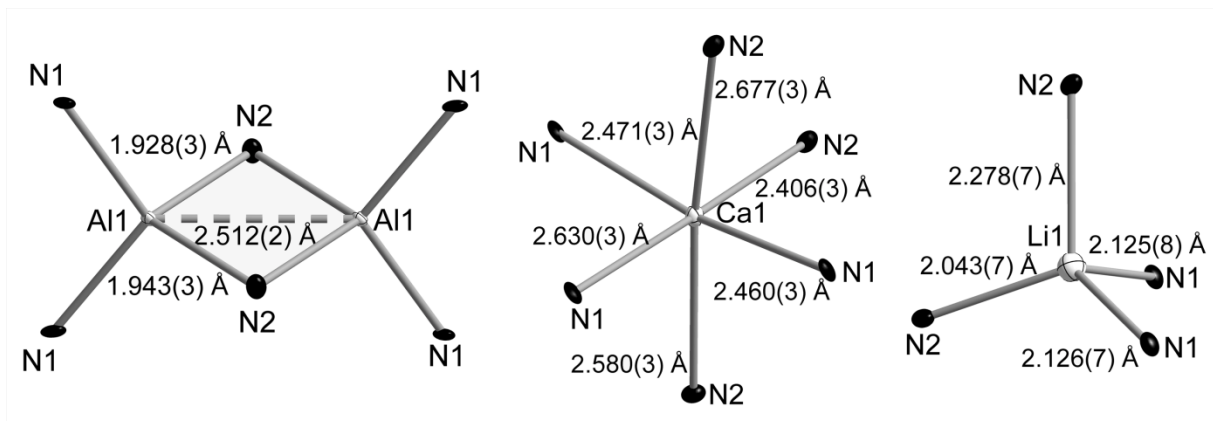


Figure 3. Coordination bond length of [Al₂N₂N_{4/2}] units (left), Ca²⁺ site (middle), and Li⁺ site (right); ellipsoids are drawn with a probability factor of 70 %.

With an angle of 99.072(6)°, N2–Al1–N2 exhibits only a small deviation from a regular tetrahedral angle in spite of the edge-sharing arrangement. Furthermore, a significant enlargement of the Al1–N2 bond length relative to Al1–N1 is not observable (see Figure 3). Comparable to AlN₄ polyhedra, LiN₄ tetrahedra are connected to each other through two corners [Li–Li 3.573(2) Å] and one edge [Li–Li 2.285(1) Å]. Although the Li atoms are arranged in planes, no endless strands or channels with short Li–Li distances (< 2.5 Å) occur like in Li₂SiN₂ or Li₄Sr₃Si₂N₆.^[9,19] The Ca site is coordinated by six N atoms and adopts a distorted-octahedral arrangement with an axial angle (N1–Ca1–N2) of 178.42(10)° (see Figure 3). Ca–N distances range from 2.460(3) to 2.677(3) Å and correspond well with typical distances in other calcium nitrides as well as with the sum of ionic radii.^[6,20–22]

Table 3. Ternary nitridoaluminates with AlN₄-tetrahedra.

	Author	Year	Entanglement of AlN ₄ tetrahedra
Ca ₃ AlN ₃	<i>Kniep et al.</i> ^[8]	1999	dimer
Sr ₃ Al ₂ N ₄	<i>Kniep et al.</i> ^[12]	1994	chain
α -Ca ₃ Al ₂ N ₄	<i>Kniep et al.</i> ^[6]	2000	layer
β -Ca ₃ Al ₂ N ₄	<i>Kniep et al.</i> ^[6]	2000	layer
Ba ₃ Al ₂ N ₄	<i>Kniep et al.</i> ^[8]	1999	chain

Rietveld refinement of powder-diffraction data validates the structure of Ca[LiAlN₂] obtained from single-crystal diffraction data (see Table S1 in the Supporting Information in Chapter 6.1 and Figure 4).

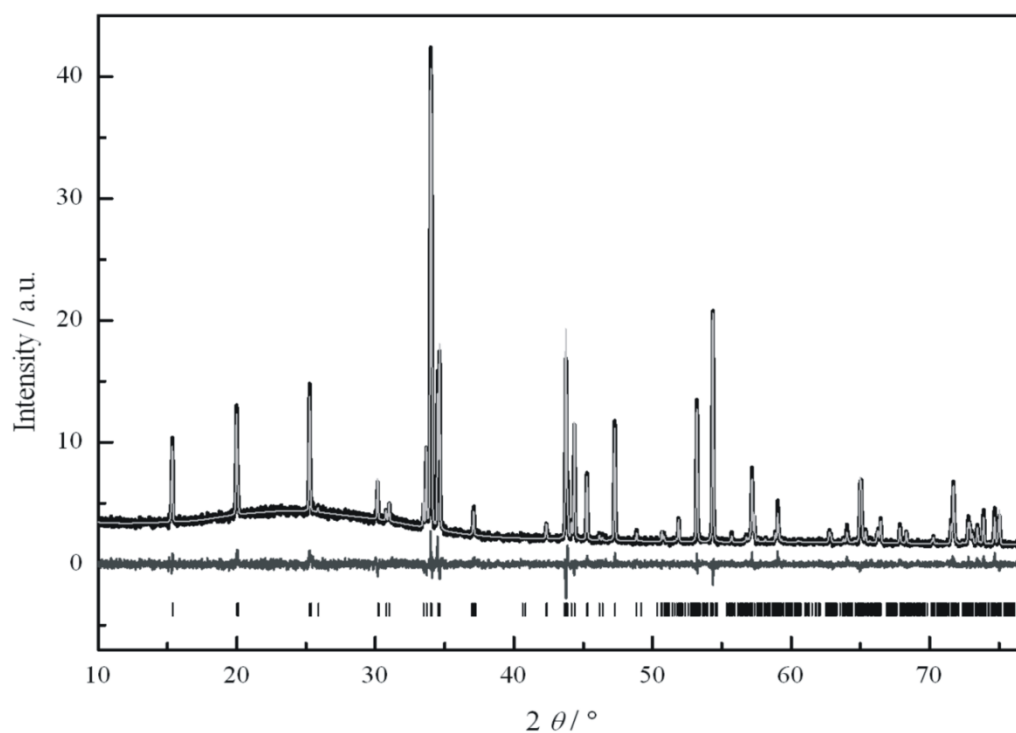


Figure 4. Observed (black) and calculated (bright gray) X-ray powder-diffraction pattern as well as the difference profile for the Rietveld refinement of Ca[LiAlN₂]. The vertical bars indicate possible peak positions.

3.1.2.2 Lattice-Energy Calculations (MAPLE)

To prove the electrostatic consistency of the crystal structure, MAPLE (Madelung part of lattice energy) calculations of the lattice energy^[22–25] were carried out. Exclusively electrostatic interactions in an ionic crystal were taken into account, depending on the charge, distance, and coordination spheres of the constituting ions. The calculated partial MAPLE values (for Li⁺, Ca²⁺, Al³⁺, and N³⁻) are in good agreement with reference values.^[20,26] The

minor deviation of 0.04 % of the total MAPLE sum of Ca[LiAlN₂] compared to the MAPLE sum of the formally constituting compounds ($1/3 \text{ Li}_3\text{N}^{[27]} + 1/3 \text{ Ca}_3\text{N}_2^{[28]} + \text{AlN}^{[29]}$) corroborates the refined crystal structure (see Table 4).

Table 4. Partial MAPLE values and MAPLE sums [kJmol^{-1}] of Ca[LiAlN₂].

Ca[LiAlN ₂] ^[a]		Model	
Ca1	1969	+1/3	Li ₃ N ^[27]
Al1	5155	+1/2	Ca ₃ N ₂ ^[28]
N1	4941	+1	AlN ^[29]
N2	4867		
Li1	671		
$\Sigma = 17594$		$\Sigma = 17665$	
		$\Delta = 0.04\%$	

[a] Typical partial MAPLE values [kJmol^{-1}]: Ca²⁺: 1930 - 2120; Al³⁺: 5000 - 6000; Li⁺: 600 - 860; N³⁻: 5000 - 6000.^[20,26]

3.1.3 Conclusion

The crystal structure of Ca[LiAlN₂] was successfully solved by using single-crystal diffraction data and was confirmed with X-ray powder-diffraction data as well as lattice-energy calculations. Ca[LiAlN₂] represents the first example of a quaternary calcium lithionitridoaluminate with tetrahedral AlN₄ and LiN₄ units. The lithium-flux method in combination with a hydride as precursor permits a convenient synthetic approach to nitridoaluminates like Ca[LiAlN₂] at moderate temperatures.

3.1.4 Experimental Section

3.1.4.1 Synthesis

All manipulations have been performed with rigorous exclusion of oxygen and moisture in flame-dried glassware on a Schlenk line attached to a vacuum (10^{-3} mbar) line or in an argon-filled glovebox (Unilab, MBraun, Garching, O₂ < 1 ppm, H₂O < 1 ppm). The synthesis of Ca[LiAlN₂] was carried out in Ta ampoules (30 mm length, 9.5 mm diameter, 0.5 mm wall thickness), which were arc-welded under a pressure of 1 bar of purified argon. The crucible holder was cooled with water during this procedure to avoid chemical reactions during welding. For the synthesis of Ca[LiAlN₂] the starting materials LiN₃ (23 mg, 0.47 mmol, synthesized according to the method by Fair et al.)^[30] and LiAlH₄ (27 mg, 0.70 mmol, Acros, 95 %) were mixed in an agate mortar, filled into a tantalum ampoule, and covered with Li

(16.2 mg, 2.33 mmol, Aldrich, 99.9 %) and Ca (28 mg, 0.70 mmol, Aldrich, 99.99 %) in a glovebox. The closed crucible was placed into a silica tube under argon and positioned in the middle of a tube furnace. The temperature was raised to 900 °C (rate 5 °Cmin⁻¹), maintained for 24 h, subsequently cooled down to 500 °C (rate 0.12 °Cmin⁻¹), and finally quenched to room temperature by switching off the furnace. From the inhomogeneous product, colorless platelet-shaped single crystals of Ca[LiAlN₂] were isolated under a microscope, which was integrated in a glovebox, enclosed in glass capillaries, and sealed under argon. Addition of 1 mol-% Eu(NH₂)₂ (2 mg, 0.01 mmol synthesized according to the method by Zeuner et al.)^[31] to the reaction mixture led to the formation of nonluminescent blue Ca[LiAlN₂]:Eu²⁺ crystals. The preparation of phase-pure powder samples was possible by collecting single crystals, pulverizing them in an agate mortar, and enclosing them in a glass capillary. Further details of the crystal structure investigations may be obtained from the Fachinformationszentrum Karlsruhe, 76344 Eggenstein-Leopoldshafen, Germany (fax: +49-7247-808-666; e-mail: crysdata@fiz-karlsruhe.de), on quoting the depository number CSD-424911.

3.1.4.2 *Single-Crystal X-ray Diffraction*

Single-crystal diffraction data were collected on a STOE IPDS I diffractometer (Mo-K α radiation, graphite monochromator). A semiempirical absorption correction using the program XPREP^[32] was applied. The crystal structure was solved by using direct methods with SHELXS.^[33] The refinement of the structure was carried out by the least-squares method using SHELXL.^[33]

3.1.4.3 *Powder X-ray Diffraction*

Powder-diffraction data were collected on a STOE STADI P diffractometer [Cu-K α ₁ radiation, Ge(111) monochromator, position-sensitive detector] in Debye–Scherrer geometry. Simulations of Bragg data were performed using the WinXPOW program package^[34] on the basis of the single-crystal structural data. Rietveld refinement was carried out using the TOPAS package.^[35]

3.1.4.4 *Electron Microscopy*

The chemical composition was confirmed by energy-dispersive X-ray spectroscopy (EDX) using a JSM-6500F scanning microscope (Jeol) equipped with a Si/Li EDX detector 7418 (Oxford Instruments). An atomic ratio of Ca/Al/N 1:1:2.4 results from the EDX analysis and agrees with the composition Ca[LiAlN₂], whereas Li is not determinable by EDX.

3.1.5 References

- [1] M. Zeuner, S. Pagano, W. Schnick, *Angew. Chem. Int. Ed.* **2011**, *50*, 7754.
- [2] H. Huppertz, W. Schnick, *Z. Anorg. Allg. Chem.* **1997**, *623*, 212.
- [3] R. Kniep, *Pure Appl. Chem.* **1997**, *69*, 185.
- [4] R. Niewa, F. J. DiSalvo, *Chem. Mater.* **1998**, *10*, 2733.
- [5] R. Niewa, H. Jacobs, *Chem. Rev* **1996**, *96*, 2053.
- [6] M. Ludwig, J. Jaeger, R. Niewa, R. Kniep, *Inorg. Chem.* **2000**, *39*, 5909.
- [7] S. J. Clarke, F. J. DiSalvo, *Inorg. Chem.* **1997**, *36*, 1143.
- [8] M. Ludwig, R. Niewa, R. Kniep, *Z. Naturforsch. B: Chem. Sci.* **1999**, *54*, 461.
- [9] S. Pagano, S. Lupart, S. Schmiechen, W. Schnick, *Z. Anorg. Allg. Chem.* **2010**, *636*, 1907.
- [10] R. Juza, F. Hund, *Z. Anorg. Allg. Chem.* **1948**, *257*, 13.
- [11] M. S. Bailey, F. J. DiSalvo, *J. Alloys Compd.* **2006**, *417*, 50.
- [12] W. Blase, G. Cordier, M. Ludwig, R. Kniep, *Z. Naturforsch. B: Chem. Sci.* **1994**, *49*, 501.
- [13] Z. A. Gál, P.M. Mallinson, H. J. Orchard, S.J. Clarke, *J. Inorg. Chem.* **2004**, *43*, 3998.
- [14] V. Bachmann, C. Ronda, O. Oeckler, W. Schnick, A. Meijerink, *Chem. Mater.* **2009**, *21*, 316.
- [15] C. Hecht, F. Stadler, P. J. Schmidt, J. Schmedt auf der Guenne, V. Baumann, W. Schnick, *Chem. Mater.* **2009**, *21*, 1595.
- [16] J. A. Kechele, C. Hecht, O. Oeckler, J. Schmedt auf der Guenne, P.J. Schmidt, W. Schnick, *Chem. Mater.* **2009**, *21*, 1288.
- [17] O. Oeckler, J.A. Kechele, H. Koss, P. J. Schmidt, W. Schnick, *Chem. Eur. J.* **2009**, *15*, 5311.
- [18] F. Liebau, *Structural Chemistry of Silicates*, Springer Verlag, Berlin, **1985**.
- [19] S. Pagano, M. Zeuner, S. Hug, W. Schnick, *Eur. J. Inorg. Chem.* **2009**, 1579.
- [20] H. Höpfe, *Doctoral thesis*, Ludwig-Maximilian-University Munich, **2003**.
- [21] F. Ottinger, R. Nesper, *Z. Anorg. Allg. Chem.* **2005**, *631*, 1597.
- [22] R. D. Shannon, *Acta Crystallogr. Sect. A: Found. Crystallogr.* **1976**, *32*, 751.
- [23] R. Hoppe, *Angew. Chem. Int. Ed. Engl.* **1970**, *9*, 25.
- [24] R. Hoppe, R. Homann, *Z. Anorg. Allg. Chem.* **1970**, *379*, 193.
- [25] R. Hübenthal, MAPLE, Programm zur Berechnung des Madelunganteils der Gitterenergie, **1993**, version 4, University of Gießen, Germany.
- [26] K. Köllisch, *Doctoral thesis*, Ludwig-Maximilian-University Munich, **2001**.

- [27] A. Rabenau, H. Schulz, *J. Less-Common Met.* **1976**, *50*, 155.
- [28] Y. Laurent, J. Lang, M. T. le Bihan, *Acta Crystallogr., Sect. B: Struct. Sci.* **1968**, *24*, 494.
- [29] W. Paszkowicz, S. Podsiadlo, R. Minikayev, *J. Alloys Compd.* **2004**, *382*, 100.
- [30] H. D. Fair, R. F. Walker, *Energetic Materials 1, Physics and Chemistry of the Inorganic Azides*, New York, London, **1977**.
- [31] M. Zeuner, F. Hintze, W. Schnick, *Chem. Mater.* **2009**, *21*, 336.
- [32] G. M. Sheldrick, XPREP, Data Preperation & Reciprocal Space Exploration, **1996**, v6.12, Siemens Analytical X-ray Instruments.
- [33] G. M. Sheldrick, *Acta Crystallogr., Sect. A: Found. Crystallogr.* **2008**, *64*, 112.
- [34] Stoe & Cie GmbH, *WINXPOW* - Program for powder data handling, **2007**, v2.21, Darmstadt, Germany.
- [35] A. Coelho, TOPAS - Academic **2007**, Brisbane: Coelho Software.

3.2 Group (III) Nitrides $M[\text{Mg}_2\text{Al}_2\text{N}_4]$ ($M = \text{Ca}, \text{Sr}, \text{Ba}, \text{Eu}$) and $\text{Ba}[\text{Mg}_2\text{Ga}_2\text{N}_4]$ - Structural Relation and Nontypical Luminescence Properties of Eu^{2+} Doped Samples

published in: *Chem. Mater.* **2014**, *26*, 6113-6119

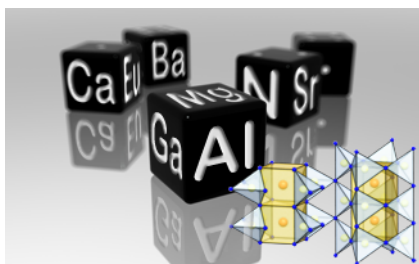
authors: Philipp Pust, Frauke Hintze, Cora Hecht, Volker Weiler, Andreas Locher, Daniela Zitnanska, Sascha Harm, Detlef Wiechert, Peter J. Schmidt and Wolfgang Schnick

DOI: 10.1021/cm502280p

Copyright © 2014 American Chemical Society

<http://pubs.acs.org/doi/abs/10.1021/cm502280p>

Abstract. The isotopic nitridomagnesoaluminates $M[\text{Mg}_2\text{Al}_2\text{N}_4]$ ($M = \text{Ca}, \text{Sr}, \text{Ba}, \text{Eu}$) as well as a novel nitridomagnesogallate $\text{Ba}[\text{Mg}_2\text{Ga}_2\text{N}_4]$ have been synthesized by high-temperature reactions in arc-welded tantalum ampules. The crystal structures were solved and refined using single-crystal X-ray diffraction or powder X-ray diffraction data, respectively. All compounds crystallize in the UCr_4C_4 -structure type (space group $I4/m$ (no. 87), $Z = 2$, $\text{Ca}[\text{Mg}_2\text{Al}_2\text{N}_4]$: $a = 8.0655(11)$, $c = 3.2857(7)$ Å, $wR2 = 0.085$ $\text{Sr}[\text{Mg}_2\text{Al}_2\text{N}_4]$: $a = 8.1008(11)$, $c = 3.3269(7)$ Å, $wR2 = 0.084$; $\text{Eu}[\text{Mg}_2\text{Al}_2\text{N}_4]$: $a = 8.1539(12)$, $c = 3.3430(7)$ Å, $wR2 = 0.033$; $\text{Ba}[\text{Mg}_2\text{Al}_2\text{N}_4]$: $a = 8.2602(9)$, $c = 3.43198(19)$ Å, $wRp = 0.031$; $\text{Ba}[\text{Mg}_2\text{Ga}_2\text{N}_4]$: $a = 8.3654(12)$, $c = 3.4411(7)$ Å, $wR2 = 0.031$) forming highly condensed anionic networks of disordered $(\text{Al}/\text{Mg})\text{N}_4$ and $(\text{Ga}/\text{Mg})\text{N}_4$ units, connected to each other by common edges and corners. The M^{2+} site is centered in *vierer* ring channels along $[001]$ and coordinated in a cuboidal surrounding by N. Eu^{2+} doped samples of $M[\text{Mg}_2\text{Al}_2\text{N}_4]$ ($M = \text{Ca}, \text{Sr}, \text{Ba}$) exhibit nontypical luminescence properties including trapped exciton emission in the red spectral region. These compounds widen the group of novel red-emitting materials such as



$\text{Ca}[\text{LiAl}_3\text{N}_4]:\text{Eu}^{2+}$, $\text{Sr}[\text{LiAl}_3\text{N}_4]:\text{Eu}^{2+}$ or $\text{Sr}[\text{Mg}_3\text{SiN}_4]:\text{Eu}^{2+}$. Therefore, deep discussion of the observed anomalous luminescence is essential to understand the correlations between all these materials, which are fundamental to design narrow band luminescence of Eu^{2+} systems.

3.2.1 Introduction

Phosphor-converted light-emitting diodes (pc-LEDs) are expected to be the light sources of the future. As the conversion of electric energy to visible light is much more efficient in pc-LEDs compared to classical light bulbs, the former are expected to be the most relevant candidates for the replacement of energy wasting incandescent light bulbs.^[1-4]

Current pc-LED solutions either suffer from lacking intensity in the red spectral region, which limits color rendition properties, or employ red phosphors, which emit a substantial portion of the radiation outside the human eye sensitivity, limiting the luminous efficacy (efficiency weighted by eye sensitivity). The enhancement of both parameters, color rendition (CRI) and luminous efficacy of a white pc-LED, critically depend on the properties (emission maximum and width) of the red-emitting phosphor material.^[5] Consequently, in order to improve the efficacy (lm/W), without compromising the CRI, there is a strong demand for novel red emitting phosphor materials with superior luminescence properties.^[6,7] Thereby, a number of multinary nitrides of group III and IV elements emerged as attractive host lattices for doping with Eu^{2+} , resulting in interesting luminescence properties. Due to parity allowed $4f^6(^7F)5d^1 \rightarrow 4f^7(^8S_{7/2})$ transitions intense emission can be observed throughout the entire visible spectrum.

Especially the material classes of nitridosilicates, nitridoalumosilicates, and related SiAlONs came into the focus of extensive investigations. In the meantime, several representatives proved to be excellent candidates for application in pc-LEDs.^[8]

Recently, a novel group of structurally related phosphor materials was investigated. We could demonstrate that the novel nitridomagnesosilicate $\text{Sr}[\text{Mg}_3\text{SiN}_4]:\text{Eu}^{2+}$ represents the most narrow red-emitting Eu^{2+} -doped phosphor material described in literature so far ($\lambda_{\text{em}} = 615 \text{ nm}$, FWHM $\sim 1170 \text{ cm}^{-1}$).^[9] The isotypic nitridolithoaluminate $\text{Ca}[\text{LiAl}_3\text{N}_4]:\text{Eu}^{2+}$ also exhibits an intense, for a Eu^{2+} -doped material exceptionally narrow, red emission.^[10] Both compounds crystallize in the $\text{Na}[\text{Li}_3\text{SiO}_4]$ structure type,^[11] which exhibits specific structural features that we believe are beneficial for narrow band red emission. Especially, the ordered and rigid host lattice and the single heavy atom site should be mentioned in this respect.

The isoelectronic compound $\text{Sr}[\text{LiAl}_3\text{N}_4]:\text{Eu}^{2+}$, which crystallizes in the $\text{Cs}[\text{Na}_3\text{PbO}_4]$ structure type, could demonstrate the high potential of such materials for industrial application.^[12] The employment of such a narrow band red-emitting system helps to increase luminous efficacy of a demonstrator pc-LED by 14% ($R_a8 = 91$, $R9 = 57$) compared to a

commercially available high CRI-LED. Therefore, we started a broadband screening of these as well as related structure types, to obtain new compound classes with adequate luminescence properties and to understand structure-property relations in more detail.

In this contribution, the novel nitridomagnesoaluminates $\text{Ca}[\text{Mg}_2\text{Al}_2\text{N}_4]$, $\text{Sr}[\text{Mg}_2\text{Al}_2\text{N}_4]$, $\text{Eu}[\text{Mg}_2\text{Al}_2\text{N}_4]$ and $\text{Ba}[\text{Mg}_2\text{Al}_2\text{N}_4]$ are presented as well as the novel nitridomagnesoaluminate $\text{Ba}[\text{Mg}_2\text{Ga}_2\text{N}_4]$. All five quaternary compounds are isotypic crystallizing in the UCr_4C_4 -structure type. Detailed investigations of the crystal structures as well as the nontypical luminescence properties of Eu^{2+} doped samples are reported.

3.2.2 Experimental Section

3.2.2.1 Synthesis

For synthesis of $M[\text{Mg}_2\text{Al}_2\text{N}_4]$ ($M = \text{Ca}, \text{Sr}, \text{Ba}, \text{Eu}$) and $\text{Ba}[\text{Mg}_2\text{Ga}_2\text{N}_4]$ different approaches have been employed. All procedures were performed under inert gas atmosphere (Ar) in glove boxes (Unilab, MBraun, Garching; $\text{O}_2 < 1$ ppm, $\text{H}_2\text{O} < 1$ ppm).

$\text{Ba}[\text{Mg}_2\text{Ga}_2\text{N}_4]$ was synthesized starting from mixtures of the respective metals and NaN_3 as nitrogen source in a sodium melt. Typically, 0.31 mmol NaN_3 (20.1 mg, Acros, 99%), 0.064 mmol Mg (1.53 mg, Alfa Aesar, 99.9%), 0.245 mmol Ga (17.1 mg, Sigma-Aldrich, 99.99%) and 1.95 mmol Na (44.9 mg, Sigma-Aldrich, 99.95%) were used. Furthermore, 0.063 mmol Ba (8.65 mg, Sigma Aldrich, 99.99%) was added. For luminescence investigations small amounts of EuF_3 (Sigma Aldrich 99.95%) were added as dopand. The starting materials were filled into Ta ampoules (30 mm length, 10 mm diameter, 0.5 mm wall thickness). The ampoules were welded shut under Ar atmosphere and placed in quartz tubes under vacuum to prevent oxidation of the ampoules. The respective reaction mixtures were heated to 760 °C in a tube furnace at 50 °/h, maintained at that temperature for 48 h and then cooled down to 200 °C at a rate of 3.4 °/h. After reaction, the ampoules were opened in a glove box and Na was separated from the reaction products by vacuum sublimation at 320 °C for 10 h.

To obtain single crystals of $M[\text{Mg}_2\text{Al}_2\text{N}_4]$ ($M = \text{Ca}, \text{Sr}, \text{Ba}, \text{Eu}$) a faster reaction compared to the above-mentioned metal route was used. Herein, the metal fluorides together with Mg_3N_2 were used. To capture the F⁻-ions, syntheses were performed in a Li-melt with LiN_3 as the nitrogen-source. Typically, 0.3 mmol MF_2 ($M = \text{Ca}, \text{Sr}, \text{Ba}$; all from Sigma-Aldrich, 99.99%) or EuF_3 (Sigma-Aldrich 99.95%), 0.6 mmol AlF_3 (50.4 mg, Sigma-Aldrich, 99.95%), 0.20 mmol Mg_3N_2 (20.2 mg, Sigma-Aldrich, 99.5%), 0.30 mmol LiN_3 (14.7 mg, synthesized

according to *Fair et al.*),^[13] and 3.0 mmol Li (20.8 mg, Sigma Aldrich, 99.9%) were added. For luminescence investigations of the alkaline-earth compounds, small amounts of EuF_3 were added as dopand. The respective mixtures of starting materials were filled into Ta ampules and sealed in a water-cooled arc-welding device under argon. The ampules were placed in silica tubes and heated in tube furnaces to 900 °C at 200 °/h, maintained at that temperature for 24 h, and slowly cooled down to 500 °C at a rate of 10 °/h. Subsequently, the furnace was turned off and the Ta-ampules were opened under inert gas atmosphere in a glove box.

Bulk samples of $M[\text{Mg}_2\text{Al}_2\text{N}_4]$ ($M = \text{Ca}, \text{Sr}, \text{Ba}$) were synthesized in a hot isostatic press under nitrogen pressure (7500 PSI) at 1450 °C. Here, stoichiometric mixtures of Mg_3N_2 (Sigma-Aldrich, 99.5%), AlN (Tokuyama, 99%) and $M\text{H}_2$ ($M = \text{Sr}, \text{Ba}$; both from Cerac, 99.5%) were used as starting materials.

3.2.2.2 *Electron Microscopy*

Electron microscopy was performed on a JEOL JSM 6500 F scanning electron microscope (SEM) equipped with a field emission gun at a maximum acceleration voltage of 30 kV. Synthesized samples were prepared on adhesive conductive carbon pads and coated with a conductive carbon film. The chemical compositions were confirmed by EDX spectroscopy (Oxford Instruments, model 7418), each spectrum recorded on an area limited to one crystal face to avoid influence of possible contaminating phases.

3.2.2.3 *Single-Crystal X-ray Diffraction*

The crystal structures of $M[\text{Mg}_2\text{Al}_2\text{N}_4]$ ($M = \text{Ca}, \text{Sr}, \text{Eu}$) and $\text{Ba}[\text{Mg}_2\text{Ga}_2\text{N}_4]$ were determined by single-crystal X-ray diffraction on a Nonius Kappa-CCD diffractometer with graded multilayer X-ray optics and Mo- $K\alpha$ radiation ($\lambda = 0.71073 \text{ \AA}$). Absorption correction for $\text{Eu}[\text{Mg}_2\text{Al}_2\text{N}_4]$ and $\text{Ba}[\text{Mg}_2\text{Ga}_2\text{N}_4]$ was carried out by means of WinGX.^[14] The structures were solved by direct methods implemented in SHELXS-97.^[15] Crystal structure refinements were carried out with anisotropic displacement parameters for all atoms by full-matrix least-squares calculation on F^2 using SHELXL-97.^[15] The corresponding single crystals were prepared in capillaries and checked for quality on a Buerger precession camera.

More details of the structure investigations are available from the Fachinformationszentrum Karlsruhe, D-76344 Eggenstein Leopoldshafen, Germany (fax: +49-7247-808-666; Email: crysdata@fiz.karlsruhe.de) on quoting the depository numbers CSD-425319 ($\text{Ca}[\text{Mg}_2\text{Al}_2\text{N}_4]$), CSD-425321 ($\text{Sr}[\text{Mg}_2\text{Al}_2\text{N}_4]$), CSD-425320 ($\text{Eu}[\text{Mg}_2\text{Al}_2\text{N}_4]$), CSD-427065 ($\text{Ba}[\text{Mg}_2\text{Al}_2\text{N}_4]$), and CSD-425318 ($\text{Ba}[\text{Mg}_2\text{Ga}_2\text{N}_4]$).

3.2.2.4 Powder X-ray Diffraction

Powder X-ray diffraction data were collected on a STOE STADI P diffractometer (Cu $K\alpha_1$ radiation, Ge(111) monochromator, position sensitive detector) in Debye-Scherrer geometry or alternatively on a Huber G670 Guinier imaging plate Diffractometer (Cu- $K\alpha_1$ radiation, Ge(111) monochromator). Simulations of Bragg intensities were performed using the WinXPOW program package^[16] on the basis of the single-crystal data. Rietveld refinement was carried out using the TOPAS package.^[17] The crystal structure of $\text{Ba}[\text{Mg}_2\text{Al}_2\text{N}_4]$ was solved and refined from X-ray powder data starting from the crystallographic data of isotypic $\text{Sr}[\text{Mg}_2\text{Al}_2\text{N}_4]$.

3.2.2.5 UV/Vis Spectroscopy

Reflectance spectra were recorded on an Edinburgh Photonics FLS920-s spectrometer with a Xe900 450 W arc lamp (Czerny-Turner monochromator with three gratings, single-photon-photomultiplier detector). The spectra were measured between 250 and 780 nm with 5 nm step size.

3.2.2.6 Luminescence

Luminescence properties of single crystals were investigated using a luminescence microscope consisting of a HORIBA Fluorimax4 Spectrofluorimeter-system which is attached to an Olympus BX51 microscope via fiber optics. Photoluminescence measurements on powder samples in PTFE sample holders were carried out using an in-house built system based on a 5.3" integrating sphere and a spectrofluorimeter equipped with a 150 W Xe lamp, two 500 mm Czerny-Turner monochromators, 1800 1/mm lattices, and 250/500 nm lamps, with a spectral range from 230 to 820 nm. Low-temperature emission spectra of powder samples were recorded with an Ocean Optics HR2000 + ES spectrometer (2.048 pixels, grating UA (200-1.100 nm), slit 50) with the samples mounted in a closed-cycle He cryostat.

The excitation wavelength was chosen to 440 nm with a spectral width of 10 nm. The emission spectra were collected in the wavelength interval between 470 and 780 nm with 2 nm step size. Excitation spectra were measured in the wavelength range between 350 and 575 nm (for $M[\text{Mg}_2\text{Al}_2\text{N}_4]:\text{Eu}^{2+}$ with $M = \text{Ca}, \text{Sr}$) or 615 nm (for $\text{Ba}[\text{Mg}_2\text{Al}_2\text{N}_4]:\text{Eu}^{2+}$) with 2 nm step size.

3.2.3 Results and Discussion

3.2.3.1 Synthesis and Chemical Analysis

With the synthesis methods described above a series of new compounds was obtained, namely $\text{Ca}[\text{Mg}_2\text{Al}_2\text{N}_4]$, $\text{Sr}[\text{Mg}_2\text{Al}_2\text{N}_4]$, $\text{Ba}[\text{Mg}_2\text{Al}_2\text{N}_4]$, $\text{Eu}[\text{Mg}_2\text{Al}_2\text{N}_4]$, and $\text{Ba}[\text{Mg}_2\text{Ga}_2\text{N}_4]$.

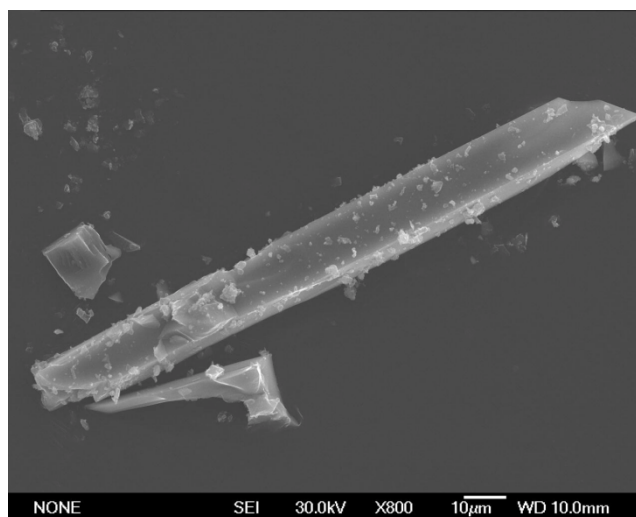


Figure 1. SEM image of rod-shaped $\text{Sr}[\text{Mg}_2\text{Al}_2\text{N}_4]$ single crystal.

The presented Mg containing nitridoaluminates are to the best of our knowledge the first of their kind. However, since Mg^{2+} and $\text{Al}^{3+}/\text{Ga}^{3+}$ are both part of the tetrahedral network, classification as nitridomagnesoaluminates and -gallates, according to *Hoppe*, is more appropriate.^[11] All compounds were obtained as rod-shaped crystals. A SEM image of $\text{Sr}[\text{Mg}_2\text{Al}_2\text{N}_4]$ is shown exemplarily in Figure 1. Table 1 summarizes the average compositions obtained from EDX-analysis (three measurements on different crystals), normalized according to the respective heavy atom. All measurements are in good accordance with the expected sum formulas.

Table 1. EDX Analyses.

EDX analysis	sum formula
$\text{Ca}_{1.0}\text{Mg}_{1.9}\text{Al}_{1.9}\text{N}_{4.6}$	$\text{CaMg}_2\text{Al}_2\text{N}_4$
$\text{Sr}_{1.0}\text{Mg}_{2.0}\text{Al}_{2.3}\text{N}_{4.6}$	$\text{SrMg}_2\text{Al}_2\text{N}_4$
$\text{Ba}_{1.0}\text{Mg}_{2.3}\text{Al}_{2.0}\text{N}_5$	$\text{BaMg}_2\text{Al}_2\text{N}_4$
$\text{Eu}_{1.0}\text{Mg}_{2.1}\text{Al}_{2.1}\text{N}_{5.1}$	$\text{EuMg}_2\text{Al}_2\text{N}_4$
$\text{Ba}_{1.0}\text{Mg}_{2.0}\text{Ga}_{2.0}\text{N}_{4.7}$	$\text{BaMg}_2\text{Ga}_2\text{N}_4$

As all compounds are isotypic; only $\text{Sr}[\text{Mg}_2\text{Al}_2\text{N}_4]$ will be described in the following sections for reasons of clarity. Further crystallographic information on remaining compounds is available in the Supporting Information.

3.2.3.2 Single-Crystal Structure Analysis

The crystal structure of $\text{Sr}[\text{Mg}_2\text{Al}_2\text{N}_4]$ was solved and refined in the tetragonal space group $I4/m$ (no. 87) with $a = 8.1008(11)$ and $c = 3.3269(7)$ Å. The crystallographic data of $\text{Sr}[\text{Mg}_2\text{Al}_2\text{N}_4]$ are listed in Table 2, the atomic coordinates and displacement parameters are given in Table 3.

Table 2. Crystallographic Data of $\text{Sr}[\text{Mg}_2\text{Al}_2\text{N}_4]$.

formula	$\text{Sr}[\text{Mg}_2\text{Al}_2\text{N}_4]$
crystal system	tetragonal
space group	$I4/m$ (no. 87)
lattice params. (Å)	$a = b = 8.1008(11), c = 3.3269(7)$
cell vol. (Å ³)	218.32(6)
formula units / cell	2
$\rho_{\text{calcd.}}$ (g·cm ⁻³)	3.75
μ (mm ⁻¹)	12.886
T (K)	293(2)
F(000)	232
diffractometer	κ CCD
radiation (Å), monochromator	Mo-K α ($\lambda = 0.71073$), graphite
absorption correction	multi-scan
θ range (deg)	3.5-39.2
index ranges	$-14 \leq h \leq 14$ $-14 \leq k \leq 14$ $-5 \leq l \leq 5$
independent reflections	365 ($R_{\text{int}} = 0.0451$)
refined params.	16
goodness of fit	1.165
$R1$ (all data); $R1$ ($F^2 > 2\sigma(F^2)$)	0.0313; 0.0309
$wR2$ (all data); $wR2$ ($F^2 > 2\sigma(F^2)$)	0.0838; 0.0834
max/min residual electron density (e·Å ⁻³)	1.74 / -1.57

$\text{Sr}[\text{Mg}_2\text{Al}_2\text{N}_4]$ crystallizes in the UCr_4C_4 -structure type^[18] forming a three-dimensional network of (Mg/Al) N_4 -tetrahedra. It is structurally related to the compounds $\text{Ca}[\text{LiAl}_3\text{N}_4]$ and

$\text{Sr}[\text{LiAl}_3\text{N}_4]$.^[10,12] The framework contains strands of edge-sharing tetrahedra which are connected to each other forming *vierer* rings^[19] along [001]. In this network structure only ammonium-type $\text{N}^{[4]}$ atoms connecting four tetrahedral centers (Mg/Al) occur (see Figure 2).

Table 3. Atomic Coordinates and Equivalent Isotropic Displacement Parameters (\AA^2) of $\text{Sr}[\text{Mg}_2\text{Al}_2\text{N}_4]$ and Site Occupancies, Standard Deviations in Parentheses.

atom (Wyck.)	x	y	z	U_{eq}	SOF
Sr ($2a$)	0	0	0	0.01357(18)	1
Al ($8h$)	0.18393(14)	0.36311(12)	0	0.0143(2)	0.5
Mg ($8h$)	0.18393(14)	0.36311(12)	0	0.0143(2)	0.5
N ($8h$)	0.4035(4)	0.2370(5)	0	0.0222(6)	1

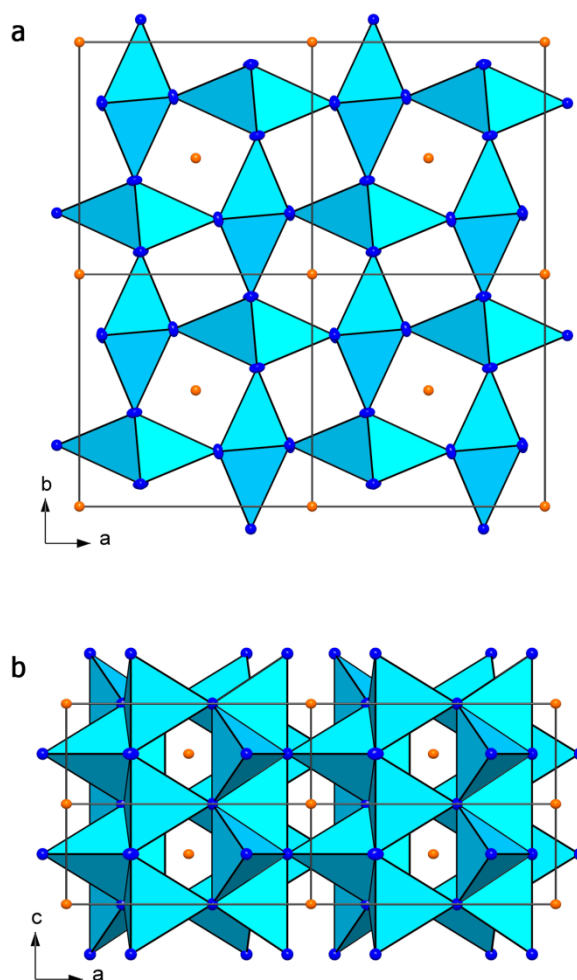


Figure 2. Crystal structure of $\text{Sr}[\text{Mg}_2\text{Al}_2\text{N}_4]$. (Mg/Al) N_4 -tetrahedra blue, nitrogen atoms dark blue and Sr^{2+} -ions orange. (a) Viewing direction along [001]; (b) viewing direction along [010].

The degree of condensation (i.e., the atomic ratio (Al/Mg):N) in this compound is $\kappa = 1$, corresponding to the value in aluminum nitride AlN. Sr^{2+} -ions are located in every second

vierer-ring channel, centered in face-sharing cuboidal polyhedra (see Figure 3) with a distance Sr-N of 2.818(2) Å. Compared to the sum of the ionic radii,^[20] a slight elongation is observed. An analogous elongation of this distance is also known from all other compounds we report here and was found in $\text{Sr}[\text{Mg}_2\text{Ga}_2\text{N}_4]$ (Sr-N: 2.855(2) Å) as well crystallizing in the same structure type.^[21] ($\text{Mg}^{2+}/\text{Al}^{3+}$)-atoms on the tetrahedrally coordinated site are statistically disordered on Wyckoff position $8h$. The distances (Mg/Al)-N vary between 1.94 and 2.05 Å. Comparable values for Al-N and Mg-N distances appear in the structures of $\text{Sr}_3\text{Al}_2\text{N}_4$ (Al-N: 1.86-1.96 Å) and CaMg_2N_2 (Mg-N: 2.13-2.30 Å),^[22, 23] whereas the reported bond lengths (Mg/Al)-N in $\text{Sr}[\text{Mg}_2\text{Al}_2\text{N}_4]$ correspond with the average of these distances. For the reported Ga containing compound similar results were obtained. Although Ga^{3+} and Mg^{2+} differ significantly in their X-ray scattering intensity no ordering of the atoms on tetrahedral position was observed and the elemental distribution was confirmed by EDX-analysis.

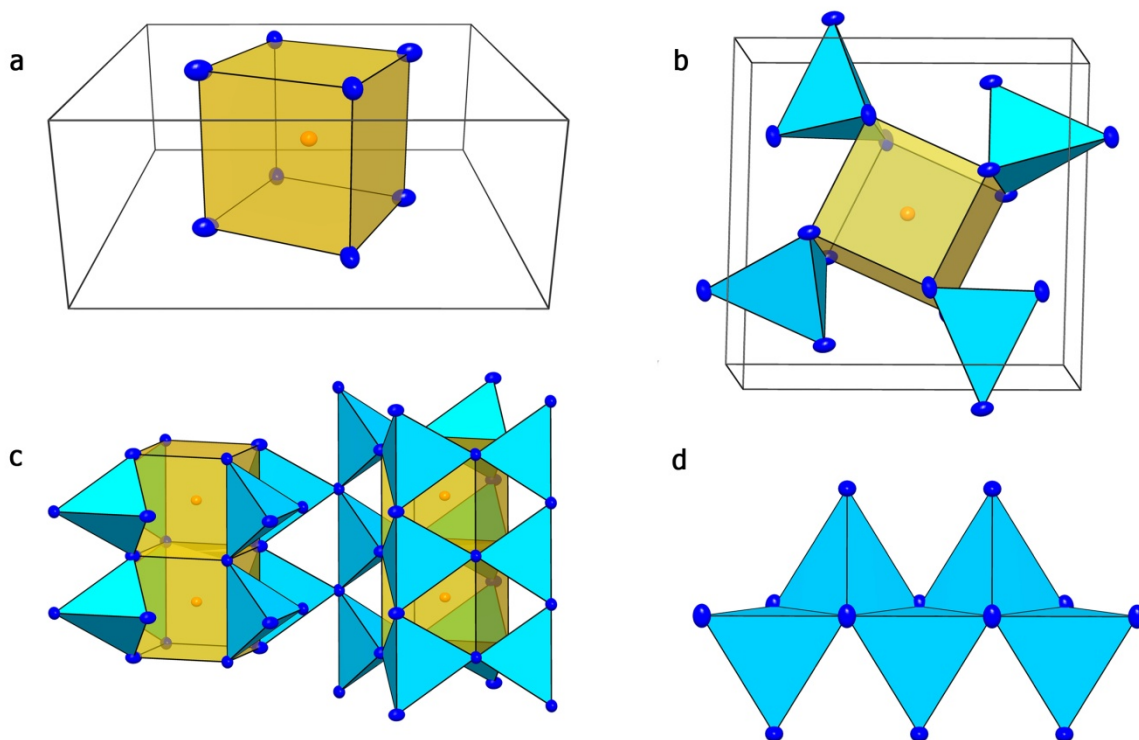


Figure 3. Structural details of $\text{Sr}[\text{Mg}_2\text{Al}_2\text{N}_4]$; all atoms are shown as ellipsoids with 50% probability. (a) Cuboid-like coordination of Sr^{2+} (orange) by nitrogen atoms (blue); (b) coordination of the Sr^{2+} centered polyhedra by (Mg/Al) N_4 -tetrahedra (blue); (c) structure assembly and conjunction of (Mg/Al) N_4 -tetrahedra (blue); (d) edge sharing of (Mg/Al) N_4 -tetrahedra strands (blue).

Rietveld refinement of powder-diffraction data validates the structure of $\text{Sr}[\text{Mg}_2\text{Al}_2\text{N}_4]$ obtained from single-crystal X-ray diffraction data (see Figure 4 and Supporting Information Table S3). However, besides $\text{Sr}[\text{Mg}_2\text{Al}_2\text{N}_4]$ small amounts of AlN can be found as side

phase. The insert in Figure 4 shows a comparison of the two most intensive reflections of $M[\text{Mg}_2\text{Al}_2\text{N}_4]$ ($M = \text{Ca}, \text{Sr}, \text{Ba}$). The ligand field increases from $M = \text{Ba}$ to Ca due to a decrease of the lattice constants and shortening of the M–N contacts (see insert Figure 4). Reflectance measurements of nominally undoped powders (see Figure 5) show onsets of the fundamental absorption edge of the host lattices in the 3.65–3.8 eV range.

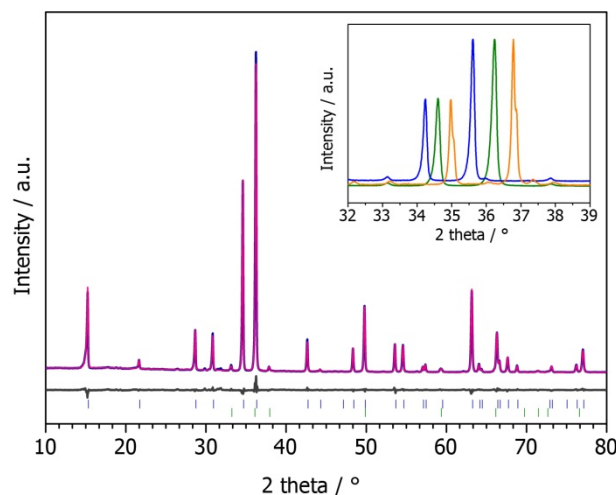


Figure 4. Rietveld refinement ($R_p = 0.0305$, $wR_p = 0.0407$; 14384 data points) of X-ray powder-diffraction pattern of $\text{Sr}[\text{Mg}_2\text{Al}_2\text{N}_4]$ with measured histogram (blue line), calculated pattern (red line), difference curve (gray line) and positions of reflections (blue bars). Positions of AlN reflections (~ 10 wt%, green bars). Insert: Comparison of the two most intensive reflections of $\text{Ca}[\text{Mg}_2\text{Al}_2\text{N}_4]$ orange, $\text{Sr}[\text{Mg}_2\text{Al}_2\text{N}_4]$ green and $\text{Ba}[\text{Mg}_2\text{Al}_2\text{N}_4]$ blue.

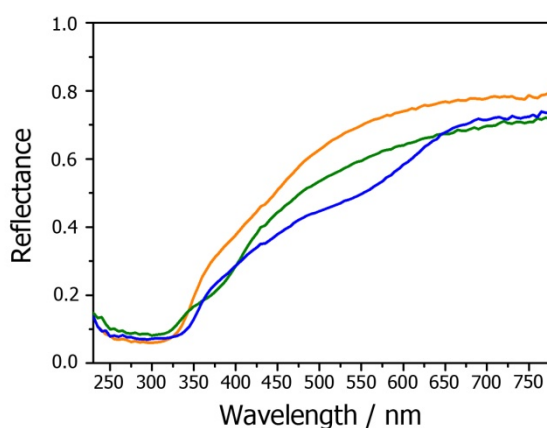


Figure 5. Reflectance spectra for nondoped powders of $\text{Ca}[\text{Mg}_2\text{Al}_2\text{N}_4]$ orange, $\text{Sr}[\text{Mg}_2\text{Al}_2\text{N}_4]$ green and $\text{Ba}[\text{Mg}_2\text{Al}_2\text{N}_4]$ blue.

3.2.3.3 Luminescence

Eu^{2+} -doped samples of $M[\text{Mg}_2\text{Al}_2\text{N}_4]$ ($M = \text{Ca}, \text{Sr}, \text{Ba}$) and $\text{Ba}[\text{Mg}_2\text{Ga}_2\text{N}_4]$ show a red body color and red luminescence is observed under irradiation with UV to green light.

Luminescence investigations were either performed on single crystals in sealed glass capillaries (for $\text{Ba}[\text{Mg}_2\text{Ga}_2\text{N}_4]:\text{Eu}^{2+}$) or on bulk material on PTFE sample holders.

With a nominal doping level of 2% $\text{Ba}[\text{Mg}_2\text{Ga}_2\text{N}_4]:\text{Eu}^{2+}$ yields an emission band peaking at $\lambda_{\text{em}} = 649 \text{ nm}$ with full width at half-maximum (FWHM) of $\sim 2168 \text{ cm}^{-1}$ when excited at 440 nm.

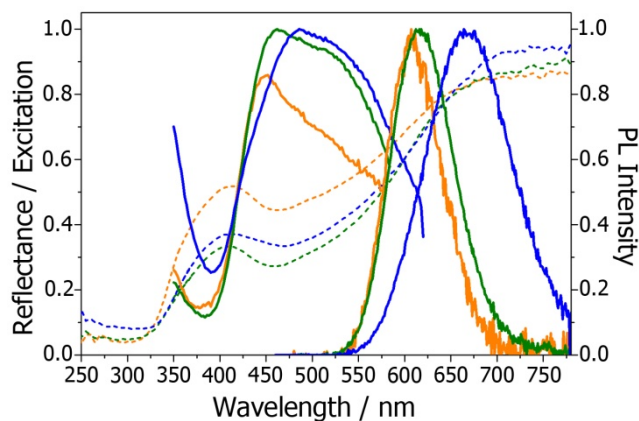


Figure 6. Excitation, reflectance (dashed curves) and emission ($\lambda_{\text{exc}} = 440 \text{ nm}$) spectra of $M[\text{Mg}_2\text{Al}_2\text{N}_4]:\text{Eu}^{2+}$ (0.1%) ($M = \text{Ca}, \text{Sr}, \text{Ba}$) bulk samples at room temperature. $\text{Ca}[\text{Mg}_2\text{Al}_2\text{N}_4]:\text{Eu}^{2+}$ orange, $\text{Sr}[\text{Mg}_2\text{Al}_2\text{N}_4]:\text{Eu}^{2+}$ green, and $\text{Ba}[\text{Mg}_2\text{Al}_2\text{N}_4]:\text{Eu}^{2+}$ blue.

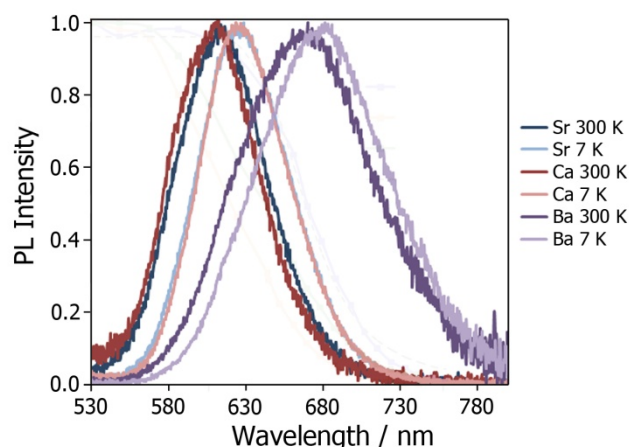


Figure 7. Normalized emission spectra for $T = 300 \text{ K}$ and $T = 7 \text{ K}$ of $M[\text{Mg}_2\text{Al}_2\text{N}_4]:\text{Eu}^{2+}$ (0.1%, $M = \text{Ca}, \text{Sr}, \text{Ba}$). The figure legend gives information about the assignment of the curves depending on M and the respective temperature.

Figure 7 shows excitation, emission and reflectance spectra of $M[\text{Mg}_2\text{Al}_2\text{N}_4]:\text{Eu}^{2+}$ (0.1%, $M = \text{Ca}, \text{Sr}, \text{Ba}$) powder samples. Excitation and reflectance spectra show very similar shapes for all samples with excitation maxima in the 450 – 480 nm range. The energetic position of the lowest lying absorption band of $\text{Eu}(\text{II})$ is estimated to be located at $\sim 540 \text{ nm}$. The strong

increase in excitability at wavelengths < 350 nm is due to absorption of the host lattice in accordance with the absorption properties of the non doped powders.

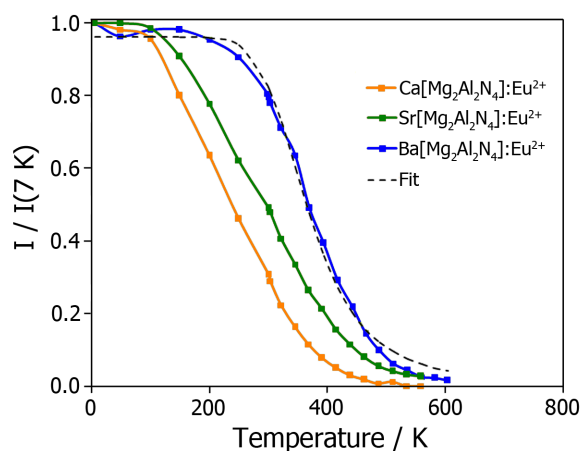


Figure 8. Temperature dependence of emission intensity of $M[\text{Mg}_2\text{Al}_2\text{N}_4]:\text{Eu}^{2+}$ (0.1%) ($M = \text{Ca}, \text{Sr}, \text{Ba}$).

The 298 K emission bands show an unusual red shift with increasing alkaline earth atom size with peak positions of $\lambda_{\text{em}} = 607$ nm (FWHM ~ 1815 cm^{-1}) for $M = \text{Ca}$, $\lambda_{\text{em}} = 612$ nm (FWHM ~ 1823 cm^{-1}) for $M = \text{Sr}$, and $\lambda_{\text{em}} = 666$ nm (FWHM ~ 2331 cm^{-1}) for $M = \text{Ba}$. While the emission band shapes are comparable for $M = \text{Ca}$ and Sr , the emission of the Ba compound is significantly red-shifted and broadened.

To study these nontypical luminescence properties in more detail, temperature dependent emission measurements were performed for these samples (see Figure 7). Samples for $M = \text{Ca}$ and Sr show a significant spectroscopic red-shift of emission at low temperatures. Below ~ 100 K both compounds show nearly identical spectra peaking at $\lambda_{\text{em}} = 625$ nm with FWHM = $1715\text{--}1785$ cm^{-1} . The intensity of emission remains nearly unchanged up to 100 K for both compounds and drops sharply when the temperature is increased (see Figure 8). From 7 to 300 K a peak shift of 474 and 340 cm^{-1} towards higher energies is observed for $M = \text{Ca}$ and Sr , respectively. The $\text{Ba}[\text{Mg}_2\text{Al}_2\text{N}_4]:\text{Eu}^{2+}$ (0.1%) sample also shows a red shift of emission at low temperatures (244 cm^{-1} from 300 to 7 K), however, the thermal quenching of the Ba compound emission can be fitted with a single activation energy ($I_T/I_0 = [1 + G \cdot \exp(-E_a/kT)]^{-1}$) (see Figure 8) with $E_a = 2022$ cm^{-1} (0.25 eV) while the thermal quenching behavior of compounds $M[\text{Mg}_2\text{Al}_2\text{N}_4]:\text{Eu}^{2+}$ (0.1%, $M = \text{Ca}, \text{Sr}$) points towards a more complex process.

The nontypical emission red-shift within the isotypic series $M[\text{Mg}_2\text{Al}_2\text{N}_4]:\text{Eu}^{2+}$ ($M = \text{Ca}, \text{Sr}, \text{Ba}$) with increasing alkaline earth cation size and the low temperature luminescence properties point toward anomalous luminescence phenomena for these compounds. Large

Stokes shifts and nontypical emission red shifts at low temperatures have been observed frequently when $\text{Eu}(\text{II})$ $5d$ levels are located close to the bottom of the host lattice conduction band leading to trapped excitation emission.^[24] We therefore conclude that normal $\text{Eu}(\text{II})$ emission from the $4f^6 5d^1$ state is only observed for $M = \text{Ca}$ and Sr at high temperatures while at low temperatures ($T > 100 \text{ K}$) and for $M = \text{Ba}$ emission from a trapped exciton state is being observed.

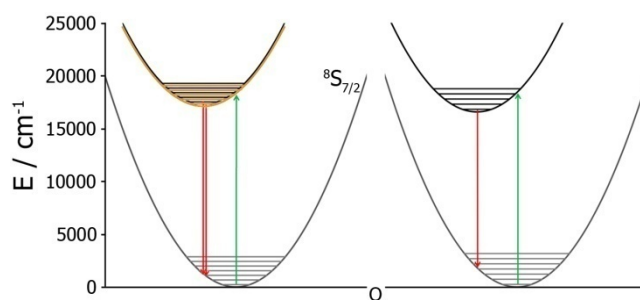


Figure 9. Configurational coordinate diagrams of $\text{Eu}(\text{II})$ in $M[\text{Mg}_2\text{Al}_2\text{N}_4]:\text{Eu}^{2+}$ ($M = \text{Ca}, \text{Sr}, \text{Ba}$). Left: $M = \text{Sr}$. The orange potential curve represents a trapped exciton state leading to red-shifted emission at low T for $M = \text{Ca}, \text{Sr}$ ($\hbar\omega = 440 \text{ cm}^{-1}$, $S = 2.8$, $U_0 = 577 \text{ nm}$). Right: $M = \text{Ba}$. The large Stokes shift indicates trapped excitation emission being visible over the whole T range ($\hbar\omega = 486 \text{ cm}^{-1}$, $S = 3.77$, $U_0 = 603 \text{ nm}$).

Figure 9 shows configurational coordinate diagrams for $\text{Eu}(\text{II})$ in $M[\text{Mg}_2\text{Al}_2\text{N}_4]:\text{Eu}^{2+}$ ($M = \text{Sr}$ and Ba) obtained by fitting the experimental data with a basic model assuming linear vibronic coupling.^[25] Positions of the lowest lying absorption bands are nearly identical for both compounds and are located at $\sim 540 \text{ nm}$. The rather high phonon frequencies in the $400\text{-}500 \text{ cm}^{-1}$ range correspond well with the observed small emission band broadening with temperature.^[26] For $M = \text{Ca}$ and Sr emission most likely originates from a trapped exciton state (orange potential curve in Figure 9) at low temperatures while at higher temperatures the $4f^6 5d^1$ state is being thermally populated and normal emission at higher energies is observed. A similar luminescence mechanism was observed recently for $\text{Sr}_4\text{Al}_{14}\text{O}_{25}:\text{Eu}^{2+}$.^[27] For $M = \text{Ba}$ the large Stokes shift and large spectral width of emission points towards trapped exciton emission taking place over the complete temperature range. It is likely that the cuboidal coordination of Eu in the title compounds and the long contact lengths for $M = \text{Ba}$ stabilizes a trapped exciton state as a comparison with the series of isotopic compounds $M\text{F}_2:\text{Eu}^{2+}$ ($M = \text{Ca}, \text{Sr}, \text{Ba}$) suggests.^[24] At room temperature the quantum efficiency of a powder layer of $\text{Sr}[\text{Mg}_2\text{Al}_2\text{N}_4]:\text{Eu}^{2+}$ is in the range of 18% for 440 nm excitation.

With respect to the emission maximum and the FWHM the luminescence properties of $M[\text{Mg}_2\text{Al}_2\text{N}_4]:\text{Eu}^{2+}$ ($M = \text{Ca}, \text{Sr}, \text{Ba}$) and $\text{Ba}[\text{Mg}_2\text{Ga}_2\text{N}_4]:\text{Eu}^{2+}$ are comparable to other red

emitting compounds reported in literature, e.g., $\text{Ba}_3\text{Ga}_3\text{N}_5:\text{Eu}^{2+}$ (ca. 2 mol% Eu; $\lambda_{\text{em}} = 638 \text{ nm}$; FWHM $\sim 2123 \text{ cm}^{-1}$),^[28] $(\text{Sr}, \text{Ba})_2\text{Si}_5\text{N}_8:\text{Eu}^{2+}$ ($\lambda_{\text{em}} = 590\text{-}625 \text{ nm}$; FWHM $\sim 2050\text{-}2600 \text{ cm}^{-1}$),^[29] or $(\text{Ca}, \text{Sr})\text{AlSiN}_3:\text{Eu}^{2+}$ ($\lambda_{\text{em}} = 610\text{-}660 \text{ nm}$; FWHM $\sim 2100\text{-}2500 \text{ cm}^{-1}$).^[30,31]

The relatively broad emission band of compounds in the UCr_4C_4 -structure type results most likely from disordering of the framework cations (here: Mg^{2+} and Al^{3+}). In this case, statistical distribution leads to constantly varying distances ($\text{Al}^{3+}/\text{Mg}^{2+}$)-N in the tetrahedrally coordinated positions, accompanied by a broad range of Eu-N bond lengths and environments. The differing crystal fields directly cause inhomogeneous line broadening of the emission band. A similar behavior has been reported for, e.g., $(\text{Ca}, \text{Sr})\text{AlSiN}_3:\text{Eu}^{2+}$, a material that also shows a statistical distribution of the host lattice cations Al and Si that occupy the same crystallographic site.^[29] The very narrow emission profiles of ordered variants of the UCr_4C_4 -structure type such as $\text{Ca}[\text{LiAl}_3\text{N}_4]:\text{Eu}^{2+}$ (ca. 5 mol% Eu; $\lambda_{\text{em}} = 668 \text{ nm}$; FWHM of $\sim 1333 \text{ cm}^{-1}$), $\text{Sr}[\text{LiAl}_3\text{N}_4]:\text{Eu}^{2+}$ (ca. 0.4 mol% Eu; $\lambda_{\text{em}} = 650 \text{ nm}$; FWHM of $\sim 1180 \text{ cm}^{-1}$) or $\text{Sr}[\text{Mg}_3\text{SiN}_4]:\text{Eu}^{2+}$ (ca. 2 mol% Eu; $\lambda_{\text{em}} = 615 \text{ nm}$; FWHM of $\sim 1170 \text{ cm}^{-1}$) corroborate this assumption.^[9,10,12]

3.2.4 Conclusions

In this contribution we present the first nitridomagnesoaluminates and a novel nitridomagnesogallate. *DiSalvo* et al. described the substitutability of Ga^{3+} and Ge^{4+} by Mg^{2+} in nitridogallates and germanates, demonstrated by the two compounds $\text{Sr}[\text{Mg}_2\text{Ga}_2\text{N}_4]$ and $\text{Sr}[\text{Mg}_3\text{GeN}_4]$ both crystallizing in the UCr_4C_4 -structure type.^[21] Back then, this structure type was already discussed as attractive host lattice for luminescent materials, due to the highly symmetric cuboid-like coordination of the heavy atom site. Furthermore, *Hoppe* et al. could demonstrate the large structural variety of this aristotype by characterizing various ordered oxidic structure types, for example, $\text{Na}[\text{Li}_3\text{SiO}_4]$.^[11] Based on this work, we started to develop different substitutional variants based on $\text{AB}_2\text{C}_2\text{X}_4$ and ABC_3X_4 structures either containing Ga/Mg, Al/Mg, Li/Al or Mg/Si on the tetrahedrally coordinated sites. However, deriving a principle for structural prediction in these systems is quite demanding.

All compounds presented in this contribution are isostructural crystallizing in the UCr_4C_4 -type with statistical distribution of the tetrahedral network cations Al/Mg or Ga/Mg, respectively. Furthermore, we could show that by employing metal fluorides in combination with Li-melts a number of quaternary compounds is accessible at moderate temperatures up to $900 \text{ }^\circ\text{C}$. The

presented compounds reveal interesting luminescence properties with emission maxima in the red spectral region and attractive FWHM values.

The nontypical emission red-shift within the isotypic $M[\text{Mg}_2\text{Al}_2\text{N}_4]:\text{Eu}^{2+}$ ($M = \text{Ca}, \text{Sr}, \text{Ba}$) compounds with increasing alkaline earth cation size and the low temperature luminescence properties give strong evidences for anomalous luminescence phenomena. Similar behavior has often been observed when $\text{Eu}(\text{II})$ 5d levels are being located close to the bottom of the host lattice conduction band leading to trapped excitation emission.^[24] Based on our results we conclude that a regular Eu^{2+} emission is only observed for $M[\text{Mg}_2\text{Al}_2\text{N}_4]:\text{Eu}^{2+}$ ($M = \text{Ca}, \text{Sr}$) at temperatures above 100 K. Below this temperature and also for $M = \text{Ba}$ emission from a trapped exciton state is observed.

These compounds widen the group of novel red-emitting systems like $\text{Ca}[\text{LiAl}_3\text{N}_4]:\text{Eu}^{2+}$, $\text{Sr}[\text{LiAl}_3\text{N}_4]:\text{Eu}^{2+}$ or $\text{Sr}[\text{Mg}_3\text{SiN}_4]:\text{Eu}^{2+}$ ^[9, 10, 12] and are fundamental to completely understand the mechanisms responsible for narrow band luminescence of Eu^{2+} systems.

3.2.5 References

- [1] C. C. Lin, R.-S. Liu, *J. Phys. Chem. Lett.* **2011**, *2*, 1268.
- [2] M. Mikami, H. Watanabe, K. Uheda, S. Shimooka, Y. Shimomura, T. Kurushima, N. Kijima, *IOP Conf. Ser.: Mater. Sci. Eng.* **2009**, *1*, 012002.
- [3] R. Mueller-Mach, G. Mueller, M. R. Krames, H. A. Höpfe, F. Stadler, W. Schnick, T. Juestel, P. Schmidt, *Phys. Status Solidi A* **2005**, *202*, 1727.
- [4] S. Ye, F. Xiao, Y. X. Pan, Y. Y. Ma, Q. Y. Zhang, *Mater. Sci. Eng. R.* **2010**, *71*, 1.
- [5] M. Krames, G. O. Mueller, R. B. Mueller-Mach, H. Bechtel, P. J. Schmidt, *PCT Int. Appl.*, WO 2010131133, A1, **2010**.
- [6] A. A. Setlur, *Electrochem. Soc. Interface* **2009**, *18*, 32.
- [7] R.-J. Xie, N. Hirosaki, T. Takeda, T. Suehiro, *ECS J Solid State Sci. Technol.* **2013**, *2*, R3031.
- [8] M. Zeuner, S. Pagano, W. Schnick, *Angew. Chem. Int. Ed.* **2011**, *50*, 7754.
- [9] S. Schmiechen, H. Schneider, P. Wagatha, C. Hecht, P. J. Schmidt, W. Schnick, *Chem. Mater.* **2014**, *26*, 2712.
- [10] P. Pust, A. S. Wochnik, E. Baumann, P. J. Schmidt, D. Wiechert, C. Scheu, W. Schnick, *Chem. Mater.* **2014**, *26*, 3544.
- [11] B. Nowitzki, R. Hoppe, *Rev. Chim. Miner.* **1986**, *23*, 217.
- [12] P. Pust, V. Weiler, C. Hecht, A. Tücks, A. S. Wochnik, A.-K. Henß, D. Wiechert, C. Scheu, P. J. Schmidt, W. Schnick, *Nat. Mater.* **2014**, *13*, 891.

- [13] H. D. Fair, R. F. Walker, *Energetic Materials 1, Physics and Chemistry of the Inorganic Azides*. New York, London, **1977**.
- [14] L. J. Farrugia, *J. Appl. Cryst.* **1999**, *32*, 837.
- [15] G. M. Sheldrick, *Acta Crystallogr., Sect. A: Found. Crystallogr.* **2008**, *64*, 112.
- [16] Stoe & Cie GmbH, WINXPOW - Program for powder data handling, **2007**, v2.21; Darmstadt, Germany.
- [17] A. Coelho, TOPAS – Academic, **2007**, Brisbane: Coelho Software.
- [18] L. G. Akselrud, O. I. Bodak, E. P. Marusin, *Sov. Phys. Crystallogr. (Engl. Transl.)* **1989**, *34*, 289.
- [19] Liebau established the terms *zweier*, *dreier*, *vierer*, *fünfer* rings. Thereby, a *vierer* ring can be described as four polyhedra connected to each other by common corners forming a ring. The terms derive from the German numerals *drei* (3), *vier* (4), etc. by adding the suffixing "er" to the numeral; F. Liebau, *Structural chemistry of silicates*. Springer, Berlin, **1985**.
- [20] R. D. Shannon, *Acta Crystallogr. Sect. A: Found. Crystallogr.* **1976**, *32*, 751.
- [21] D. G. Park, Y. Dong, F. J. DiSalvo, *Solid State Sci.* **2008**, *10*, 1846.
- [22] W. Blase, G. Cordier, M. Ludwig, R. Kniep, *Z. Naturforsch. B: Chem. Sci.* **1994**, *49*, 501.
- [23] V. Schultz-Coulon, W. Schnick, *Z. Naturforsch. B* **1995**, *50*, 619.
- [24] P. Dorenbos, *J. Phys.: Condens. Matter* **2003**, *15*, 2645.
- [25] M. Nazarow, B. Tsukerblat, D. Y. Noh, *J. Phys. Chem. Solids* **2008**, *69*, 2605.
- [26] D. Curie, *Absorption and emission spectra*, in: *Di Bartolo, Optical Properties of Ions in Solids*. Plenum Press, New York, **1975**.
- [27] D. Dutczak, C. Ronda, T. Juestel, A. Meijerink, *J. Phys. Chem. A.* **2014**, *118*, 1617.
- [28] F. Hintze, F. Hummel, P. J. Schmidt, D. Wiechert, W. Schnick, *Chem. Mater.* **2012**, *24*, 402.
- [29] M. Zeuner, P. J. Schmidt, W. Schnick, *Chem. Mater.* **2009**, *21*, 2467.
- [30] K. Uheda, N. Hirosaki, H. Yamamoto, *Phys. Stat. Sol. A* **2006**, *11*, 2712.
- [31] K. Uheda, N. Hirosaki, Y. Yamamoto, A. Naita, T. Nakajima, H. Yamamoto, *Electrochem. Solid State Lett.* **2006**, *9*, H22.

3.3 Ca[LiAl₃N₄]:Eu²⁺ - A Narrow Band Red-Emitting Nitridolithoaluminate

published in: *Chem. Mater.* **2014**, *26*, 3544-3549

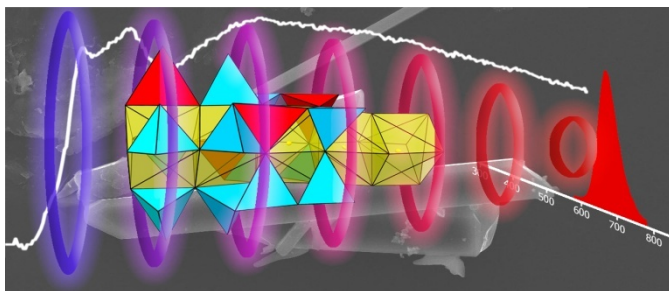
authors: Philipp Pust, Angela S. Wochnik, Elen Baumann, Peter J. Schmidt, Detlef Wiechert, Christina Scheu and Wolfgang Schnick

DOI: 10.1021/cm501162n

Copyright © 2014 American Chemical Society

<http://pubs.acs.org/doi/abs/10.1021/cm501162n>

Abstract. Ca[LiAl₃N₄]:Eu²⁺ is an intriguing new narrow-band red-emitting phosphor material with potential for application in high-power phosphor-converted light-emitting diodes (pc-LEDs). With excitation by blue InGaN-based LEDs, the compound exhibits an emission maximum at 668 nm with a full width at half maximum of only 1333 cm⁻¹ (~60 nm). Ca[LiAl₃N₄]:Eu²⁺ was synthesized from Ca, LiAlH₄, LiN₃, AlF₃, and EuF₃ in weld-shut Ta ampules, and the structure was solved and refined on the basis of single-crystal X-ray diffraction data. After isotypical crystallization with Na[Li₃SiO₄], the compound forms a highly condensed framework of AlN₄ and LiN₄ tetrahedra [*I*4₁/*a* (no. 88), *Z* = 16, *a* = 11.1600(16) Å, and *c* = 12.865(3) Å] and can thus be classified as a nitridolithoaluminate. Both types of polyhedra are connected to each other by common edges and corners, yielding a high degree of condensation, $\kappa = 1$. The Ca site is positioned in the center of *vierer* ring channels along [001] and coordinated in a cuboidal manner by eight N atoms. To validate the presence of Li, transmission electron microscopy (TEM) investigations employing electron



energy-loss spectroscopy (EELS) were carried out. Furthermore, to confirm the electrostatic bonding interactions and the chemical composition, lattice energy calculations [Madelung part of lattice energy (MAPLE)] have been performed.

3.3.1 Introduction

During the last couple of years, white phosphor-converted light-emitting diodes (pc-LEDs) have emerged as superior candidates to replace incandescent light bulbs because of their much more efficient conversion of electric energy to visible light.^[1-4] To further improve the luminous efficacy (efficiency of light conversion subject to the human eye sensitivity), there is a huge demand for novel phosphor materials with superior luminescence properties and light quality.^[5,6] Thereby, ternary and multinary alkaline-earth nitrides emerged as important host lattices for doping with Eu²⁺, exhibiting intense emission because of parity allowed $4f^6(^7F)5d^1 \rightarrow 4f^7(^8S^{7/2})$ transitions. Especially, nitridosilicates, nitridoalumosilicates, and related SiAlONs have been extensively investigated, whereas several compounds turned out to be excellent luminescent materials for application in pc-LEDs.^[7] Achieving accurate color rendition with pc-LED light without compromising energy efficiency calls for better adaptation of the pc-LED emission spectrum to the spectral region of the human eye sensitivity, resulting in high luminous efficacy values. Optimization of both requirements, quantified by the color rendering index (CRI) and the luminous efficacy of a white pc-LED, critically depends upon the emission maximum and width of the red-emitting component. Thus, there is a huge demand for narrow band red-emitting phosphors being applicable in high power pc-LEDs (blue light output > 100 W/cm²). This particularly requires short decay times of the excited state of the activators to avoid saturation, high chemical stability, and high thermal quenching temperatures above 100 °C.^[8] However, the number of red-emitting materials, which fulfill these demanding requirements for the application in high-luminance pc-LED devices, are quite small. (Sr,Ba)₂Si₅N₈:Eu²⁺ [$\lambda_{em} \sim 590\text{--}625$ nm; full width at half maximum (FWHM) $\sim 2050\text{--}2600$ cm⁻¹] and (Ca,Sr)SiAlN₃:Eu²⁺ [$\lambda_{em} \sim 610\text{--}660$ nm; FWHM $\sim 2100\text{--}2500$ cm⁻¹] convinced regarding their chemical and thermal stabilities; however, both suffer from rather broad emission bands, which greatly limit the achievable luminous efficacy values of high-luminance warm-white pc-LEDs because a significant part of the emitted light is above 700 nm and, thus, outside the human eye sensitivity.^[3,8-11] Recently, we have demonstrated that the novel nitridomagnesosilicate Sr[Mg₃SiN₄]:Eu²⁺ represents the most narrow red emitting Eu²⁺-doped phosphor material described in the literature thus far.^[12] This compound crystallizes in the Na[Li₃SiO₄] structure type,^[13] which exhibits specific structural features facilitating narrow-band red emission. Now, we are searching for further new nitride compounds crystallizing in this structure type. In this contribution, we describe the novel

Eu²⁺-doped nitridolithoaluminate Ca[LiAl₃N₄]:Eu²⁺, which is isotypic with Sr[Mg₃SiN₄]:Eu²⁺ and exhibits an intriguing narrow-band red emission as well.

3.3.2 Experimental Section

3.3.2.1 Synthesis

Ca[LiAl₃N₄]:Eu²⁺ (5 mol % Eu) was synthesized by firing a mixture of AlF₃ (75.6 mg, 0.90 mmol, Sigma-Aldrich, 95%), LiN₃ (22.0 mg, 0.45 mmol, synthesized according to Fair et al.),^[14] EuF₃ (3.1 mg, 0.015 mmol, Sigma-Aldrich, 99.99%), and metallic Ca (11.4 mg, 0.285 mmol, Sigma-Aldrich, 99.99%) in an arc-welded tantalum ampule. The starting materials were thoroughly ground in an agate mortar, filled into a Ta ampule, covered with Ca metal pieces, and sealed by arc-melting under argon. These procedures were performed in either Ar-filled glove boxes (Unilab, MBraun, Garching; O₂ < 1 ppm; H₂O < 1 ppm) or Schlenk-type glassware under an inert gas atmosphere. The ampules were placed in quartz tubes, heated in tube furnaces to 1000 °C within 4.5 h, maintained at that temperature for 24 h, and subsequently cooled to 500 °C within 40 h. After reaction, the furnace was turned off and the Ta ampules were opened in a glovebox. Pink rod-shaped crystals of Ca[LiAl₃N₄]:Eu²⁺ were obtained next to colorless crystals of LiF and small amounts of CaLiAlN₂^[15] as byproducts. The pink crystals are stable in air and exhibit intense red luminescence, when excited by ultraviolet (UV) to green light.

3.3.2.2 Single-Crystal X-ray Diffraction

The crystal structure of Ca[LiAl₃N₄] was determined by means of single-crystal X-ray diffraction data on a Bruker D8 Quest diffractometer (Mo-K α radiation). A numerical absorption correction using the program PLATON^[16] was applied. The crystal structure was solved using direct methods with SHELXS.^[17] The structure refinement was carried out by the method of least-squares using SHELXL.^[17] Prior to this selected red luminescence, Ca[LiAl₃N₄]:Eu²⁺ single crystals were picked on a glass wire, sealed in a glass capillary, and checked for quality on a Buerger precession camera.

Further details of the crystal structure investigations can be obtained from Fachinformationszentrum Karlsruhe, Eggenstein-Leopoldshafen, Germany, upon quoting the depository number CSD-427066.

3.3.2.3 Electron Microscopy

For scanning electron microscopy (SEM) investigations, a JSM-6500F SEM (JEOL) equipped with a Si/Li energy-dispersive X-ray (EDX) detector (Oxford Instruments, model 7418) was used. For transmission electron microscopy (TEM) measurements, a FEI Titan 80-300

(accelerating voltage of 300 kV) TEM equipped with a post-column energy filter GIF Tridiem from Gatan and an EDAX EDX detector for analytical characterizations was employed. To identify investigated particles by interpretation of d values of observed reflections, selected area diffraction (SAD) patterns were recorded with a Gatan UltraScan 1000 (2000 × 2000) charge-coupled device (CCD) camera and evaluated using a calibrated camera constant obtained using a Si standard.

3.3.2.4 EDX Spectroscopy

To analyze the chemical composition of different crystallites, EDX data were collected with an accelerating voltage of 12 kV. Furthermore, SEM was used to collect images of particles to investigate the morphology.

3.3.2.5 Electron Energy-Loss Spectroscopy (EELS)

The EELS investigations were performed in diffraction mode in TEM with the use of a SAD aperture choosing a circular area of about 150 nm in diameter to avoid beam damage. An entrance aperture of the spectrometer of 2 mm and a camera length of 130 mm were used, resulting in a collector angle of 13.5 mrad. Dispersions of 0.3 eV/channel were used, leading to a fwhm of around 0.9–1.2 eV of the zero-loss peak. The acquisition time for the Li–K and Al–L_{2,3} edges was 10 s. The obtained data were corrected for dark current and channel-to-channel gain variation. The pre-edge background was approximated by a first-order log-polynomial function and subtracted from the original data.^[18]

3.3.2.6 Luminescence

For luminescence investigations, a luminescence microscope, consisting of a HORIBA Fluorimax4 spectrofluorimeter system attached to an Olympus BX51 microscope via fiber optics, was applied. The samples were measured in glass capillaries. Excitation wavelength was chosen to 470 nm with a spectral width of 10 nm. The emission spectra were measured in the wavelength range between 580 and 780 nm with 2 nm step size. For color point calculations, the range between 600 and 780 nm was used. Excitation spectra were measured in the wavelength range between 380 and 550 nm with 2 nm step size. The integral range was therefore between 630 and 690 nm.

3.3.3 Results and Discussion

3.3.3.1 Synthesis and Chemical Analysis

The synthesis of Ca[LiAl₃N₄]:Eu²⁺ according to the above-mentioned route yielded rod-shaped crystals with an average length between 40 and 70 μm (see Figure 1). EDX analysis

yields an average composition (five measurements, each on different crystals), normalized according to the Ca content, of Ca₁Al_{2.8}N_{4.4}, which corroborates the sum formula obtained from single-crystal structure refinement (within the standard deviation of the EDX device). Eu was not detected in SEM/EDX because of the low accelerating voltage of 12 kV. During all measurements, the oxygen content was zero within the accuracy of this method. However, TEM/EDX measurements and luminescence investigations obtained evidence for the presence of Eu. Light atoms, such as Li, are not determinable with this EDX setup.

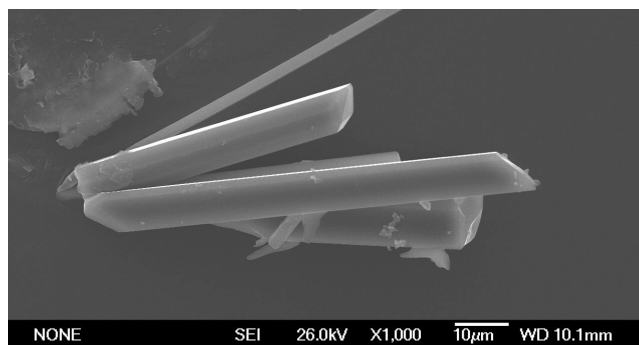


Figure 1. SEM image of rod-shaped Ca[LiAl₃N₄]:Eu²⁺ crystals.

3.3.3.2 Single-Crystal Structure Analysis

The crystal structure of Ca[LiAl₃N₄]:Eu²⁺ was solved and refined in the tetragonal space group *I*₄₁/*a* (no. 88) with *a* = 11.1600(16) Å and *c* = 12.865(3) Å. The crystallographic data are summarized in Table 1, and atomic coordinates and isotropic displacement parameters are given in Table 2.

The small amount of Eu²⁺ as a dopant was neglected for refinement of the crystal structure because of the insignificant contribution of the scattering density. For lattice energy calculations (see below), Eu²⁺ was neglected as well. The crystal structure of Ca[LiAl₃N₄] is displayed in Figure 2. The compound is isotypic to Na[Li₃SiO₄]^[13] and the recently discovered nitridosilicates M[Mg₃SiN₄] with M = Ca, Sr, and Eu.^[12] Ca[LiAl₃N₄] also shows a close structural relation to compounds crystallizing in UCr₄C₄ structure type, such as Sr[Mg₃GeN₄], by only differing in the distribution of network cation positions.^[19,20] Sr[Mg₃GeN₄] shows disordering of the tetrahedrally coordinated network cations (Mg/Ge).^[19] In contrast, Ca[LiAl₃N₄] can be described as crystallizing in an ordered variant of the UCr₄C₄ type.^[20] A highly condensed network of vertex- and corner-sharing AlN₄ and LiN₄ tetrahedra forming *vierer* ring^[21] channels along [001] is formed (see Figure 2a), and because Al³⁺ and Li⁺ are both part of the tetrahedra network, the more precise classification for Ca[LiAl₃N₄] as a nitridolithoaluminate, according to Nowitzki and Hoppe,^[13] should be chosen. The Li site is affected by a 4₁ screw axis around the *vierer* ring channels (see Figure 2c). The degree of

condensation [i.e., atomic ratio (Al,Li)/N] is $\kappa = 1$ and, thus, comparable to the binary nitride AlN. Because of the high value of κ , each N site is coordinated by four tetrahedral centers, resulting exclusively in ammonium-type N^[4] atoms. Al–N [1.8273(2)–1.9511(3) Å] and Li–N [1.9680(2)–2.2788(3) Å] distances are in good agreement with other nitridolithoaluminates, such as Ca[LiAlN₂] [Al–N, 1.917(3)–1.958(3) Å; Li–N, 2.043(3)–2.278(7) Å], as well as with the sum of the ionic radii.^[15,22] Along [001], every second *vierer* ring channel contains endless strands of Ca atoms. The Ca site is in 6 + 2 coordination with eight N atoms, forming a cuboidal arrangement with Ca–N distances ranging from 2.5202(3) to 2.9075(3) Å (see Figure 2b).

Table 1. Crystallographic Data of Single-Crystal Structure Determination of Ca[LiAl₃N₄]

formula	Ca[LiAl ₃ N ₄]
crystal system	tetragonal
space group	<i>I</i> 4 ₁ / <i>a</i> (no. 88)
lattice parameters (Å)	<i>a</i> = 11.1600(16) and <i>c</i> = 12.865(3)
cell volume (Å ³)	1602.3(5)
formula units per unit cell	16
density (g·cm ⁻³)	3.051
μ (mm ⁻¹)	2.055
T (K)	293(2)
diffractometer	Bruker D8 Quest
radiation (Å)	Mo-K α (λ = 0.71073 Å)
F(000)	1440
profile range	2.42 \leq θ \leq 30.00
index ranges	-14 \leq <i>h</i> \leq 14 -14 \leq <i>k</i> \leq 14 -17 \leq <i>l</i> \leq 16
independent reflections	1014 [<i>R</i> _{int} = 0.0569]
refined parameters	82
goodness of fit	1.072
<i>R</i> 1 (all data); <i>R</i> 1 (<i>F</i> ² > 2 σ (<i>F</i> ²))	0.0341, 0.0303
<i>wR</i> 2 (all data); <i>wR</i> 2 (<i>F</i> ² > 2 σ (<i>F</i> ²))	0.0787, 0.0762
$\Delta\rho_{\max}$, $\Delta\rho_{\min}$ (e·Å ⁻³)	0.807, -1.007

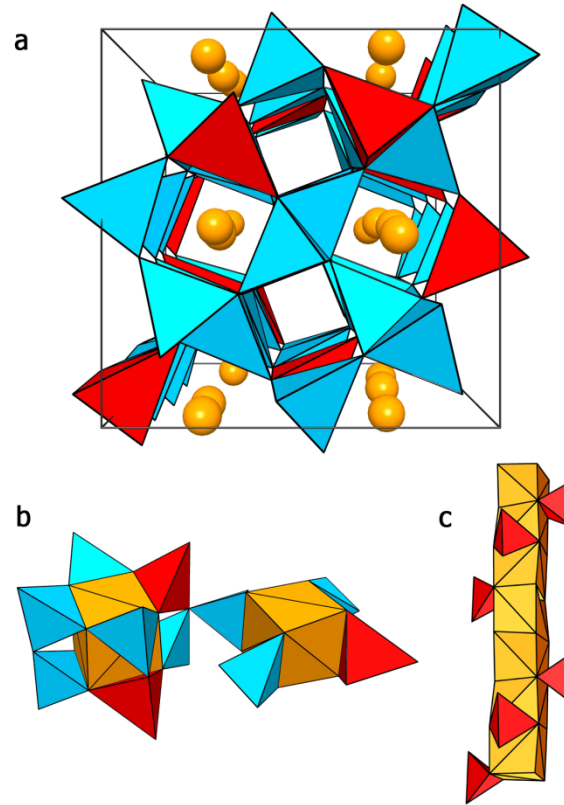


Figure 2. Crystal structure of Ca[LiAl₃N₄], with AlN₄ tetrahedra (blue), LiN₄ tetrahedra (red), and Ca atoms and CaN₈ polyhedra (orange): (a) unit cell in projection along [001], (b) coordination of CaN₈ polyhedra, and (c) strands of face-sharing CaN₈ polyhedra with surrounding LiN₄ tetrahedra.

Table 2. Atomic Coordinates and Isotropic Displacement Parameters (\AA^2) of Ca[LiAl₃N₄]:Eu²⁺, with Standard Deviations in Parentheses^a

Atom	x	y	z	$U_{\text{eq}} / \text{\AA}^3$
Ca1	0.26627(4)	0.00441(3)	0.18602(2)	0.00747(14)
Al1	0.03325(5)	0.08002(4)	0.30855(3)	0.00431(16)
Al2	0.02082(4)	0.09016(4)	0.55935(3)	0.0041(16)
Al3	0.02192(4)	0.0857(4)	0.06621(3)	0.00416(16)
Li1	0.35466(3)	0.2348(3)	0.06581(17)	0.0086(6)
N1	0.44053(12)	0.08009(12)	0.06858(7)	0.0054(3)
N2	0.15659(12)	0.18508(13)	0.05929(7)	0.0060(3)
N3	0.17564(11)	0.16539(12)	0.29918(9)	0.0055(3)
N4	0.16319(12)	0.17089(12)	0.57203(8)	0.0059(3)

^aAll atoms occupy the Wyckoff position 16f.

In comparison to values from the literature, some Ca–N bonds in this compound show slight elongation; therefore, 6 + 2 specification has been chosen. The CaN₈ polyhedra are connected to each other by common faces, forming endless strands parallel to [001] (see Figure 2c). The Ca–Ca distances [3.2271(6) Å] are in good agreement to comparable compounds, such as Ca₃Al₂N₄ [Ca–Ca, 2.941(5)–3.3573(5) Å].^[23] In doped samples, the activator ion Eu²⁺ is

expected to occupy the Ca positions comparable to other nitride phosphor materials, such as Ca₂Si₅N₈:Eu²⁺ or CaAlSiN₃:Eu²⁺.^[10,11,24,25]

3.3.3.3 Lattice-Energy Calculations

To proof electrostatic consistency of the crystal structure, Madelung part of lattice energy (MAPLE)^[22,26–28] calculations of the lattice energy were carried out. Exclusively electrostatic interactions in an ionic crystal were taken into account, depending upon the charge, distance, and coordination spheres of the constituting ions. The calculated partial MAPLE values (for Li⁺, Ca²⁺, Al³⁺, and N³⁻) are in good accordance with reference values.^[29,30] The minor deviation of 0.9% of the total MAPLE sum of Ca[LiAl₃N₄] compared to the MAPLE sum of the formally constituting compounds (Ca[LiAlN₂] + 2 AlN)^[15,31] corroborates the refined crystal structure (see Table 3).

Table 3. Partial MAPLE values and MAPLE sums [kJ/mol] of Ca[LiAl₃N₄]:Eu²⁺

Ca[LiAl ₃ N ₄] ^a		Model	
Ca1	1841	1	Ca[LiAlN ₂] ^[14]
Al1	5441	2	AlN ^[30]
Al2	5302		
Al3	5372		
Li1	785		
N1	5134		
N2	5194		
N3	5153		
N4	5236		
Σ = 39421		Σ = 39064	
		Δ = 0.9%	

^aTypical partial MAPLE values [kJ/mol]:

Ca²⁺: 1930 - 2120; Al³⁺: 5000 - 6000; Li⁺: 600 - 860; N³⁻: 5000 - 6000.^[29,30]

3.3.3.4 EELS

To confirm the presence of Li in the structure, EELS measurements were performed in TEM. The Li–K edge in Figure 3 occurs at around 61 eV and shows two main peaks at 70 eV with a split of 0.8 eV and a smaller peak at around 63 eV. The Al–L_{2,3} and Al–L₁ edges can be seen in the spectrum, but they overlap with the higher energy loss region of the Li–K edge. The Al–L_{2,3} edge shows a maximum peak at 90.5 eV. The onset of the Al–L_{2,3} edge at 73 eV overlaps with the Li–K edge, but the shape of the Al edges is in accordance with published data.^[32] The Li–K edge is varying compared to data from the literature, for example, of Li, LiMn₂O, Li₂O, Li₂CaSi₂N₄, or Li₂SrSi₂N₄, which is due to the different bonding types.^[33,34]

However, the EELS measurements clearly show the presence of Li and Al being integrated in the structure.

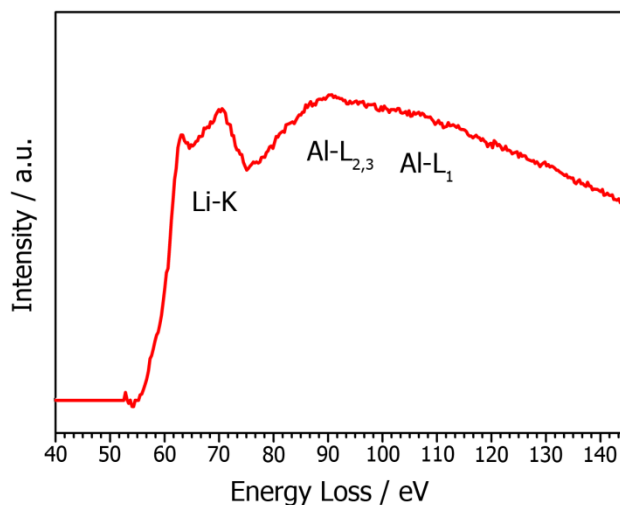


Figure 3. EELS spectrum of Ca[LiAl₃N₄]:Eu²⁺. The energy loss region of Li-K edge, Al-L_{2,3} and Al-L₁ is shown. The background left to the Li-K edge has been subtracted.

3.3.3.5 Luminescence

Eu²⁺-doped samples of the title compound show red luminescence by irradiation with blue light. Luminescence investigations have been performed on single crystals of Ca[LiAl₃N₄]:Eu²⁺ (5 mol% Eu nominal composition) sealed in silica glass capillaries. All measurements show comparable results; therefore, an exemplary spectrum is shown in Figure 4. Excitation at 470 nm yields an emission band peaking at 668 nm with a remarkably narrow FWHM of ~1333 cm⁻¹ (~60 nm) and CIE color coordinates of $x = 0.720$ and $y = 0.280$. The excitation spectrum shows two maxima at ~485 and ~560 nm. In comparison to other known red-emitting luminescent materials, such as (Sr,Ba)₂Si₅N₈:Eu²⁺ ($\lambda_{em} = 590\text{--}625$ nm; FWHM ~2050–2600 cm⁻¹),^[3,8,9,35] Ba₃Ga₃N₅:Eu²⁺ (ca. 2 mol% Eu; $\lambda_{em} = 638$ nm; FWHM ~2123 cm⁻¹),^[36] or (Ca,Sr)AlSiN₃:Eu²⁺ ($\lambda_{em} = 610\text{--}660$ nm; FWHM ~2100–2500 cm⁻¹)^[10,11] the FWHM of Ca[LiAl₃N₄]:Eu²⁺ (5 mol% Eu nominal composition) is rather narrow. The recently discovered isotypic compound Sr[Mg₃SiN₄]:Eu²⁺ ($\lambda_{em} = 615$ nm; FWHM ~1170 cm⁻¹) exhibits a very similar narrow band emission,^[12] which is most likely due to similar structural features. Therefore, both materials could be attractive candidates for application in warm-white pc-LEDs. However, for practical use, the emission maximum is too red-shifted and should be below 650 nm to compete with commercially available phosphor materials. There are two possible options to obtain a narrow-band emission at shorter wavelength in this system. On the one hand, a smaller dopant concentration should lead to a blue shift of the emission maximum, and on the other hand, the crystal field splitting could be

reduced by partial substitution of Ca by Sr, which should also lead to a hypsochrome emission band shift. The intriguing luminescence properties of Ca[LiAl₃N₄]:Eu²⁺ can be ascribed to structural features of the host lattice, which is built up by an ordered, rigid [LiAl₃N₄]²⁻ framework with $\kappa = 1$.

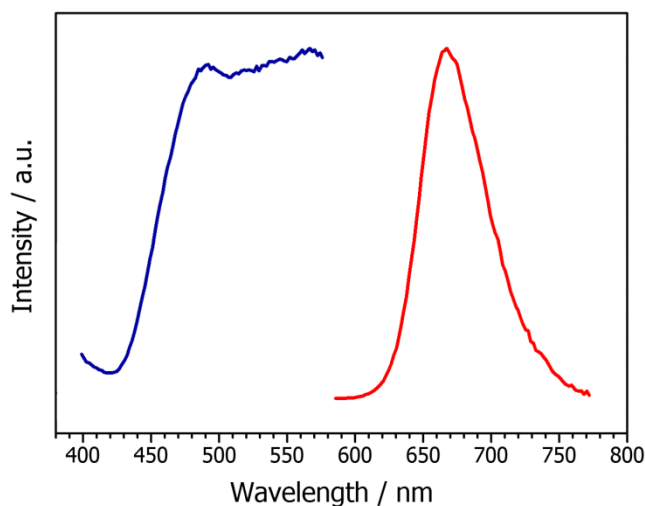


Figure 4. Excitation (blue) and emission (red) spectra of a Ca[LiAl₃N₄] (5 mol% Eu) single crystal. Excitation spectrum: $\lambda_{\text{exc, max}} = 485 \text{ nm}, 560 \text{ nm}$. Emission spectrum: $\lambda_{\text{exc}} = 470 \text{ nm}$, $\lambda_{\text{em}} = 668 \text{ nm}$, FWHM $\sim 1333 \text{ cm}^{-1}$ ($\sim 60.3 \text{ nm}$); CIE color coordinates: $x = 0.720$, $y = 0.280$.

This high degree of condensation may be beneficial for reducing structural relaxation around the activator in its excited state. Also, experimental observations (especially in Eu²⁺ phosphors) suggest that a cuboidal coordination with longer activator–ligand contact lengths around the activator site, such as in Ca[LiAl₃N₄]:Eu²⁺, can result in a narrow emission bandwidth. This has also been observed for nitridosilicate phosphors, such as Sr[Mg₃SiN₄]:Eu²⁺,^[12] BaSi₂O₂N₂:Eu²⁺, or Sr_{0.25}Ba_{0.75}Si₂O₂N₂:Eu²⁺.^[37–43] Larger Stokes shifts and, thus, broader emission bands observed for Eu²⁺ phosphors have been commonly associated with more asymmetric dopant site geometry^[44,45] or with smaller coordination numbers, leading to more pronounced structural relaxation around the Eu²⁺ ion in its excited state.^[46]

3.3.4 Conclusion

In this contribution, a new nitridolithoaluminate, namely, Ca[LiAl₃N₄]:Eu²⁺, with intriguing luminescence properties is reported. The compound consists of a highly condensed rigid framework of AlN₄ and LiN₄ tetrahedra with Ca atoms positioned in *vierer* ring channels along [001]. To verify the structural model, lattice energy calculations using MAPLE were carried out. Furthermore, to corroborate incorporation of Li ions in the structure, EELS

spectroscopy was applied. Luminescence investigations of doped samples show an intense red emission peaking at 668 nm with an exceptionally narrow FWHM of $\sim 1333 \text{ cm}^{-1}$ ($\sim 60 \text{ nm}$) for Eu²⁺ phosphors, when irradiated with UV to green light. The strong absorption in the blue to green spectral region ($\lambda_{\text{exc,max}} \sim 465 \text{ nm}$) makes the material attractive for application in phosphor-converted InGaN LEDs. The remarkable luminescence properties can be traced back to structural features of the host lattice. The high degree of condensation in the [LiAl₃N₄]²⁻ framework is beneficial to reduce phonon energies. Furthermore, there is only one crystallographic Ca site in a rather symmetric 8-fold surrounding (CaN₈ polyhedra), which is quite favorable to reduce inhomogeneous line-broadening effects (e.g., caused by different crystal fields around the activator sites). Additionally, Ca[LiAl₃N₄]:Eu²⁺ is in close structural relation to the recently discovered Sr[Mg₃SiN₄]:Eu²⁺,^[12] which also exhibits highly attractive luminescence. Here, further substitutions on the network cation positions could reveal even more attractive luminescence features. The results of these investigations illustrate the high suitability of both nitridosilicates and nitridoaluminates as host lattices for Eu²⁺-doped phosphor materials. Beneficial for narrow-band red emission seems to be a highly condensed, rigid network structure (e.g., Na[Li₃SiO₄] structure type), which comprises a single, highly symmetric alkaline earth atom position and a larger number of nearly equidistant N ligands surrounding this site. Consequently, we claim that Ca[LiAl₃N₄]:Eu²⁺ has the potential for application in high-power pc-LEDs, and there is strong incentive to further optimize the synthesis and enhance the luminescence properties.

3.3.5 References

- [1] C. C. Lin, R.-S. Liu, *J. Phys. Chem. Lett.* **2011**, *2*, 1268.
- [2] M. Mikami, H. Watanabe, K. Uheda, S. Shimooka, Y. Shimomura, T. Kurushima, N. Kijima, *IOP Conf. Ser.: Mater. Sci. Eng.* **2008**, *1*.
- [3] R. Mueller-Mach, G. Mueller, M. R. Krames, H. A. Höpfe, F. Stadler, W. Schnick, T. Juestel, P.J. Schmidt, *Phys. Status Solidi A* **2005**, *202*, 1727.
- [4] S. Ye, F. Xiao, Y. X. Pan, Y. Y. Ma, Q. Y. Zhang, *Mater. Sci. Eng. R.* **2010**, *71*, 1.
- [5] A. A. Setlur, *Electrochem. Soc. Interface* **2009**, *18*, 32.
- [6] R.-J. Xie, N. Hirosaki, T. Takeda, T. Suehiro, *ECS J Solid State Sci. Technol.* **2013**, *2*, R3031.
- [7] M. Zeuner, S. Pagano, W. Schnick, *Angew. Chem. Int. Ed.* **2011**, *50*, 7754.

- [8] M. Krames, G.O. Mueller, R.B. Mueller-Mach, H. Bechtel, P.J. Schmidt, *PCT Int. Appl.*, WO 2010131133, A1, **2010**.
- [9] H. A. Höpfe, H. Lutz, P. Morys, W. Schnick, A. Seilmeier, *J. Phys. Chem. Solids* **2000**, *61*, 2001.
- [10] K. Uheda, N. Hirosaki, H. Yamamoto, *Phys. Stat. Sol. A* **2006**, *11*, 2712.
- [11] K. Uheda, N. Hirosaki, Y. Yamamoto, A. Naita, T. Nakajima, H. Yamamoto, *Electrochem. Solid State Lett.* **2006**, *9*, H22.
- [12] S. Schmiechen, H. Schneider, P. Wagatha, C. Hecht, P.J. Schmidt, W. Schnick, *Chem. Mater.* **2014**, *26*, 2712.
- [13] B. Nowitzki, R. Hoppe, *Rev. Chim. Min.* **1986**, *23*, 217.
- [14] H. D. Fair, R. F. Walker, *Energetic Materials 1, Physics and Chemistry of the Inorganic Azides*, New York, London, **1997**.
- [15] P. Pust, S. Pagano, W. Schnick, *Eur. J. Inorg. Chem.* **2013**, 1157.
- [16] A. L. Spek, PLATON - A Multipurpose Crystallographic Tool, v1.07; Utrecht University: Utrecht, Netherlands, **2003**
- [17] G. M. Sheldrick, *Acta Crystallogr., Sect. A: Found. Crystallogr.* **2008**, *64*, 112.
- [18] R. F. Egerton, *Electron Energy-Loss Spectroscopy in the Electron Microscope*; 3rd ed., Springer, New York, **2011**.
- [19] D. G. Park, Y. Dong, F. J. DiSalvo, *Solid State Sci.* **2008**, *10*, 1846.
- [20] R. K. Behrens, W. Jeitschko, *Monatsh. Chem.* **1987**, *118*, 43.
- [21] Liebau established the terms *zweier*, *dreier*, *vierer*, *fünfer* rings. Thereby, a *vierer* ring can be described as four polyhedra connected to each other by common corners forming a ring. The terms derive from the German numerals *drei* (3), *vier* (4), etc. by adding the suffixing "er" to the numeral; F. Liebau, *Structural chemistry of silicates*, Springer, Berlin, **1985**.
- [22] R. D. Shannon, *Acta Crystallogr. Sect. A: Found. Crystallogr.* **1976**, *32*, 751.
- [23] M. Ludwig, J. Jaeger, R. Niewa, R. Kniep, *Inorg. Chem.* **2000**, *39*, 5909.
- [24] Y. Q. Li, J. E. J. van Steen, J. W. H. van Krevel, G. Botty, A. C. A. Delsing, F. J. DiSalvo, G. deWith, H. T. Hintzen, *J. Alloys Compd.* **2006**, *417*, 273.
- [25] T. Schlieper, W. Schnick, *Z. Anorg. Allg. Chem.* **1995**, *621*, 1535.
- [26] R. Hoppe, *Angew. Chem. Int. Ed. Engl.* **1970**, *9*, 25.
- [27] R. Hoppe, R. Z. Homann, *Anorg. Allg. Chem.* **1970**, *379*, 193.
- [28] R. Hübenthal, MAPLE, Programm zur Berechnung des Madelunganteils der Gitterenergie, version 4, University of Gießen, **1993**.

- [29] H. Höpfe, *Doctoral thesis*, Ludwig-Maximilian-University Munich, **2003**.
- [30] K. Köllisch, *Doctoral thesis*, Ludwig-Maximilian-University Munich, **2001**.
- [31] W. Paszkowicz, S. Podsiadlo, R. Minikayev, *J. Alloys Compd.* **2004**, *382*, 100.
- [32] C. Scheu, G. Dehm, H. Müllejans, R. Brydson, M. Rühle, *Microsc. Microanal. Microstruct.* **1995**, *6*, 19.
- [33] V. Mauchamp, P. Moreau, L. Monconduit, M.-L. Doublet, F. Boucher, G. Ouvrard, *J. Phys. Chem. C* **2007**, *111*, 3996.
- [34] M. Zeuner, S. Pagano, S. Hug, P. Pust, S. Schmiechen, C. Scheu, W. Schnick, *Eur. J. Inorg. Chem.* **2010**, 4945.
- [35] M. Zeuner, P.J. Schmidt, W. Schnick, *Chem. Mater.* **2009**, *21*, 2467.
- [36] F. Hintze, F. Hummel, P.J. Schmidt, D. Wiechert, W. Schnick, *Chem. Mater.* **2012**, *24*, 402.
- [37] J. Botterman, K. Van den Eeckhout, I. de Baere, D. Poelman, P. F. Smet, *Acta Mater.* **2012**, *60*, 5494.
- [38] J. A. Kechele, O. Oeckler, F. Stadler, W. Schnick, *Solid State Sci.* **2009**, *11*, 537.
- [39] Y. Q. Li, A. C. A. Delsing, G. de With, H. T. Hintzen, *Chem. Mater.* **2005**, *17*, 3242.
- [40] M. Seibald, T. Rosenthal, O. Oeckler, W. Schnick, *Crit. Rev. Solid State Mater. Sci.* **2014**, *39*, 215.
- [41] L. Wang, H. Ni, Q. Zhang, F. Xiao, *J. Alloys Compd.* **2011**, *509*, 10203.
- [42] B.-G. Yun, T. Horikawa, H. Hanzawa, K. Machida, *J. Electrochem. Soc.* **2010**, *157*, J364.
- [43] M. Seibald, T. Rosenthal, O. Oeckler, F. Fahrnbauer, A. Tücks, P.J. Schmidt, W. Schnick, *Chem. Eur. J.* **2012**, *18*, 13446.
- [44] G. J. Dirksen, G. Blasse, *J. Solid State Chem.* **1991**, *92*, 591.
- [45] A. Diaz, D. A. Keszler, *Chem. Mater.* **1997**, *9*, 2071.
- [46] A. Meijerink, G. Blasse, *J. Lumin.* **1989**, *43*, 283.

3.4 Narrow-Band Red-Emitting Sr[LiAl₃N₄]:Eu²⁺ as a Next-Generation LED-Phosphor Material

published in: *Nat. Mater.* **2014**, *13*, 891-896

authors: Philipp Pust, Volker Weiler, Cora Hecht, Andreas Tücks, Angela S. Wochnik, Ann-Kathrin Henß, Detlef Wiechert, Christina Scheu, Peter J. Schmidt and Wolfgang Schnick

DOI: 10.1038/NMAT4012

Copyright © 2014 Nature Publishing Group

<http://www.nature.com/nmat/journal/v13/n9/full/nmat4012.html>

Abstract. To facilitate the next generation of high-power white-light-emitting diodes (white LEDs), the discovery of more efficient red-emitting phosphor materials is essential. In this regard, the hardly explored compound class of nitridoaluminates affords a new material with superior luminescence properties. Doped with Eu²⁺, Sr[LiAl₃N₄] emerged as a new high-performance narrow-band red-emitting phosphor material, which can efficiently be excited by



GaN-based blue LEDs. Owing to the highly efficient red emission at $\lambda_{\text{max}} \sim 650 \text{ nm}$ with a full-width at half-maximum of $\sim 1,180 \text{ cm}^{-1}$ ($\sim 50 \text{ nm}$) which shows only very low thermal quenching ($>95\%$ relative to the quantum efficiency at $200 \text{ }^\circ\text{C}$), a prototype phosphor-converted LED (pc-LED), employing Sr[LiAl₃N₄]:Eu²⁺ as the red-emitting component, already shows an increase of 14% in luminous efficacy compared to a commercially available high colour rendering index (CRI) LED, together with an excellent colour rendition ($R_{a8} = 91$, $R_9 = 57$). Therefore, we predict great potential for industrial applications in high-power white pc-LEDs.

3.4.1 Article

Energy efficiency has become an increasingly important criterion for pervasive products such as light sources. Replacing energy-wasting traditional light sources such as incandescent lamps with energy-efficient LED lamps is considered a major step towards reducing electrical energy consumption worldwide.^[1-7] LEDs are based on semiconductor technology, where each single emitter can produce only one single colour tone. General lighting and illumination, however, require white light covering the whole spectral range (blue to red). To create a white-light phosphor-converted (pc-)LED, a blue LED die (440-470 nm) is typically covered with either a yellow-green phosphor (single phosphor approach) or a combination of red and green phosphors (multi-phosphor approach), such that the combination of the light generated by the phosphor layer and the blue light leaking through creates white light.^[8,9] Most commercially available single-phosphor pc-LEDs are based on Ce³⁺-doped garnet materials (YAG:Ce; Y_{3-x}Gd_xAl_{5-y}Ga_yO₁₂:Ce) as the yellow-emitting phosphor material. YAG:Ce possesses many favourable properties, such as broadband emission in the visible spectral region (500-700 nm), efficient absorption of blue light (~420-480 nm) and excellent chemical and thermal stability.^[10,11] A major drawback of this material is the limited spectral power distribution in the red spectral range, which limits the application range to cool white light (correlated colour temperature 4,000-8,000 K), and limited colour rendering index (CRI usually < 75; see detailed explanation in the Supplementary Information; refs 12-14). For illumination-grade lighting, however, lower correlated colour temperatures (2,700-4,000 K) and higher CRIs ($R_a > 80$) are required.^[15] The challenge for the solid-state lighting industry is to further improve the colour rendition of illumination-grade light sources without compromising energy efficiency, by means of better adapting the pc-LED emission to the sensitivity of the human eye, resulting in a high luminous efficacy (efficiency of light conversion relative to human vision; see detailed explanation in the Supplementary Information in chapter 6.3). Achieving this goal depends critically on the spectral peak position and width of the red-emitting component.^[8] At present, the number of red-emitting phosphor materials which are adequate for high-luminance pc-LED applications (blue light output >100 W·cm⁻²) is rather small owing to the very demanding requirements (high conversion efficiency at temperatures up to 200 °C and high degradation resistance). Eu²⁺ doped materials such as (Ba,Sr)₂Si₅N₈:Eu²⁺ ($\lambda_{em} \sim 590-625$ nm, full-width at half-maximum (FWHM) $\sim 2,050-2,600$ cm⁻¹; refs 8,16,17) or (Ca,Sr)SiAlN₃:Eu²⁺ ($\lambda_{em} \sim 610-660$ nm, FWHM $\sim 2,100-2,500$ cm⁻¹; refs 18,19) have found applications in commercially available illumination-grade white pc-LEDs. The rather broad emission bands of these materials greatly

limit the maximum achievable luminous efficacies of high-quality warm-white pc-LEDs (CRI > 90) because a significant part of the light is produced outside the sensitivity range of the human eye above 700 nm. Materials with narrower emission such as the sulphide material Sr_{1-x}Ca_xS:Eu²⁺ ($\lambda_{em} \sim 615\text{-}650$ nm, FWHM $\sim 1,550\text{-}1,840$ cm⁻¹) exhibit attractive luminescence properties,^[20] but limitations such as strong emission quenching with temperature, high sensitivity towards hydrolysis (due to the rather ionic nature of binary sulphides) and the toxicity of the hydrolysis products (H₂S gas) hinders practical application. Here we report on a new, environmentally friendly, next-generation red-emitting phosphor material with superior luminescence properties.

The design of a new narrow-band red-emitting nitride phosphor material was successfully accomplished by synthesizing a nitridoaluminate as a novel type of host lattice for Eu²⁺ activators. The replacement of commercial red phosphor materials by the narrow-band red-emitting Sr[LiAl₃N₄]:Eu²⁺ (FWHM $\sim 1,180$ cm⁻¹, ~ 50 nm) results in a significant increase of luminous efficacy in white pc-LEDs with excellent colour rendition (CRI > 90). In the following Sr[LiAl₃N₄]:Eu²⁺ will be abbreviated to SLA.

In the compound class of silicon-free nitridoaluminates, systematic investigations on host lattices for efficient luminescent materials have not yet been performed.

Inspired by naturally occurring minerals such as aluminates or silicates, we adopted the structural chemistry to an oxygen-free nitride material, which has been synthesized at a relatively moderate temperature of 1,000 °C. However, the creation of synthetic nitridoaluminates means more than simply substituting O by N in classical (oxo)aluminates. The introduction of nitrogen leads to a significantly increased structural variety, up to highly condensed sphalerite-type frameworks of AlN₄ tetrahedra, even with highly condensed ammonium-type N^[4], connecting up to four neighbouring Al tetrahedral centres.^[21] The higher degree of condensation leads not only to increased stability of the materials compared to phosphors with terminal or ionic O or S atoms, which tend to hydrolyse over time, but also to high rigidity of the host lattice and thus to limited local structural relaxation of the Eu²⁺ site in its excited state - a prerequisite for the desired small Stokes shifted, narrow-band emission.^[22]

Excitation and emission spectra of SLA with a 0.4% dopant concentration are shown in Fig. 1a. SLA exhibits an excitation minimum at 375 nm followed by a broad absorption band with a maximum value at ~ 466 nm. Up to 490 nm the absorption is still above 98% relative to the apex at 466 nm.

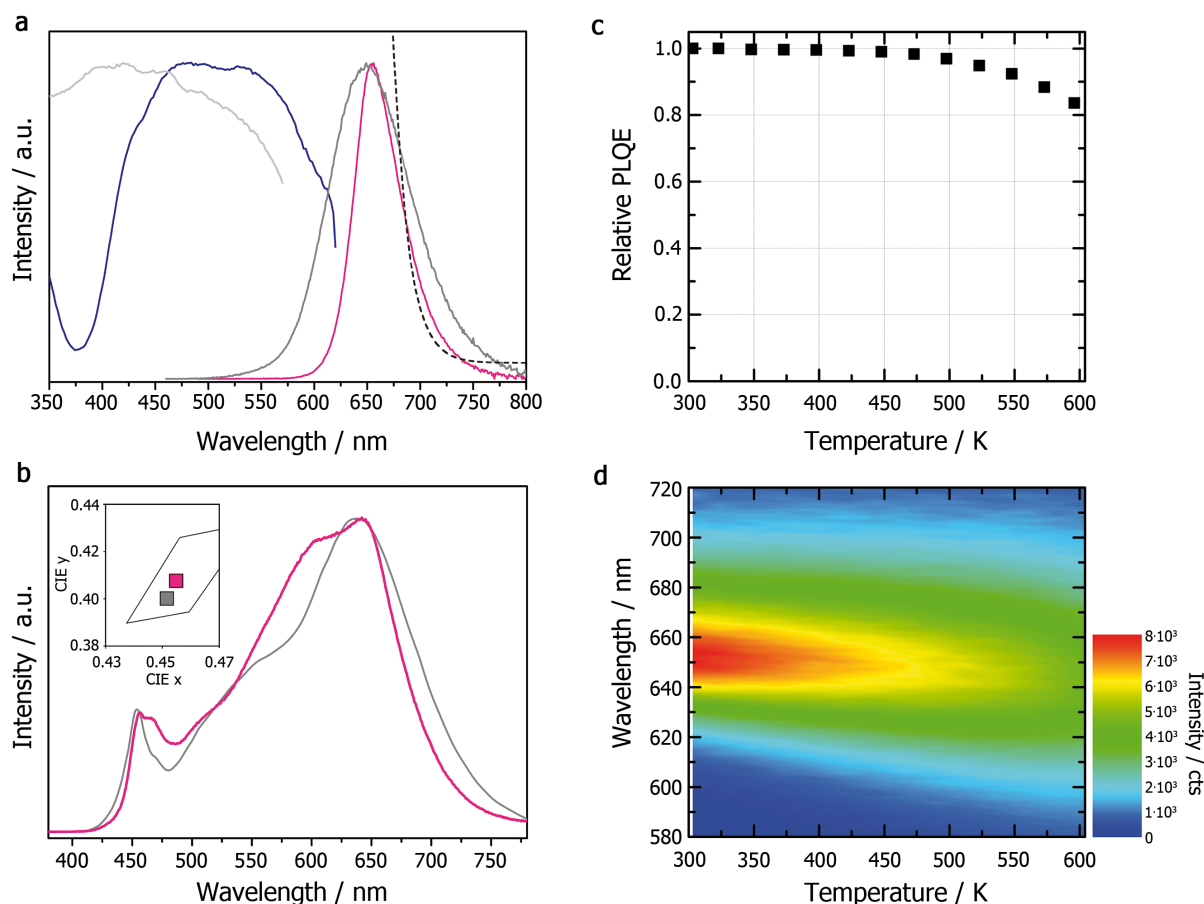


Figure 1. Photoluminescence properties of next-generation red-emitting Sr[LiAl₃N₄]:Eu²⁺. **a**, Excitation (SLA (blue); CaAlSiN₃:Eu²⁺ (grey)) and emission spectra for $\lambda_{\text{exc}} = 440$ nm of SLA (pink) and of CaAlSiN₃:Eu²⁺ (dark grey). The dotted curve indicates the upper limit of sensitivity of the human eye.^[23] **b**, Luminescence spectra of pc-LEDs with a correlated colour temperature of 2,700 K. Pink curve: LED with Lu₃Al₅O₁₂:Ce³⁺ (green phosphor), (Ba,Sr)₂Si₅N₈:Eu²⁺ (orange phosphor) and SrLiAl₃N₄:Eu²⁺ (red phosphor) mix. Grey curve: commercially available high-CRI LED. The pc-LED consisting of the narrow-band red-emitting phosphor shows a 14% increased luminous efficacy and excellent colour rendition ($R_a = 91$, $R_9 = 57$). The inset shows the CIE 1931 colour coordinates of the LEDs. Both LEDs show colour coordinates within the 2,700 K ANSI C78.377A white colour bin (black line). **c**, Temperature dependence of the relative integrated photoluminescence intensity for SLA, revealing a decrease of only 5% from the room-temperature quantum efficiency at 500 K. **d**, Temperature dependence of the spectral emission, showing a small shift towards higher energies with temperature.

The maximum of the emission is at $\lambda_{\text{em}} = 654$ nm, with a FWHM of only 1,180 nm. The external (internal) quantum efficiency of a powder layer of SLA is close to 52 (76)% for 440 nm excitation. The grey curve in Fig. 1a shows the emission of a commercially available CaAlSiN₃:Eu²⁺ phosphor (external (internal) quantum efficiency of 74 (96)% for 440 nm excitation) which is currently applied in warm-white high-power pc-LEDs, with a similar

peak wavelength of $\lambda_{\text{em}} = 649$ nm. Here a significant part of the emission is produced in spectral regions where the human eye sensitivity is low (dotted curve; ref. 23), resulting in a significantly limited luminous efficacy of the warm-white pc-LED. A comparison of emission intensities under 440 nm steady-state excitation of both materials can be found in Supplementary Fig. 1 in chapter 6.3. The remarkably reduced FWHM of SLA (Fig. 1a) concentrates the emitted light in the visible spectral region while further enhancing the chromatic saturation of the red spectrum with respect to the reference material.

As shown in Fig. 1, the emission spectrum of SLA is remarkably narrow for an efficient Eu²⁺-system emitting in the red spectral region. Such a uniquely narrow red emission band, combined with strong absorption in the blue spectral range (Fig. 1a), is highly desirable for high-quality solid-state lighting applications. The origin of this narrow red emission can be ascribed to a combination of properties of the host lattice. Diffuse reflection spectra of doped and undoped samples are shown in Supplementary Fig. 2 in chapter 6.3. Two broad absorption bands with maxima at ~ 320 and ~ 470 nm are observed for the Eu²⁺-doped sample. With respect to the spectrum of the undoped sample, the high-energy band corresponds mainly to absorption of the host lattice, whereas the low-energy absorption band can be assigned to $4f^7(^8S_{7/2}) \rightarrow 4f^6(^7F)5d^1$ transitions within Eu²⁺. The optical bandgap is estimated to 4.7 eV. A comparison with the energy levels determined for cubic CaS:Eu²⁺ indicates that the bandgap of SLA is smaller (~ 0.5 eV), although the position, shape and width of the low-energy absorption bands are very similar, indicating comparable centroid shifts and energetic separation of the Eu²⁺ 5d levels.^[24]

In Fig. 1b, the luminescence spectrum of a commercially available high-CRI LED (grey curve) is compared with the spectrum of a prototype pc-LED with a Lu₃Al₅O₁₂:Ce³⁺ (green), (Ba,Sr)₂Si₅N₈:Eu²⁺ (orange) and SrLiAl₃N₄:Eu²⁺ (red) phosphor mix (pink curve). Both pc-LEDs exhibit a correlated colour temperature of 2,700K (see Fig. 1b inset). The pc-LED consisting of the narrow-band red-emitting phosphor shows a 14% increased luminous efficacy and excellent colour rendition ($R_a = 91$, $R_9 = 57$). Figure 1c,d shows the temperature dependence of the relative integrated photoluminescence intensity of a typical SLA sample. At 500 K the integrated light output drops by only 5%, which is comparable to the performance of highly efficient Ce³⁺ doped garnet phosphors. The change in chromaticity with temperature is low - from 303 K to 465 K the CIE (Commission Internationale de l'Éclairage) colour coordinates and the lumen equivalent of the emission shift from $x, y = 0.692, 0.306$ and $LE = 77$ lm/W_{opt} to $x, y = 0.668, 0.330$ and $LE = 114$ lm/W_{opt}. In this temperature range the emission band shifts by ~ 1 nm towards higher energies while the

spectrum broadens by 374 cm⁻¹. As the sensitivity curve of the human eye is very steep in the saturated red spectral range (see Fig. 1a, dashed curve), even small changes in emission peak position and width have a great impact on the spectral lumen equivalent. However, for a composed white spectrum with a centroid wavelength at approximately 580 nm the impact of these changes is small, because the human eye is most sensitive in the green-yellow spectral range. Hence, the colour point of a white pc-LED in the given temperature range shifts within a three-step MacAdam ellipse.^[25] Furthermore, the temperature rise of the LED chip from room temperature to operating temperature (~330-360 K) is typically reached within milliseconds and can therefore hardly be noticed by the human eye. Moreover, adjustments of colour rendering parameters for a given application temperature can be carried out by tuning the relative concentrations of the different phosphor materials in a pc-LED.

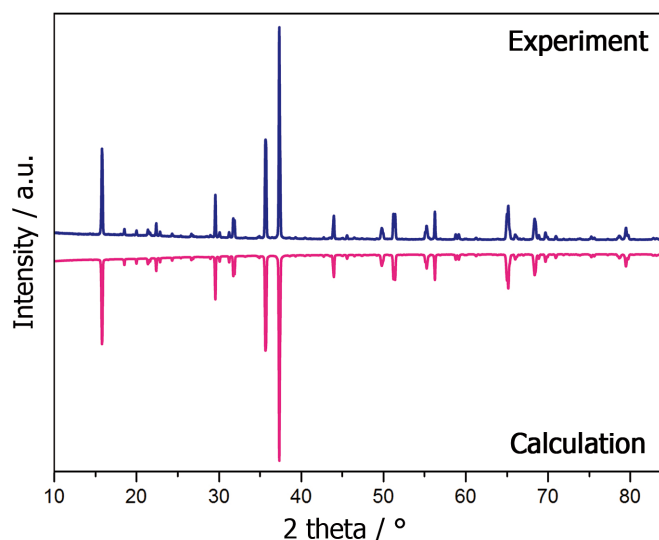


Figure 2. Crystal structure characterization of next-generation red-emitting Sr[LiAl₃N₄]:Eu²⁺. X-ray powder diffraction pattern of SLA with the measured histogram (blue line) and the calculated pattern based on Rietveld refinement data (pink line).

The crystal structure of Sr[LiAl₃N₄]:Eu²⁺ was solved and refined from single-crystal and powder X-ray diffraction (XRD) data in the triclinic space group $P\bar{1}$ (no. 2) with unit cell parameters $a = 5.86631(12)$ Å, $b = 7.51099(15)$ Å, $c = 9.96545(17)$ Å, $\alpha = 83.6028(12)^\circ$, $\beta = 76.7720(13)^\circ$ and $\gamma = 79.5650(14)^\circ$, and is isotypic to the oxoplumbate Cs[Na₃PbO₄] (ref. 26). To validate the triclinic structure model, theoretical calculations were performed using Rietveld methods on powder XRD data. A comparison of the measured powder XRD with the results of the calculation is shown in Fig. 2 and a detailed plot of the Rietveld refinement is presented in Supplementary Fig. 3 in chapter 6.3. Eu²⁺ as dopant (0.2 mol%) was neglected for structure determination because of its insignificant contribution to the

scattering density. In addition to the reflections of SLA, some weak reflections of SrO have been found in the XRD (Supplementary Fig. 3 in chapter 6.3). The secondary phase was quantified to 0.28 wt% from Rietveld refinement. The crystallographic data of SLA is summarized in Supplementary Table 1 and the atomic coordinates and isotropic displacement parameters are given in Supplementary Table 2 in chapter 6.3. Selected interatomic distances and bond angles are listed in Supplementary Tables 3 and 4 in chapter 6.3.

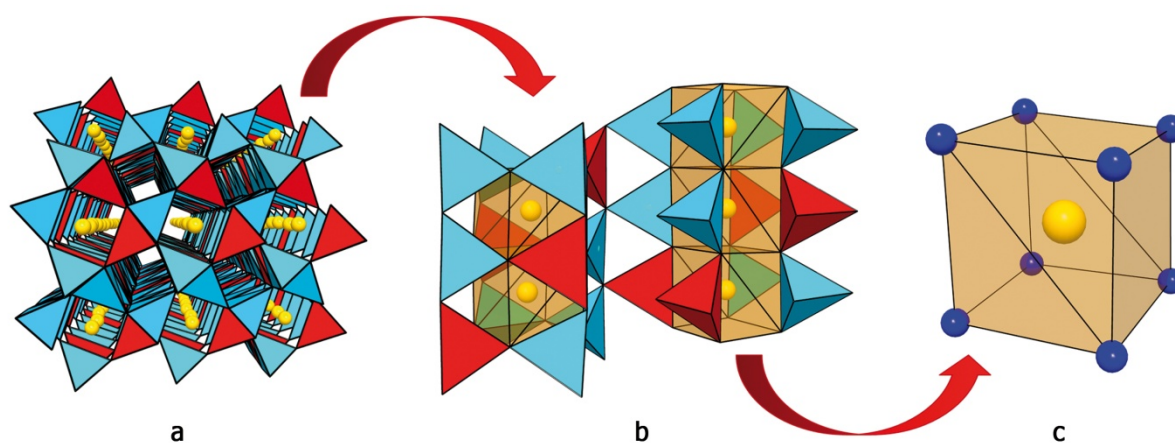


Figure 3. Structural overview of next-generation red-emitting Sr[LiAl₃N₄]:Eu²⁺. Yellow spheres are Sr; blue tetrahedra are AlN₄; red polyhedra are LiN₄, blue spheres are N. **a**, Perspective view with channels of *vierer* rings along [011]. **b**, Strands of face-sharing cuboid-like SrN₈ polyhedra coordinated by AlN₄ and LiN₄ tetrahedra. **c**, Cuboid-like SrN₈ polyhedron.

Figure 3 shows a structural overview of the host lattice, where a highly condensed, rigid framework of ordered edge- and corner-sharing AlN₄ and LiN₄ tetrahedra (Al-N: 1.87-2.00 Å and Li-N: 1.98-2.10 Å) with channels of vierer rings along [011] is obtained (see Fig. 3b; the term *vierer* ring refers to four polyhedra connected to each other to form a ring, and is a nomenclature established in ref. 27). The degree of condensation κ , which is equal to the atomic ratio (Al,Li):N, in this compound is unity, like in aluminium nitride. The net negative charge of the [LiAl₃N₄]²⁻ framework is compensated by incorporating Sr²⁺ ions in every second channel. There are two crystallographic Sr sites, each coordinated by eight N atoms (Sr-N: 2.69-2.91 Å) in a highly symmetric cuboid-like environment (Fig. 3c), which is extremely favourable for narrow emission bands (see below). The SrN₈ polyhedra are connected by common faces, forming endless strands along [011], with Sr-Sr distances of 3.27 Å. The Eu²⁺ dopant is expected to replace Sr ions, as the ionic radii of Eu²⁺ (1.25 Å) and Sr²⁺ (1.26 Å) are almost identical.^[28]

The atomic ratios Sr(1):Al(3.2):N(4.7) determined by energy-dispersive X-ray (EDX) spectroscopy are in good accordance with the formula Sr[LiAl₃N₄]:Eu²⁺ obtained from single-

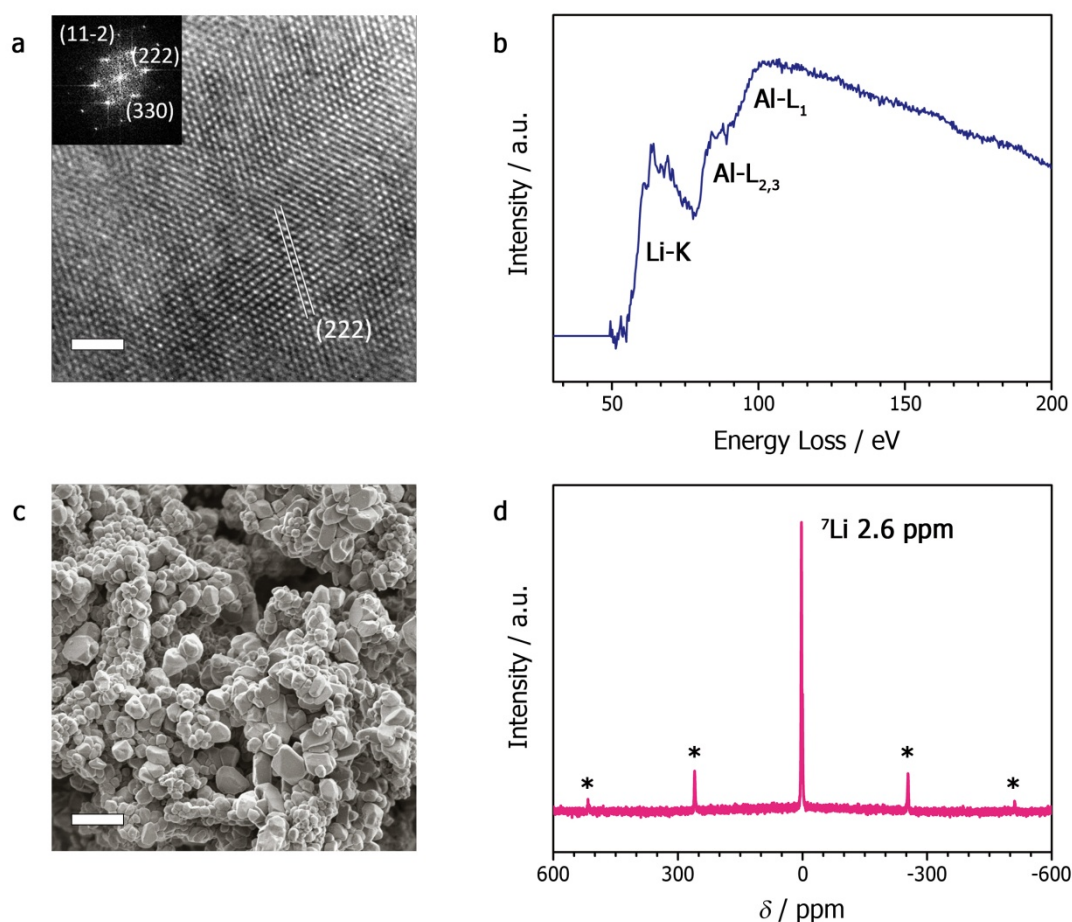


Figure 4. Morphology and composition of next-generation red-emitting Sr[LiAl₃N₄]:Eu²⁺. **a**, High-resolution TEM image of SLA and the corresponding fast Fourier transformation in the inset. The image was detected in the zone axis $[\bar{1}10]$ orientation. Scale bar, 2 nm. **b**, EELS spectrum of SLA. The energy loss region of the Li-K, Al-L_{2,3} and Al-L₁ edges is shown. The background in front of the Li-K edge is subtracted. **c**, SEM image of SLA bulk material. Scale bar, 5 μm . **d**, ⁷Li solid-state MAS-NMR spectrum. Rotation sidebands are indicated by asterisks (rotation frequency 50 kHz).

crystal and powder XRD data. Within the estimated standard deviation of this method oxygen concentrations are below the detection limit.

High-resolution transmission electron microscopy (HRTEM) images of SLA, shown in Fig. 4a, confirmed the ordered structure. The image was taken in the $[\bar{1}10]$ zone axis orientation, as visible in the fast Fourier transformation investigations (inset Fig. 4a). To verify the inclusion of Li in the structure, electron energy-loss spectroscopy (EELS) measurements were performed in TEM. The Li-K edge in Fig. 4b occurs at around 58 eV and shows a main peak at 64 eV, which exhibits a split of 1 eV and a smaller peak at around 61 eV. Also the Al-L_{2,3} and Al-L₁ edges can be seen in the spectrum shown in Fig. 4b. The onset at 73 eV of the Al-L_{2,3} edge overlaps with the Li-K edge, but the shape of the Al edges correlates with data published in the literature, the peak maximum being determined to be 85 eV, which is in

good accordance with the values obtained from the literature.^[29] The Li-K edge shows a slight deviation compared to the literature data; for example, Li_xTiP (x = 2-11), Li₂CaSi₂N₄ or Li₂SrSi₂N₄, due to different bonding types.^[30,31] However, the EELS measurements clearly confirm the presence of Li and Al in the structure. The scanning electron microscope (SEM) image in Fig. 4c shows the crystalline morphology of SLA, with particle sizes below 5 μm. To further confirm the incorporation of Li, we carried out ⁷Li solid-state magic angle spinning nuclear magnetic resonance (MAS-NMR) spectroscopy. The NMR spectrum of SLA in Fig. 4d indicates one sharp isotropic signal, giving some evidence for the incorporation of Li in the framework. The observed chemical shift value of δ = 2.6 ppm with a FWHM of 2.1 ppm (Fig. 4d) is comparable to that of nitridosilicates such as LiCa₃Si₂N₅ (δ = 2.7 ppm; ref. 32) or Li₂SrSi₂N₄ (δ = 2.0 ppm; ref. 31). The existence of only one signal in the ⁷Li spectra can be ascribed to the limited resolution of ⁷Li, as also observed, for example, in Li₂SiN₂, where eight independent crystallographic positions for lithium also result in only one signal in the solid-state MAS NMR-spectroscopy.^[33]

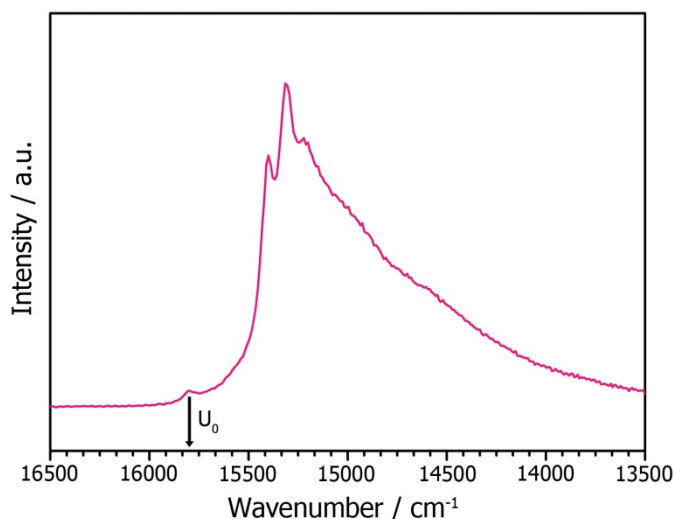


Figure 5. Low-temperature luminescence of next-generation red-emitting Sr[LiAl₃N₄]:Eu²⁺. Emission spectrum for excitation of SLA at λ_{exc} = 470 nm at 6 K with the vibronic structure of the emission transitions. The black arrow indicates the zero phonon line energy U₀ at 15,797 cm⁻¹.

As indicated, the structural features are in direct correlation with the luminescence properties. The host lattice is built up from an ordered, rigid [LiAl₃N₄]²⁻ framework with κ = 1. We believe that the rigidity limits geometrical relaxations and thus the Stokes shift of the luminescence (956 cm⁻¹) which could be accurately determined by low-temperature emission measurements, shown in Fig. 5, because of the well-resolved vibronic structure of the emission transitions, with the zero phonon line energy U₀ at 15,797 cm⁻¹. Also the low number of vibronic structures in the high-energy tail of the emission band (derived phonon

energy from the separation of the vibronic features: $\sim 202\text{ cm}^{-1}$) indicate only a weak electron-phonon coupling of Eu²⁺ in SrLiAl₃N₄ (ref. 34). Furthermore, it is beneficial that both Sr sites are coordinated in almost identical spheres and not affected by the statistical distribution of the surrounding network cations Al and Li. A statistical distribution in this case, as observed for Si and Al in CaAlSiN₃:Eu²⁺, would lead to constantly varying bonding distances (Al,Li)-N in the tetrahedral spheres, attended by a wide variety of activator-N bond length and environments. Owing to comparable crystal-field splitting effects for both sites, inhomogeneous line broadening of the emission band, resulting from different activator environments, is reduced to a minimum. (Ba,Sr)₂Si₅N₈:Eu²⁺ also shows two crystallographic sites that can be occupied by Eu²⁺. As a result of the larger chemical differences of the respective sites, the emission maxima and Stokes shifts are more distinct and thus lead to a relatively broad composite emission (FWHM $\sim 2,050\text{-}2,600\text{ cm}^{-1}$; refs 8,16,17,35). A comparison of the local Eu²⁺ coordination geometry of SLA with Eu²⁺ in BaSi₂O₂N₂:Eu²⁺, a narrow-band green emitter (490 nm peak emission, FWHM $\sim 1,250\text{ cm}^{-1}$) with a surprisingly similar cuboidal coordination,^[36-41] suggests that such a structural motif results in a small Stokes shift and thus in a narrow emission bandwidth, most likely due to hindered structure relaxation around the activator in its excited state.^[42] Larger Stokes shifts and thus broader emission bands observed for Eu²⁺ phosphors have been commonly associated with a more asymmetric dopantsite geometry.^[43] The energy position of the Eu²⁺ $4f^65d^1$ excited state and the $4f^7(^8S_{7/2}) \rightarrow 4f^6(^7F)5d^1$ transition in inorganic hosts is modified by the covalence and polarizability of the Eu²⁺-ligand interactions.^[21,44-47] In SLA, the activator ion is surrounded by a network of condensed AlN₄ and LiN₄ tetrahedra. Therefore, the more polarizable nitridic surroundings lower the excited $4f^65d^1$ state of Eu²⁺ owing to a large crystal field splitting and a strong nephelauxetic effect compared with more ionic-for example, oxidic-environments. This shifts the absorption and emission transitions towards the red spectral region, because the energy difference between the $4f^7$ ground state and the $4f^65d^1$ excited state is reduced.

A variation in dopant concentration hardly changes the emission band position (peak shift from 656 nm for 1mol% Eu to 651 nm for 0.05mol% Eu). This indicates low fluctuations of the local activator chemical environment (no statistical site occupation). In contrast, phosphor materials such as $M_2\text{Si}_5\text{N}_8:\text{Eu}^{2+}$ ($M = \text{Ca, Sr, Ba}$) or $M\text{SiAlN}_3:\text{Eu}^{2+}$ ($M = \text{Ca, Sr}$) exhibit a strong emission band shift with varying activator concentration, owing to more than one alkaline earth cation position in the structure enabling multiple activator sites.^[8,16-19,48]

In summary, we have successfully synthesized a new, unique narrow-band red-emitting nitride phosphor material at a rather moderate temperature of 1,000 °C. Sr[LiAl₃N₄]:Eu²⁺,

with its highly condensed, rigid framework structure, fulfils the requirements for a red emitter in illumination-grade, high-power pc-LED applications. We expect that the superior emission properties of SLA, with $\lambda_{\max} \sim 650$ nm, FWHM $\sim 1,180$ nm, in combination with a very high thermal quenching temperature (>95% relative quantum efficiency at 200 °C) will result in high colour rendition pc-LED light sources with significantly increased luminous efficacies.

3.4.2 Methods

Sr[LiAl₃N₄]:Eu²⁺ (0.4 mol% Eu nominal composition) was synthesized by heating a stoichiometric mixture of LiAlH₄ (Sigma-Aldrich, 95%), AlN (Tokuyama, 99%), SrH₂ (Cerac, 99.5%) and EuF₃ (Sigma-Aldrich, 99.99%) for 2 h to 1,000 °C in a forming gas atmosphere (N₂:H₂ = 95:5). The starting materials were thoroughly ground in a ball mill, filled in a tungsten crucible and heated to the target temperature at a rate of 50 °C·min⁻¹ in a radio-frequency furnace. After a short reaction period the product is obtained in the form of a pink coloured powder, which is stable in ambient air up to 400 °C. Likewise, the material is fully stable under normal air humidity conditions in the LED application (>1,000 h reliability test under industry standard test conditions passed for technology demonstrator LEDs). To meet the long-term reliability requirements of the lighting industry for very harsh environments (for example, T_{ambient} >85 °C, relative humidity >85%) application of a barrier layer coating as applied to most commercial Eu(II) doped LED phosphors may be needed. Extensive reliability investigations of SLA will be part of the further development towards an industrial product.

The crystal structure of Sr[LiAl₃N₄]:Eu²⁺ was determined by single-crystal X-ray diffraction on a Bruker D8 Venture diffractometer (Mo-K α radiation, rotating anode generator, graphite monochromator). Numerical absorption correction using the program PLATON (ref. 49) was applied. The crystal structure was solved using direct methods with SHELXS (ref. 50). The refinement of the structure was carried out by the method of least-squares using SHELXL (ref. 50). Prior to this, selected red luminescent Sr[LiAl₃N₄]:Eu²⁺ single crystals were placed on micromounts (MiTeGen) and checked for quality on a Buerger precession camera.

The crystal structure was also refined using Rietveld methods on the powder X-ray diffraction pattern. Powder diffraction data were collected on a STOE STADI P diffractometer (Cu-K α_1 radiation, Ge(111) monochromator, position sensitive detector) in a transmission geometry. Simulations of Bragg data were performed using the WinXPOW package.^[51] Rietveld refinement was carried out using the TOPAS package.^[52]

Further details of the investigations of the crystal structure can be obtained from the Fachinformationszentrum Karlsruhe, 76344 Eggenstein-Leopoldshafen, Germany (Fax: +49-7247-808-666; E-mail: crysdata@fiz-karlsruhe.de) on quoting the depository number CSD-427067.

The chemical composition of different crystallites was analysed by EDX spectroscopy using a JSM-6500F scanning electron microscope (SEM, Jeol) equipped with a Si/Li EDX detector (Oxford Instruments, model 7418). The EDX data were collected from several particles at an accelerating voltage of 30 kV. Furthermore, the scanning electron microscope was used to collect images of particles to investigate the morphology.

TEM investigations were done using a FEI Titan 80-300 kV microscope equipped with a post-column energy filter (GIF Tridiem from Gatan) and an EDAX energy-dispersive X-ray detector for analytical characterizations. The electron diffraction data were evaluated using a calibrated camera constant obtained by means of a Si standard. The EELS measurements were done in diffraction mode using a selected area diffraction aperture giving a circular area of about 150 nm in diameter to prevent beam damage. We used a 2 mm entrance aperture in the spectrometer and a camera length of 130 mm, resulting in a collector angle of 13.5 mrad.

The EELS data were detected with an energy resolution of about 0.9-1.2 eV, as determined by the FWHM of the zero loss peak. The data were obtained with a dispersion of 0.3 eV/channel. The acquisition time was 10 s for the Li-K, Al-L_{2,3} and Al-L₁ edges. All data were corrected for channel-to-channel gain variation and dark current. The pre-edge background of the Li-K edge was extrapolated by using a first-order log-polynomial function and subtracted from the original spectra.^[53]

Solid-state MAS-NMR experiments were performed at 11.74 T on a Bruker 500 Advance III FT spectrometer equipped with a commercial 1.3 mm triple-resonance MAS probe at a ⁷Li frequency of 194.416 MHz. All experiments were performed in ZrO₂ rotors at room temperature. The chemical shift of ⁷Li is reported using the frequency ratios published by IUPAC [δ scale relative to 1% tetramethylsilane (TMS) in CDCl₃] (ref. 54). The ⁷Li MAS-NMR spectrum was acquired with a 90° pulse length of 1.0 μ s, a recycle delay of 64 s and a sample spinning frequency of 50 kHz.

Initial luminescence investigations on single crystals of the title compound have been performed with the aid of a luminescence microscope consisting of a Horiba Fluorimax4 spectrofluorimeter system attached to an Olympus BX51 microscope via fibre optics. Photoluminescence measurements on powder samples were carried out with an in-house-built system based on a 5.3" integrating sphere and a spectrofluorimeter equipped with a 150 W Xe

lamp, two 500 mm Czerny-Turner monochromators, 1,800 1/mm lattices and 250/500 nm lamps, with a spectral range from 230 to 820 nm. Low-temperature emission spectra of powder samples were recorded with an Ocean Optics HR2000 + ES spectrometer (2,048 pixels, grating UA (200-1,100 nm), slit-50) with the samples mounted in a closed-cycle He cryostat.

The samples were measured on PTFE sample holders. The excitation wavelength was chosen to be 440 nm with a spectral width of 10 nm. The emission spectra were recorded in the wavelength range between 460 nm and 820 nm with a 1 nm step size. Excitation spectra were monitored in the 630-690 nm wavelength range under an excitation wavelength range from 350 to 570 nm with a 2 nm step size. For the measurement of the photoluminescence quantum efficiency, commercially available CaAlSiN₃:Eu²⁺ with an external (internal) quantum efficiency of 74 (96)% at a 440 nm excitation wavelength was used as the reference phosphor.

3.4.3 References

- [1] C. Che, R.-S. Liu, *J. Phys. Chem. Lett.* **2011**, *2*, 1268.
- [2] X.-H. He, N. Lian, J.-H. JSun, M.-Y. Guan, *J. Mater. Sci.* **2009**, *44*, 4763.
- [3] H. A. Höpfe, *Angew. Chem. Int. Ed.* **2009**, *48*, 3572.
- [4] M. Mikami, H. Watanabe, K. Uheda, S. Shimooka, Y. Shimomura, T. Kurushima, N. Kijima, *IOP Conf. Ser.: Mater. Sci. Eng.* **2009**, *1*, 012002.
- [5] R.-J. Xie, N. Hirosaki, *Sci. Technol. Adv. Mater.* **2007**, *8*, 588.
- [6] R.-J. Xie, N. Hirosaki, Y. Li, T. T., *Materials* **2010**, *3*, 3777.
- [7] S. Ye, F. Xiao, Y. X. Pan, Y. Y. Ma, Q. Y. Zhang, *Mater. Sci. Eng. R.* **2010**, *71*, 1.
- [8] M. Krames, G. O. Mueller, R. B. Mueller-Mach, H. Bechtel, P. J. Schmidt, *PCT Int. Appl.*, WO 2010131133, A1, **2010**.
- [9] R. Mueller-Mach, G. O. Mueller, M. R. Krames, T. Trottier, *IEEE J. Select. Top. Quant. Electron.* **2002**, *8*, 339.
- [10] A. A. Setlur, *Electrochem. Soc. Interface* **2009**, *18*, 32.
- [11] D. J. Robbins, *J. Electrochem. Soc.* **1979**, *126*, 1150.
- [12] S. Nakamura, G. Fasol, *The blue laser diode*, Springer, Berlin, Germany, **1997**.
- [13] S. Nakamura, *Proc. SPIE* **1997**, *3002*, 26.
- [14] P. Schlotter, R. Schmidt, J. Schneider, *Appl. Phys. A.* **1997**, *64*, 417.
- [15] M. R. Krames, O. B. Shchekin, R. Mueller-Mach, G. O. Mueller, L. Zhou, G. Harbers, M. G. Craford, *J. Disp. Tech.* **2007**, *3*, 160.

- [16] H. A. Höpfe, H. Lutz, P. Morys, W. Schnick, A. Seilmeier, *J. Phys. Chem. Solids* **2000**, *61*, 2001.
- [17] R. Mueller-Mach, G. Mueller, M. R. Krames, H. A. Höpfe, F. Stadler, W. Schnick, T. Juestel, P. Schmidt, *Phys. Status Solidi A* **2005**, *202*, 1727.
- [18] K. Uheda, N. Hirosaki, H. Yamamoto, *Phys. Stat. Sol. A* **2006**, *11*, 2712.
- [19] K. Uheda, N. Hirosaki, Y. Yamamoto, A. Naita, T. Nakajima, H. Yamamoto, *Electrochem. Solid State Lett.* **2006**, *9*, H22.
- [20] R. Mueller-Mach, G. Mueller, *Proc. of SPIE* **2000**, 3938, 30.
- [21] M. Zeuner, S. Pagano, W. Schnick, *Angew. Chem. Int. Ed.* **2011**, *50*, 7754.
- [22] G. Blasse, A. Bril, *Philips Tech. Rev.* **1970**, *31*, 314.
- [23] J. J. Vos, *Color Research and Application* **1978**, *3*, 125.
- [24] N. Yamashita, O. Harada, K. Nakamura, *Jpn. J. Appl. Phys.* **1995**, *34*, 5539.
- [25] D. L. MacAdam, *J. Opt. Soc. Amer.* **1942**, *32*, 247.
- [26] H. Stoll, R. Hoppe, *Rev. Chim. Min.* **1987**, *24*, 96.
- [27] F. Liebau, *Structural chemistry of silicates*, Springer, Berlin, **1985**.
- [28] R. D. Shannon, *Acta Crystallogr. Sect. A: Found. Crystallogr.* **1976**, *32*, 751.
- [29] C. Scheu, G. Dehm, H. Müllejans, R. Brydson, M. Rühle, *Microsc. Microanal. Microstruct.* **1995**, *6*, 19.
- [30] V. Mauchamp, P. Moreau, L. Monconduit, M.-L. Doublet, F. Boucher, G. Ouvrard, *J. Phys. Chem. C* **2007**, *111*, 3996.
- [31] M. Zeuner, S. Pagano, S. Hug, P. Pust, S. Schmiechen, C. Scheu, W. Schnick, *Eur. J. Inorg. Chem.* **2010**, 4945.
- [32] S. Lupart, W. Schnick, *Z. Anorg. Allg. Chem.* **2012**, 638, 2015.
- [33] S. Pagano, M. Zeuner, S. Hug, W. Schnick, *Eur. J. Inorg. Chem.* **2009**, 1579.
- [34] B. Henderson, G. F. Imbusch, *Optical spectroscopy of inorganic solids*, Oxford University Press, **2006**.
- [35] T. Schlieper, W. Milius, W. Schnick, *Z. Anorg. Allg. Chem.* **1995**, *621*, 1380.
- [36] J. Botterman, K. Van den Eeckhout, I. de Baere, D. Poelman, P. F. Smet, *Acta Mater.* **2012**, *60*, 5494.
- [37] J. A. Kechele, O. Oeckler, F. Stadler, W. Schnick, *Solid State Sci.* **2009**, *11*, 537.
- [38] Y. Q. Li, A. C. A. Delsing, G. de With, H. T. Hintzen, *Chem. Mater.* **2005**, *17*, 3242.
- [39] M. Seibald, T. Rosenthal, O. Oeckler, W. Schnick, *Crit. Rev. Solid State Mater. Sci.* **2014**, *39*, 215.
- [40] L. Wang, H. Ni, Q. Zhang, F. Xiao, *J. Alloys Compd.* **2011**, *509*, 10203.

- [41] B.-G. Yun, T. Horikawa, H. Hanzawa, K. Machida, *J. Electrochem. Soc.* **2010**, *157*, J364.
- [42] A. Meijerink, G. Blasse, *J. Lumin.* **1989**, *43*, 283.
- [43] G. J. Dirksen, G. Blasse, *J. Solid State Chem.* **1991**, *92*, 591.
- [44] P. Dorenbos, *J. Solid State Sci. Technol.* **2013**, *2*, R3001.
- [45] P. Dorenbos, *Phys. Rev. B.* **2000**, *62*, 15640.
- [46] P. Dorenbos, *Phys. Rev. B.* **2001**, *64*, 125117.
- [47] P. Dorenbos, *Phys. Rev. B.* **2002**, *65*, 235110.
- [48] Y. Q. Li, J. E. J. van Steen, J. W. H. van Krevel, G. Botty, A. C. A. Delsing, F. J. DiSalvo, G. deWith, H. T. Hintzen, *J. Alloys Compd.* **2006**, *417*, 273.
- [49] A. L. Spek, PLATON - A Multipurpose Crystallographic Tool, v1.07; Utrecht University: Utrecht, Netherlands, **2003**.
- [50] G. M. Sheldrick, *Acta Crystallogr., Sect. A: Found. Crystallogr.* **2008**, *64*, 112.
- [51] Stoe & Cie GmbH, WINXPOW - Program for powder data handling, **2007**, v2.21, Darmstadt, Germany.
- [52] A. Coelho, TOPAS - Academic **2007**, Brisbane: Coelho Software.
- [53] R. F. Egerton, *Electron Energy-Loss Spectroscopy in the Electron Microscope*; 3rd ed., Springer, New York, **2011**.
- [54] R. K. Harris, E. D. Becker, S. M. Cabral de Menezes, R. Goodfellow, P. Granger, *Solid State Nucl. Magn. Reson.* **2002**, *22*, 458.

3.5 Investigations of the Electronic Structure and Bandgap of the Next-Generation LED-Phosphor Sr[LiAl₃N₄]:Eu²⁺ - Experiment and Calculations

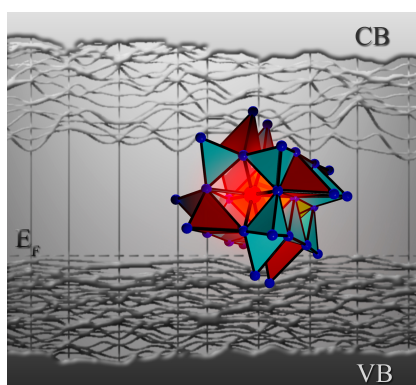
Published in: *Adv. Opt. Mater.* **2015**, 3, 546-550

authors: Thomas M. Tolhurst, Teak D. Boyko, Philipp Pust, Neil W. Johnson, Wolfgang Schnick, Alexander Moewes

DOI: 10.1002/adom.201400558

Copyright © 2015 Wiley-VCH Verlag GmbH & Co. KGaA, Weinheim

<http://onlinelibrary.wiley.com/doi/10.1002/adom.201400558/abstract>



3.5.1 Communication

The research on novel, suitable materials for phosphor-converted light-emitting diodes (pc-LEDs) has attracted a lot of attention in recent years, due to their dramatically increased energy efficiency compared to conventional light sources. The replacement of conventional sources, such as incandescent lamps, is considered a fundamental step toward reducing worldwide electrical energy consumption.^[1] LED efficiency can be captured by the luminous efficacy of the LED, which relates power input to emitted intensity, weighted by the sensitivity of the human eye.^[2,3] The dispersion of the emitted light is therefore of the utmost importance. This will also affect the perceived color of illuminated objects, and is captured by the color rendering index (CRI).^[2] The luminous efficacy is at odds with the CRI and a balance between the two must be struck. The appropriate combination of luminescent materials (phosphors) and excitation method must be selected in order to achieve the desired CRI and luminous efficacy. The resulting pc-LED can be tailored to a variety of lighting needs. Efficient pc-LEDs are typically fabricated using UV to blue emitting InGaN

semiconductor LED chips to excite other phosphors.^[4] The additive mixture of emissions creates white light.^[5] Blue-LED chips coated with broadband yellow emitting Ce³⁺-doped garnet materials have been commercialized, but suffer from variations in color output with applied current and undesirable, low CRI values.^[5,6] An alternative for generating illumination-grade light is the combination of several different phosphor materials on the chip surface (e.g., a yellow-green and red-emitting material).^[7,8] This style gives a high CRI, fair luminous efficacy and stable emissions, but has often suffered from the inefficiency of the available red phosphors.^[5] The ultimate goal is to produce an efficient illumination-grade white light, as measured by the correlated color temperature (CCT). Here, a CCT in the range of 2700–4000 K is desired, which combines a brilliant CRI with optimized luminous efficacy values.^[2,9–11] The spectral position and width of the red-emitting component have the greatest influence on CRI as well as on the luminous efficacy.^[12]

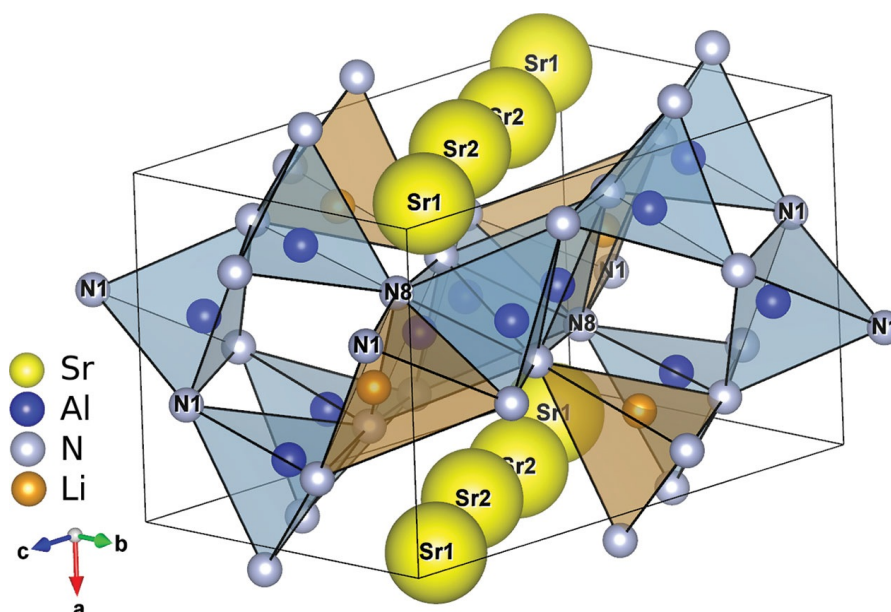


Figure 1. Crystal structure of SLA.

Many red emitters in commercial use produce a significant portion of their light outside of the visible range, limiting their luminous efficacy.^[2] These infrared emissions result in wasted power input and undesirable heating in the device. Therefore, the discovery of a narrow-band red-emitting phosphor material would be a breakthrough in LED technology. On this front, the recently reported nitridolithoaluminate Sr[LiAl₃N₄]:Eu²⁺ (SLA) can be considered a breakthrough material.^[2] With its high emission intensity in the red region of the electromagnetic spectrum and its uniquely narrow bandwidth for an Eu²⁺-doped phosphor, this material shows great potential for use in illumination-grade pc-LEDs. To fully understand the complex structure-property relationships and to enable further optimization of the material properties of Sr[LiAl₃N₄]:Eu²⁺, an in-depth presentation of the electronic structure determined

through experimental soft X-ray spectroscopy measurements and density functional theory calculations is presented here. SLA is found to have an indirect bandgap of (4.56 ± 0.25) eV, highly similar local electronic structure at non-equivalent Sr sites, and the necessary characteristics for a uniform shift in the centroid of the Eu²⁺ 5d states. This clarifies why, with two sites which can be occupied by the activator ion Eu²⁺, such a narrow emission band is still observed and re-enforces the importance of SLA as a phosphor for LED applications.

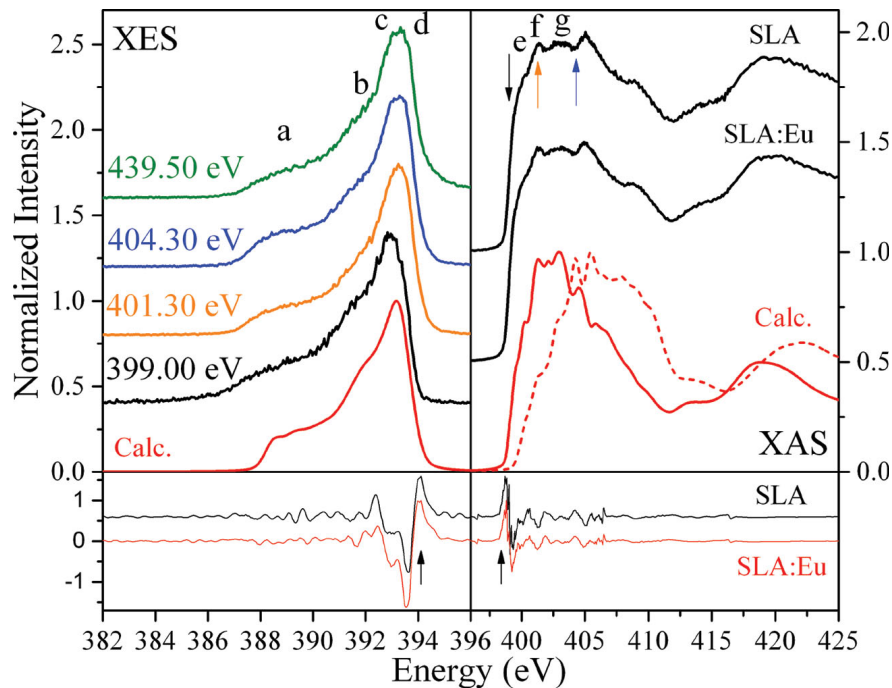


Figure 2. Comparison of XES and XAS spectra from SLA. The XAS spectra for the doped and undoped material are shown. The XES spectra for the doped and undoped sample are identical, therefore only those from the undoped sample are shown. The excitation energy for each XES spectrum is as indicated. Colored arrows on the undoped SLA XAS spectrum indicate excitation energy locations. The red curves are the calculated spectra. The calculated XAS for the ground (dashed line) and excited (solid line) states are shown. Second derivatives of the non-resonant spectra, used to determine the bandgap, are in the lower window. Arrows indicate the maxima selected for the onset of the VB and CB. Prominent features are labeled with lower case Latin letters. The calculated spectra are shifted in energy and slightly broadened to facilitate comparison.

The synthesis and the determination of the crystal structure of SLA are described elsewhere.^[2] The crystal structure of SLA is shown in Figure 1, where the XN₄ (X = Li, Al) tetrahedra can be seen surrounding the Sr sites. The labeling in this figure will be used throughout. The Eu²⁺ ions are assumed to occupy the Sr sites due to their similar ionic radii. X-ray emission spectroscopy (XES) and X-ray absorption spectroscopy (XAS) measurements for the undoped and doped (0.4% Eu²⁺) samples are shown in Figure 2, where they are compared to the calculated spectra. The measured spectra for the doped and undoped sample are largely

identical. This is expected for the low dopant concentrations dealt with here, because it is the N sites being probed and the RE ions are expected to be largely atomic in nature, having little influence on the bonding in the crystal. It can be safely assumed that the calculation results for the undoped sample are largely applicable to the doped sample.

In the XES spectra the same peaks (*a*, *b*, *c*, and *d* as marked on the non-resonant spectrum) are observed throughout. The high-energy shoulder *d* becomes suppressed at the lowest excitation energy. This same feature is augmented under 401.30 eV excitation. Feature *a* increases in intensity under 404.30 eV excitation. These slight changes in the emission spectra are attributed to the preferential excitation of non-equivalent N sites. By comparing the calculated density of states (DOS) of the non-equivalent N sites, the variations can be accounted for, supporting the calculated electronic structure of SLA.

Table 1. Determined experimental and theoretical bandgaps for SLA.

SLA Band Gap			
Experimental	GGA-PBE	LDA-mBJ	Literature ^[2]
(4.56 ± 0.25) eV	2.90 eV	4.14 eV	≈4.7 eV

Using the second derivative method on the non-resonant (439.50 eV excitation) XES and XAS spectra, an initial estimate of the bandgaps for the undoped and doped samples is found to be (4.30 ± 0.25) eV and (4.31 ± 0.25) eV respectively. The peaks in the second derivatives of the spectra used to determine the bandgaps,^[13] are shown in Figure 2. It is the bandgap of the material in its ground state that is desired, making it necessary to account for the core-hole effect.^[13] In this vein the Density Functional Theory (DFT) calculations suggest a 0.26 eV increase in energy for each of these values, leading to final, experimental bandgaps of (4.56 ± 0.25) eV and (4.57 ± 0.25) eV respectively for the undoped and doped samples. These constitute an upper limit for the bandgap, due to the inevitable overestimation of the core hole effect. This stems from differences in the shielding of the effective charge of the core hole in the modeled system, when compared to the actual system during collection of the XAS spectra. The bandgap determined through the GGAPBE (Generalized Gradient Approximation of Perdew, Burke, and Ernzerhof) calculations is 2.90 eV, which as expected is much smaller than the experimental value. For accurate results a LDA-mBJ (Local Density Approximation with modified Becke-Johnson potential) calculation was performed, which yielded a bandgap of 4.14 eV. There is near agreement between the shifted, measured bandgaps, and the mBJ value. Considering the uncertainty in the measured bandgaps and a 10% error margin for the mBJ calculation,^[14] the results agree. The final experimental

bandgap of SLA is (4.56 ± 0.25) eV. A summary of the bandgap results is shown in Table 1. This result compares well with the estimated optical bandgap of ≈ 4.7 eV and what is seen in sphalerite Li₃AlN₂, a 4.4 eV bandgap.^[2,15]

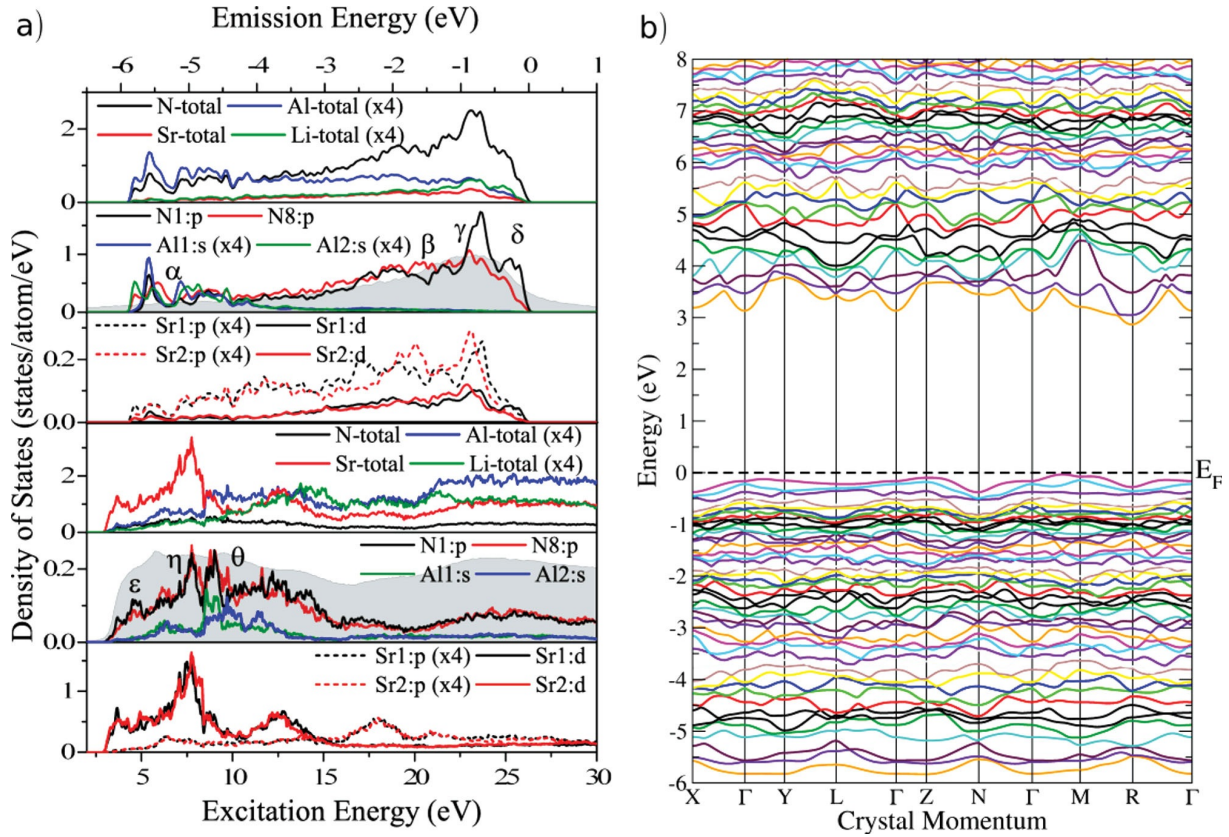


Figure 3. a) Calculated DOS in the VB (upper half) and CB (lower half) of SLA. The DOS of non-equivalent N sites and several coordinating atoms are given (all with Wyckoff position 2i), along with atomic totals in the unit cell. Normalized, measured spectra are included for comparison and are shaded grey. To aid comparison, measured and calculated band edges are aligned and select DOS are scaled by the factors indicated. Greek letters denote prominent features in the DOS. b) The band structure of SLA based on ground state GGA-PBE calculations. The bandgap is indirect. The CB minimum is at the R-point and the VB maximum between the Γ and M points. The energy scales are set with respect to the Fermi energy.

The band structure as determined by the GGA-PBE calculation can be seen in Figure 3. The bandgap is predicted to be indirect, with the valence band (VB) maximum between the Γ and M points and the conduction band (CB) minimum at the R point. The energy needed for direct transitions from the VB to the CB will therefore be a few tenths of an eV greater than the band separation determined through the XAS and XES measurements. This result is somewhat dissimilar to that of Li₃AlN₂, a direct bandgap analogue of AlN.^[15] Were the host lattice itself expected to emit light this would be a disadvantageous result, but its purpose is to provide an appropriate environment for the Eu²⁺ states.^[16,17] It should also be noted that the

high density of bands inhibits the measurement of RIXS features,^[18–20] leading to the interpretation of the variations in the XES spectra with excitation energy in terms of the variation in the DOS of the non-equivalent N sites.

The DOS for the VB and CB, as determined by the ground-state GGA-PBE calculation, are shown in Figure 3. The DOS of N1 (2i), N8 (2i), atoms with which they coordinate, and atomic totals are shown alongside non-resonant XES and XAS spectra. The non-equivalent N sites are similarly coordinated and between N1 and N8 the principal features of the N sites are represented. Most of these sites can be distinguished by their behavior in regions α and δ .

From Figure 3 it can be seen that the N:p states dominate the VB. In addition, the variations in the N DOS are mirrored in the DOS of the coordinating atoms. This not only suggests covalent bonding with the N sites, but a degree of sp-hybridization in Li and Al, as well as pd-hybridization in Sr. Strong peaks are observed in Al:s states corresponding to α in the N:p DOS of the lower VB, implying this region is characterized by Al:s–N:p covalent bonds. This is a trend seen in other materials based on XN₄ tetrahedra.^[17,21,22] The Sr:d states dominate the lower CB, although N:p states are also present. The N states largely mirror the Sr:d states in this region, suggesting that the Sr:d states determine the lower CB as N:p states do the VB. Coincident peaks suggesting shared Al:s–N:p states are present at feature θ , similar to what was seen in the lower VB. The presence of N:p states in the lower CB and upper VB supports the use of N XES and XAS to determine the bandgap. The DOS show contributions from all elements in the VB and CB, including strong participation of the N states, suggesting a rigid lattice with pervasive covalent bonding.

It can be seen in the XES spectra that excitation to $e, f,$ and g results in variations in the size of regions d and a . These preferential excitations can be explained in terms of the calculated DOS for non-equivalent N sites in the regions α through θ , supporting the varied contributions of non-equivalent N sites to the upper VB and lower CB as predicted in the DOS. The nearly unvarying shape of the XES spectra with changes in excitation energy and that the subtle changes can be explained in terms of the preferential excitation of non-equivalent N sites, points to the purity of the samples used. The presence of leftover reactants or contaminants can often be detected through such selective excitations.^[23] The calculated density of states accounts for the variations in the XES spectra with excitation energy and suggests the influence of impurities is negligible. That these variations are subtle also reflects a general similarity in the DOS of non-equivalent N sites.

The calculated CB and VB DOS in Figure 3 show considerable similarity between the DOS of the non-equivalent Sr sites, Sr1 (2i) and Sr2 (2i). There is some variation observable in the height of a few peaks in the CB, but it is slight.

In the VB the DOS are again very similar. However, there are some notable fluctuations at the upper edge of the VB at features γ and δ . These fluctuations link directly to what is seen in the coordinating N DOS. In Sr2 feature δ is suppressed, a trait seen in the associated N states. In contrast, this feature is present in Sr1 and its coordinating N atoms. For instance, δ is most prominent in N1 and N5 (2i), which coordinate solely with Sr1. In N2 (2i) and N7 (2i), which coordinate with Sr2 only, this feature is absent. N sites that coordinate with both Sr sites show the presence of δ to varying degrees. This lends further support to the Sr:pd–N:p covalent bonding in the VB. Overall the DOS suggests a similar degree of covalency between the non-equivalent Sr sites and their coordinating N sites, with slight site-specific variations. This will have an impact on the centroid shift of the Eu²⁺ ions occupying the Sr sites, which will strongly influence the material's luminescence properties.

General features of SLA's electronic structure, such as the nature of the bonding in the XN₄ tetrahedra, are shared by other phosphor materials, which in turn do not have the same luminescence properties as SLA.^[17,21,22] These general features are clearly insufficient for efficient visible light emissions. The bandgap must be large enough as to be transparent to the RE ion's emissions or house the relevant ground and excited states of the RE ion.^[17,21] For efficient luminescence in the desired spectral range, the crystal field splitting (CFS), centroid shift and Stokes shift are also key considerations for phosphor design.^[2,16,24,25]

A reoccurring theme for narrow-band emissions is a small Stokes shift. The covalent nature of N bonding in SLA suggests it should exhibit considerable rigidity and as a result, a limited Stokes shift. The principal factor for determining the CFS experienced by metal cations is the geometry of the ligands, as opposed to the ligands themselves.^[25] The two non-equivalent Sr sites in SLA have a very similar cuboidal coordination.^[2] The similarity in the crystal fields experienced at the Sr sites in SLA is further supported by their highly similar DOS. Elsewhere, substantial variation in the DOS of non-equivalent metal sites is seen,^[23] alongside broader emissions.^[21] The uniformity of the crystal field experienced by the two non-equivalent Sr sites in SLA is supported by the similarity in their DOS.

The nephelauxetic effect is largely accredited with introducing the appropriate centroid shift in the RE cation d-orbitals and can be attributed to the covalency between the RE cation and the surrounding anions, as well as their polarizability.^[16,24,26] The anion polarizability is similarly influenced by its own coordination environment.^[24,25] The centroid shift occurs

independently of the CFS,^[24,25] therefore both must be considered to engineer phosphor emissions. The calculated DOS for SLA show covalent interaction between the non-equivalent Sr and surrounding N sites, in conjunction with a high degree of similarity in that interaction. The coordination of the N sites is known to be similar from X-ray diffraction measurements.^[2] As with Sr, the N DOS reflect this. Despite the slight variations pointed to, the N DOS and the implied interactions with coordinating atoms are quite uniform across non-equivalent sites. Therefore, the centroid shift for the Eu²⁺ ions occupying either of the Sr sites can be anticipated to be similar. Since the CFS is largely determined by the ligand geometry, similar CFS at the non-equivalent sites demands similar centroid shifts if a narrow emission bandwidth is to result. To that end the information from the DOS overwhelmingly supports that conditions in SLA are highly favorable for narrow band emissions.

The band structure and DOS for the promising new LED-phosphor SLA have been calculated and related to the observed luminescence properties of the material. The calculated XAS and XES spectra reproduce those observed experimentally. The site-selective XES spectra also lend strong support to the predicted DOS. The experimentally determined bandgaps of undoped and doped SLA are (4.56 ± 0.25) eV and (4.57 ± 0.25) eV, respectively. The bandgap is predicted to be indirect by the GGA-PBE calculations. The VB of SLA is characterized by Al:s–N:p covalent bonds at lower energies and N:p–Sr:pd covalent bonds towards higher energies. The CB is characterized by N:p and Sr:d states in the lower CB, with a notable N:p–Al:s contribution. The strongly covalent nature of the bonding in SLA, the interaction of the N:p and Sr:pd states and high degree of similarity in the DOS of the two non-equivalent Sr sites all re-enforce its importance as a phosphor for LED applications. These results help in understanding the structure-property relations in Sr[LiAl₃N₄]:Eu²⁺ and explain the narrow-band emission despite the presence of two crystallographically independent Sr-sites. This study should prove informative to further studies advancing the research field of developing phosphors for illumination-grade pc-LEDs.

3.5.2 Experimental Section

XES and XAS measurements were performed at Beamline 8.0.1 of the Advanced Light Source (Berkeley, California, USA) and the Spherical Grating Monochromator (SGM) beamline at the Canadian Light Source (Saskatoon, Saskatchewan, Canada),^[27–29] respectively. Beamline 8.0.1 is equipped with a Rowland circle X-ray spectrometer, spherical gratings and area sensitive multichannel detector.^[27] The XAS spectra were measured through the partial fluorescence yield (PFY), detected with silicon drift X-ray fluorescence detectors.

The resolving power for the XES measurements, given in terms of the photon energy E as $E/\Delta E$ is approximately 800. The XAS measurements have approximate resolving powers of 4000 and 2000 at Beamline 8.0.1 and the SGM beamline, respectively.

The powdered samples were stored and prepared for measurement under dry N₂ or Ar atmospheres to avoid possible oxidation or hydrolysis. Samples were pressed into freshly exposed indium foil before being placed into the sample transfer chambers, which were initially filled with dry N₂, then evacuated. No other treatment of the samples was carried out. Measurements were conducted under a high vacuum of 5×10^{-7} Torr or better. The XES and XAS energy scales were calibrated using the XES and XAS spectra of hexagonal boron nitride (h-BN) powder (99.5% purity, Alfa Aesar). The peaks used for XES calibration are the two dominant peaks in the h-BN non-resonant emissions, positioned at 392.75 eV and 394.60 eV. The lowest energy peak in the XAS spectrum of h-BN is taken to lie at 402.1 eV.

Calculations: DFT calculations were performed using the WIEN2k software package. This software uses the full potential (linearized) augmented plane waves with local orbitals (LAPW + LO) to self consistently solve the Kohn–Sham equations.^[30] The generalized gradient approximation of Perdew, Burke and Ernzerhof (GGA-PBE) is used for the exchange and correlation energies.^[30,31] Additional calculations were performed using the local density approximation (LDA) with a modified Becke–Johnson (LDA-mBJ) potential to predict the bandgap of the material.^[14] Core hole calculations with a $2 \times 2 \times 2$ supercell were performed to model the experimental XAS as necessitated by the final state rule.^[32,33] The ground state calculation is sufficient for describing the XES spectra and in addition to the DOS, is used to provide the predicted band structure of SLA.

The broadening of the calculated spectra was done in a way that accounts for both instrumental and lifetime broadening. The lifetime broadening for a particular transition is determined by the final state of the system, in accordance with the final state rule.^[33] A Lorentz profile is used for the lifetime broadening for both the XES and XAS spectra. In both cases the energy width is taken as the sum of contributions from the core hole lifetime and a term quadratic in the energy difference between the decaying state and the conduction band edge. The latter term accounts for the variation in the lifetime of the state with its depth in the VB or CB.^[34] Gaussian instrumental broadening is also applied to the spectra. For the XES spectra each emitted energy is broadened individually in accordance with the spectrometer resolution. The XAS spectra are broadened by considering that the spectral weight given to a particular energy is due to the excitation of the sample by a Gaussian incident spectrum from the monochromator.

3.5.3 References

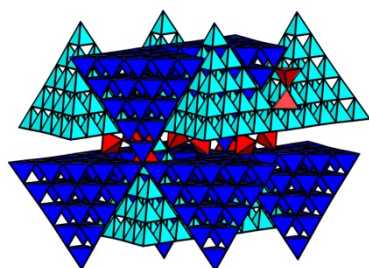
- [1] U.S. Energy Information Administration (EIA) – FAQ, <http://www.eia.gov/tools/faqs/faq.cfm?id=99&t=3>, accessed: **December 2014**.
- [2] P. Pust, V. Weiler, C. Hecht, A. Tücks, A. S. Wochnik, A.-K. Henß, D. Wiechert, C. Scheu, P. J. Schmidt, W. Schnick, *Nat. Mater.* **2014**, *13*, 891.
- [3] Y. Q. Li, N. Hirosaki, H. Yamamoto, *Nitride Phosphors and Solid-State Lighting*, Taylor & Francis, Boca Raton, FL, USA, **2011**.
- [4] W. B. Im, N. George, J. Kurzman, S. Brinkley, A. Mikhailovsky, J. Hu, B. Chmelka, F. Bradley, S. P. Denbaars, R. Seshadri, *Adv. Mater.* **2011**, *23*, 2300.
- [5] C. C. Lin, R.-S. Liu, *J. Phys. Chem. Lett.* **2011**, *2*, 1268.
- [6] H. Yang, S. W. Kim, J. Y. Han, S. Lee, D. Y. Jeon, *Adv. Mater.* **2008**, *20*, 2696.
- [7] R. Mueller-Mach, G. Mueller, M. R. Krames, H. A. Höpfe, F. Stadler, W. Schnick, T. Jüstel, P. Schmidt, *Phys. Status Solidi A* **2005**, *202*, 1727.
- [8] X. Wang, X. Yan, W. Li, K. Sun, *Adv. Mater.* **2012**, *24*, 2742.
- [9] S. Schmiechen, H. Schneider, P. Wagatha, C. Hecht, P. J. Schmidt, W. Schnick, *Chem. Mater.* **2014**, *26*, 2712.
- [10] P. Pust, A. Wochnik, E. Baumann, P. J. Schmidt, D. Wiechert, C. Scheu, W. Schnick, *Chem. Mater.* **2014**, *26*, 3544.
- [11] S. Schmiechen, H. Schneider, P. Wagatha, C. Hecht, P. J. Schmidt, W. Schnick, *Chem. Mater.* **2014**, *26*, 2712.
- [12] M. Krames, G. O. Mueller, R. B. Mueller-Mach, H. Bechtel, P. J. Schmidt, *PCT Int. Appl., WO 2010131133*, A1, **2010**.
- [13] E. Z. Kurmaev, R. G. Wilks, A. Moewes, L. Finkelstein, S. Shamin, J. Kunes, *Phys. Rev. B* **2008**, *77*, 165127.
- [14] F. Tran, P. Blaha, *Phys. Rev. Lett.* **2009**, *102*, 226401.
- [15] K. Kuriyama, Y. Kaneko, K. Kushida. *J. Cryst. Growth* **2005**, *275*, 395.
- [16] M. Mikami, H. Watanabe, K. Uheda, S. Shimooka, Y. Shimomura, T. Kurushima, N. Kijima, *IOP Conf. Ser.: Mater. Sci. Eng.* **2009**, *1*, 012002.
- [17] Y. Q. Li, N. Hirosaki, R. J. Xie, T. Takeka, M. Mitomo, *J. Solid State Chem.* **2009**, *182*, 301.
- [18] L. Ament, M. van Veenendaal, T. P. Devereaux, J. P. Hill, J. van den Brink, *Rev. Mod. Phys.* **2011**, *83*, 705.
- [19] S. Eisebitt, W. Eberhardt, *J. Electron Spectrosc. Relat. Phenom.* **2000**, *110–111*, 335.
- [20] A. Kotani, S. Shin, *Rev. Mod. Phys.* **2001**, *73*, 203.

- [21] C. J. Duan, X. J. Wang, W. M. Otten, A. C. A. Delsing, J. T. Zhao, H. T. Hintzen, *Chem. Mater.* **2008**, *20*, 1597.
- [22] M. Dadsetani, S. Namjoo, H. Hejati, *J. Electron. Mater.* **2010**, *39*, 1186.
- [23] C. Braun, M. Seibald, S. L. Börger, O. Oeckler, T. D. Boyko, A. Moewes, G. Mieke, A. Tücks, W. Schnick, *Chem. Eur. J.* **2010**, *16*, 9646.
- [24] P. Dorenbos, *Phys. Rev. B* **2001**, *64*, 125117.
- [25] P. Dorenbos, *Phys. Rev. B* **2002**, *65*, 235110.
- [26] C. Housecroft, A. Sharpe, *Inorganic Chemistry*, 2nd ed., Pearson Education Limited, Harlow, UK, **2005**.
- [27] J. J. Jia, T. A. Callcott, J. Yurkas, A. W. Ellis, F. J. Himpsel, M. G. Samant, J. Stöhr, D. L. Ederer, J. A. Carlisle, E. A. Hudson, L. J. Terminello, D. K. Shuh, R. C. C. Perera, *Rev. Sci. Instrum.* **1995**, *66*, 1394.
- [28] T. Regier, J. Krochak, T. K. Sham, Y. F. Hu, J. Thompson, R. I. R. Blyth, *Nucl. Instrum. Methods Phys. Res. Sect. A* **2007**, *582*, 93.
- [29] T. Regier, J. Paulsen, G. Wright, I. Coulthard, K. Tan, T. K. Sham, R. I. R. Blyth, *AIP Conf. Proc.* **2007**, *879*, 473.
- [30] K. Schwarz, P. Blaha, *Comput. Mater. Sci.* **2003**, *28*, 259.
- [31] S. Cottenier, *Density Functional Theory and the Family of (L)APWMethods: A Step-by-Step Introduction*, 2nd ed., **2002–2013**, (freely available at: http://www.wien2k.at/reg_user/textbooks/).
- [32] G. D. Mahan, *Phys. Rev. B* **1980**, *21*, 1421.
- [33] U. von Barth, G. Grossman, *Solid State Commun.* **1979**, *32*, 645.
- [34] D. A. Goodings, R. Harris, *J. Phys. C: Solid State Phys.* **1969**, *2*, 1808.

3.6 $\text{Ca}_{18.75}\text{Li}_{10.5}\text{Al}_{39}\text{N}_{55}:\text{Eu}^{2+}$ - Supertetrahedron Phosphors for Solid-State Lighting

to be published Philipp Pust, Volker Weiler, Angela S. Wochnik, Peter J. Schmidt, Christina Scheu and Wolfgang Schnick

Abstract. Highly efficient red-emitting phosphor materials deliver the basis for next-generation illumination-grade light-emitting diodes (LEDs). Recent studies demonstrated that the hardly explored class of nitridoaluminates comprise several interesting phosphor materials like $\text{Sr}[\text{LiAl}_3\text{N}_4]:\text{Eu}^{2+}$ or $\text{Ca}[\text{LiAl}_3\text{N}_4]:\text{Eu}^{2+}$. Here we describe the novel material $\text{Ca}_{18.75}\text{Li}_{10.5}\text{Al}_{39}\text{N}_{55}:\text{Eu}^{2+}$, with highly efficient narrow band red emission ($\lambda_{\text{em}} \sim 647$ nm, full width at half maximum ~ 1190 cm^{-1}). This compound features a rather uncommon crystal structure, forming sphalerite-like T5-supertetrahedra of AlN_4 tetrahedra which are interconnected by additional AlN_4 tetrahedra. The network is stabilized by Ca and Li ions located on the faces of the supertetrahedra. The crystal structure was solved and refined from single-crystal and powder X-ray diffraction data in the cubic space group $Fd\bar{3}m$ (no. 227) with



$a = 22.415(3)$ Å and $Z = 8$. To ensure the presence of Li, transmission electron microscopy investigations including electron energy-loss spectroscopy were carried out. Based on the intriguing luminescence properties we proclaim strong potential for industrial application in white high-power phosphor-converted LEDs.

3.6.1 Introduction

Worldwide electricity demand is expected to increase by more than 50% until 2040.^[1] About 20% of this energy is consumed by lighting applications. Therefore, one of the major interests in environmental policy is to reduce energy consumption by replacing inefficient lighting technologies with modern systems. The European Union for example introduced a stepwise ban of inefficient incandescent light bulbs.^[2] A classical light bulb converts only about 5% of the used energy into visible light.^[3] The residual 95% are typically emitted as heat by the glowing tungsten filaments. Phosphor-converted light-emitting diodes (pc-LEDs) emerged as attractive light sources for the replacement of incandescent light. In general, the conversion efficiency of LED-based technology reaches up to 50% at lifetimes greater than 25.000 h.^[4-6] However, a major drawback of this technology is the often limited color rendering index (CRI). The CRI of a classical incandescent light bulb is around 100, comparable to that of daylight. The CRI of pc-LED devices is often only around 80. Better CRI values are easily attainable with pc-LEDs, yet at the expense of reduced energy efficiency. Recent studies proved, that the CRI and the luminous efficacy (efficiency of light generation relating to human eye sensitivity) critically depend on the spectral position and width of the red emitting component.^[7] Using state of the art red emitting materials like $(\text{Ba},\text{Sr})_2\text{Si}_5\text{N}_8:\text{Eu}^{2+}$ ($\lambda_{\text{em}} \sim 590\text{--}625$ nm, full width at half maximum (FWHM) $\sim 2050\text{--}2600$ cm^{-1}) or $(\text{Ca},\text{Sr})\text{SiAlN}_3:\text{Eu}^{2+}$ ($\lambda_{\text{em}} \sim 610\text{--}660$ nm, FWHM $\sim 2100\text{--}2500$ cm^{-1}) the luminous efficacy is significantly reduced with increasing CRI, obtained by an increased content of the red emitter.^[5,8-10] This is due to the relatively broad emission bands of current red-emitting materials. This results in a substantial portion of light being emitted in the infrared region, outside the visible spectrum. Therefore, the development of a narrow band red-emitting material without infrared emission is of major interest for the LED-industry. Recently, several novel “narrow red” phosphors have been published. They are all based on highly condensed host lattices with a nearly cubical coordination sphere of the Eu^{2+} dopable heavy atom site. All of these recently reported compounds exhibit a structure type comparable to that of UCr_4C_4 ,^[11] with some of them crystallizing in ordered variants of the UCr_4C_4 structure type.^[12-14]

In this contribution we present the novel nitridolithoaluminate $\text{Ca}_{18.75}\text{Li}_{10.5}\text{Al}_{39}\text{N}_{55}:\text{Eu}^{2+}$, featuring a highly condensed host lattice. Doped with Eu^{2+} this new material shows intense emission in the red spectral region with a narrow FWHM similar to $\text{Sr}[\text{LiAl}_3\text{N}_4]:\text{Eu}^{2+}$.^[12] However, the structural motif differs fundamentally from the previously published compounds.

3.6.2 Experimental Section

3.6.2.1 Synthesis

All manipulations were performed under rigorous exclusion of oxygen and moisture in flame-dried glassware on a Schlenk line attached to a vacuum line (10^{-3} mbar) or in an argon-filled glovebox (Unilab, MBraun, Garching, O₂ <1 ppm, H₂O <1 ppm). The synthesis of Ca_{18.75}Li_{10.5}Al₃₉N₅₅:Eu²⁺ (nominal Eu²⁺ concentration 0.5 mol%) was carried out in molybdenum lined corundum crucibles in a hot isostatic press. The starting materials Li₃N (Sigma-Aldrich, 99.99%), CaH₂ (Cerac, 99.5%), AlN (Tokuyama, 99%) and EuF₃ (Sigma-Aldrich, 99.99%, dopand) were pre-mixed in stoichiometric amounts in an agate mortar, followed by fine mixing in a ball mill. The mixture was subsequently filled into the crucibles and heated for 5 h at 1250 °C and 7500 PSI nitrogen pressure. Red octahedral-shaped single crystals of Ca_{18.75}Li_{10.5}Al₃₉N₅₅:Eu²⁺ were isolated from the yellowish product under a microscope integrated in a glovebox. The crystals were enclosed in glass capillaries and sealed under argon.

3.6.2.2 Single-Crystal X-ray Diffraction

Single-crystal diffraction data were collected on a STOE IPDS I diffractometer (Mo-K α radiation, graphite monochromator). The crystal structure was solved by using direct methods with SHELXS.^[15] The refinement of the structure was carried out by the least-squares method using SHELXL.^[15]

Further details of the investigations of the crystal structure can be obtained from the Fachinformationszentrum Karlsruhe, 76344 Eggenstein-Leopoldshafen, Germany (Fax: +49-7247-808-666; E-mail: crysdata@fiz-karlsruhe.de) on quoting the depository number CSD-428388.

3.6.2.3 Powder X-ray Diffraction

Powder X-ray diffraction data were collected on a Huber G670 Guinier imaging plate diffractometer (Cu-K α_1 radiation, Ge(111) monochromator). Simulations of Bragg data were performed based on the single-crystal structural data using the WinXPOW program package.^[16] Rietveld refinement was carried out using the TOPAS package.^[17]

3.6.2.4 Electron Microscopy

For scanning electron microscope (SEM) investigations a JSM-6500F SEM (Jeol) equipped with a Si/Li energy-dispersive X-ray (EDX) detector (Oxford Instruments, model 7418) was used. For transmission electron microscope (TEM) measurements a FEI Titan 80-300 microscope equipped with a post-column energy filter GIF Tridiem from Gatan and an EDAX

EDX detector for analytical characterisations was employed. Diffraction patterns were recorded with a Gatan UltraScan 1000 ($2\text{k} \times 2\text{k}$) CCD camera and evaluated using a calibrated camera constant obtained by using a Si standard. The TEM investigations were carried out at an accelerating voltage of 300 kV.

3.6.2.5 EDX Spectroscopy

To analyze the chemical composition of different crystallites, EDX data were collected with an accelerating voltage of 12 kV. Furthermore, the SEM was used to collect images for investigating particle morphology.

3.6.2.6 Electron Energy-Loss Spectroscopy (EELS)

The EELS measurements were performed in diffraction mode in the TEM with a selected area diffraction aperture choosing a circular area of about 150 nm in diameter to avoid beam damage. A 2 mm entrance aperture of the spectrometer and a camera length of 130 mm were applied resulting in a collector angle of 13.5 mrad. Dispersions of 0.3 eV/channel were used, leading to a FWHM of around 0.9–1.2 eV of the zero loss peak. The acquisition time for the Li-K and Al-L_{2,3} edges was 10 s. The obtained data were corrected for dark current and channel-to-channel gain variation. The pre-edge background was approximated by a 1st order-log-polynomial function and subtracted from the original data.^[18]

3.6.2.7 Luminescence

Luminescence investigations were performed with the aid of a luminescence microscope consisting of a HORIBA Fluorimax4 Spectrofluorimeter-system attached to an Olympus BX51 microscope via fiber optics. Single crystals were measured in glass capillaries. Bulk samples were investigated in PTFE sample holders. The excitation wavelength was set to 450 nm with a spectral width of 10 nm. The emission spectra were measured in the wavelength range between 460 nm and 800 nm with a step size of 1 nm. Excitation spectra were measured in the wavelength range between 350 nm and 570 nm with a step size of 1 nm using a monitor wavelength of 650 nm.

3.6.3 Results and Discussion

3.6.3.1 Synthesis and Chemical Analysis

The synthesis mentioned above enabled access to the system $\text{Ca}_{(20-x)}\text{Li}_{(8+2x)}\text{Al}_{39}\text{N}_{55}:\text{Eu}^{2+}$ in which the phase $\text{Ca}_{18.75}\text{Li}_{10.5}\text{Al}_{39}\text{N}_{55}:\text{Eu}^{2+}$ could be isolated in form of single crystals (see Figure 1). SEM/EDX investigations (five measurements on different crystals) show an atomic ratio of $\text{Ca}_1\text{Al}_{2.1}\text{N}_{4.0}$ (normalized with respect to the heavy atom) which is in good accordance

with the sum formula. However, a slight overestimation of nitrogen is observed. Eu was not detected in SEM/EDX because of the low accelerating voltage of 12 kV. The oxygen content is zero within the e.s.d.

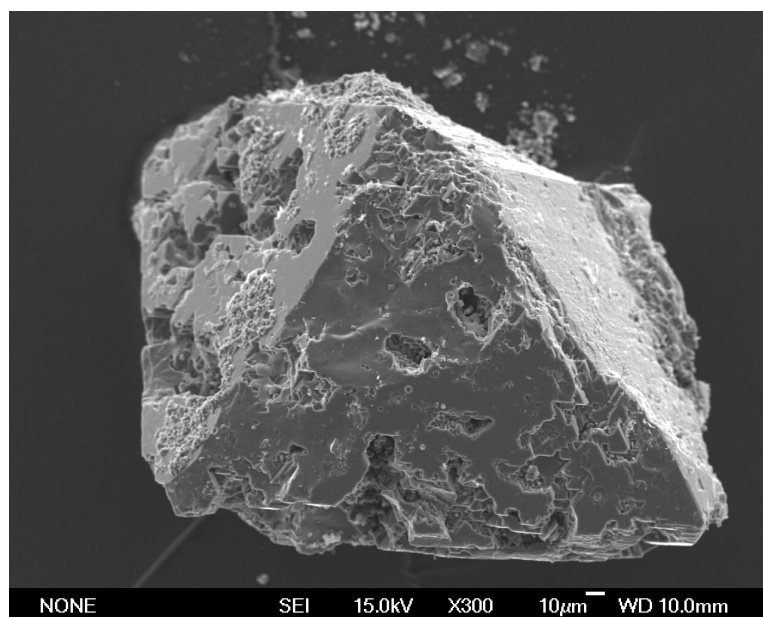


Figure 1. SEM image of $\text{Ca}_{18.75}\text{Li}_{10.5}\text{Al}_{39}\text{N}_{55}:\text{Eu}^{2+}$.

3.6.3.2 Crystal Structure

The crystal structure of $\text{Ca}_{18.75}\text{Li}_{10.5}\text{Al}_{39}\text{N}_{55}$ was solved and refined in the cubic space group $Fd\bar{3}m$ (no. 227) with $a = 22.415(3)$ Å and $Z = 8$. The crystallographic data are summarized in Table 1. The atomic coordinates, isotropic displacement parameters, Wyckoff positions and site occupancy factors (SOF) are specified in the supporting information Table S1 in chapter 6.4. Selected interatomic distances are listed in supporting information Table S2 in chapter 6.4. Eu^{2+} was neglected during structure refinement due to the small amounts of dopant concentration and the therefore nonsignificant scattering density.

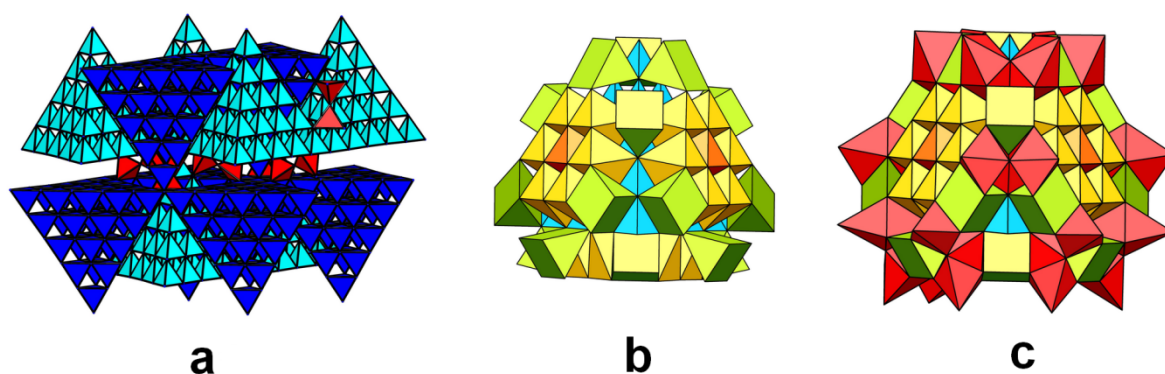


Figure 2. Sketched structure of $\text{Ca}_{18.75}\text{Li}_{10.5}\text{Al}_{39}\text{N}_{55}$ showing the characteristic structural feature of T5-supertetrahedra. (a) AlN_4 -tetrahedra network, (b) Three different Ca sites (Ca1: yellow, Ca2: green; Ca3: orange), (c) Two Li sites (red).

$\text{Ca}_{18.75}\text{Li}_{10.5}\text{Al}_{39}\text{N}_{55}:\text{Eu}^{2+}$ is built up by a network of connected $\text{Al}_{35}\text{N}_{56}$ T5-supertetrahedra, each consisting of 35 AlN_4 tetrahedra. The network itself consists of up and down pointing interdigitating T5-tetrahedra (Figure 2a blue) bridged by AlN_4 tetrahedra (Figure 2a red). Ca^{2+} and Li^+ fill the interstitial spaces between the T5-supertetrahedra. The three different Ca sites are pictured in Figure 2b (Ca1: yellow, Ca2 green, Ca3: orange), the two Li sites in Figure 2c (red). Ca1 and Ca3 are coordinated octahedrally by nitrogen with Ca-N distances ranging from 2.39 to 2.73 Å. Ca2 shows trigonal prismatic coordination with Ca-N distances from 2.49 to 2.73 Å. Structural refinement of single-crystal and powder XRD data revealed a partial occupation for Ca2 (SOF = 0.375). All values are in fair accordance with the sum of the ionic radii and in the range of other known nitridoaluminates like Ca_3AlN_3 (Ca-N: 2.4-2.8 Å).^[19, 20] The two Li positions result from a split refinement forming rings around the N1 position and exhibiting Li-N distances from 1.94 to 2.52 Å. The compound $\text{Ca}_{18.75}\text{Li}_{10.5}\text{Al}_{39}\text{N}_{55}$ is structurally related to the manganate $\text{Na}_{26}\text{Mn}_{39}\text{O}_{55}$.^[21] Both compounds display very similar structural motifs. However, the coordination of the Ca2 site in $\text{Ca}_{18.75}\text{Li}_{10.5}\text{Al}_{39}\text{N}_{55}$ differs from the corresponding Na site in $\text{Na}_{26}\text{Mn}_{39}\text{O}_{55}$ (see Figure 3). In the latter compound the respective Na ions occupy the Wyckoff position 96g and are coordinated by five N atoms forming quadratic pyramids. In $\text{Ca}_{18.75}\text{Li}_{10.5}\text{Al}_{39}\text{N}_{55}$, Ca2 is located at the Wyckoff position 48f which is centered between the Na atoms (see Figure 3). Therefore, both compounds can be considered homeotypic.

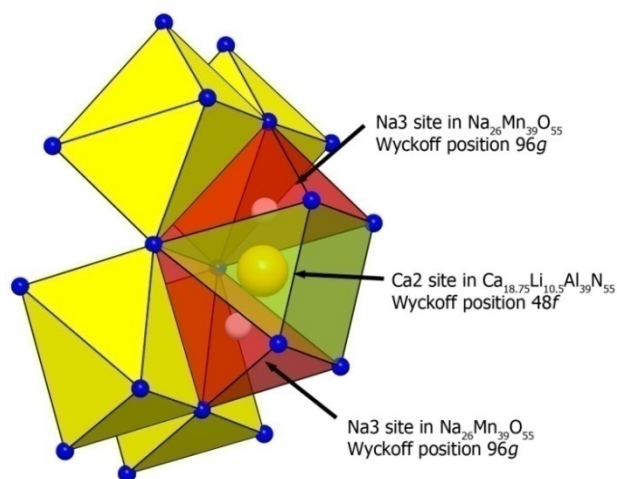


Figure 3. Sketched structure showing the Ca2 site (Wyckoff position 48f) coordinated trigonally prismaticly by nitrogen (green) in $\text{Ca}_{18.75}\text{Li}_{10.5}\text{Al}_{39}\text{N}_{55}$, which is different to the published Na coordination in $\text{Na}_{26}\text{Mn}_{39}\text{O}_{55}$ (red polyhedra).

Table 1. Crystallographic data of the single-crystal structure determination of Ca_{18.75}Li_{10.5}Al₃₉N₅₅.

formula	Ca _{18.75} Li _{10.5} Al ₃₉ N ₅₅
crystal system	cubic
space group	<i>Fd</i> $\bar{3}$ <i>m</i> (no. 227)
lattice parameters (Å)	<i>a</i> = 22.415(3)
cell volume (Å ³)	11263(2)
formula units per unit cell	8
density (g·cm ⁻³)	3.123
μ (mm ⁻¹)	2.432
T (K)	293(2)
diffractometer	Stoe IPDS I
radiation (Å)	Mo-K α (λ = 0.71073 Å), graphite monochromator
F(000)	10389.9
profile range	2.57 \leq θ \leq 30.35
index ranges	-29 \leq <i>h</i> \leq 29 -31 \leq <i>k</i> \leq 31 -30 \leq <i>l</i> \leq 31
independent reflections	854 [<i>R</i> _{int} = 0.0845]
refined parameters	74
Goodness of fit	0.991
<i>R</i> 1 (all data); <i>R</i> 1 (<i>F</i> ² > 2 σ (<i>F</i> ²))	0.0414, 0.0257
<i>wR</i> 2 (all data); <i>wR</i> 2 (<i>F</i> ² > 2 σ (<i>F</i> ²))	0.0604, 0.0569
$\Delta\rho_{\max}$, $\Delta\rho_{\min}$ (e·Å ⁻³)	0.616, -0.475

3.6.3.3 Powder X-ray Diffraction

Rietveld refinement of powder X-ray diffraction data validates the structure of Ca_{18.75}Li_{10.5}Al₃₉N₅₅ obtained from single-crystal X-ray diffraction data (see Figure 4 and supporting information Table S3 in chapter 6.4). The side-phase AlN was quantified to ~40 wt% from Rietveld refinement.

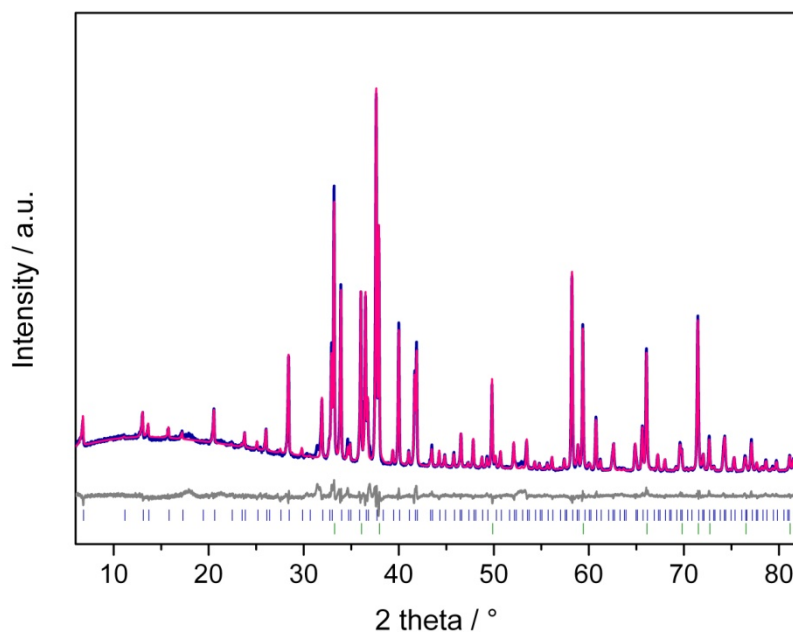


Figure 4. Observed (blue) and calculated (red) XRD pattern as well as the difference profile of the Rietveld refinement of $\text{Ca}_{18.75}\text{Li}_{10.5}\text{Al}_{39}\text{N}_{55}$ (gray). The vertical blue bars indicate possible peak positions of the title compound; green bars indicate the peak positions of the side-phase AlN.

3.6.3.4 Luminescence

Eu^{2+} -doped samples of the title compound exhibit intense red luminescence when irradiated with UV to green light. Luminescence investigations were either performed on single crystals sealed in silica glass capillaries or on bulk samples in PTFE sample holders. Both methods deliver comparable results. Therefore, only one measurement of a bulk sample with 0.5 mol% Eu (nominal composition) is shown in Figure 5. Excitation at 450 nm yields an emission band with a maximum at 647 nm and an extraordinarily narrow FWHM of 1190 cm^{-1} ($\sim 54\text{ nm}$). Peak emission and FWHM values are in the range of the recently published $\text{Sr}[\text{LiAl}_3\text{N}_4]:\text{Eu}^{2+}$ ($\lambda_{\text{em}} \sim 650\text{ nm}$, $\text{FWHM} \sim 1180\text{ cm}^{-1}$),^[12] a narrow-band red-emitting material with expected industrial relevance. The excitation spectrum shows two bands, one in the UV to blue range peaking at $\sim 380\text{ nm}$ and another broader band in the blue to green spectral region (see figure 5 blue line). The excitation maximum of the title compound is located at 525 nm. Compared to other red LED phosphor materials like $(\text{Ba},\text{Sr})_2\text{Si}_5\text{N}_8:\text{Eu}^{2+}$ ($\lambda_{\text{em}} \sim 590\text{--}625\text{ nm}$, $\text{FWHM} \sim 2050\text{--}2600\text{ cm}^{-1}$)^[5,7,8] or $(\text{Ca},\text{Sr})\text{SiAlN}_3:\text{Eu}^{2+}$ ($\lambda_{\text{em}} \sim 610\text{--}660\text{ nm}$, $\text{FWHM} \sim 2100\text{--}2500\text{ cm}^{-1}$),^[9,10] $\text{Ca}_{18.75}\text{Li}_{10.5}\text{Al}_{39}\text{N}_{55}:\text{Eu}^{2+}$ shows a dramatically reduced FWHM. This extremely narrow emission is probably due to the highly symmetric coordination of the Ca sites. $\text{Ca}_{18.75}\text{Li}_{10.5}\text{Al}_{39}\text{N}_{55}:\text{Eu}^{2+}$ is one composition in the theoretical solid solution of $\text{Ca}_{(20-x)}\text{Li}_{(8+2x)}\text{Al}_{39}\text{N}_{55}:\text{Eu}^{2+}$ ($x = 0\text{--}2$). The great variability in the Ca:Li ratio possibly enables

an intriguing tunability of the luminescence properties by simply modifying the host lattice composition. More thorough investigations of this tunability are part of further work and not discussed here.

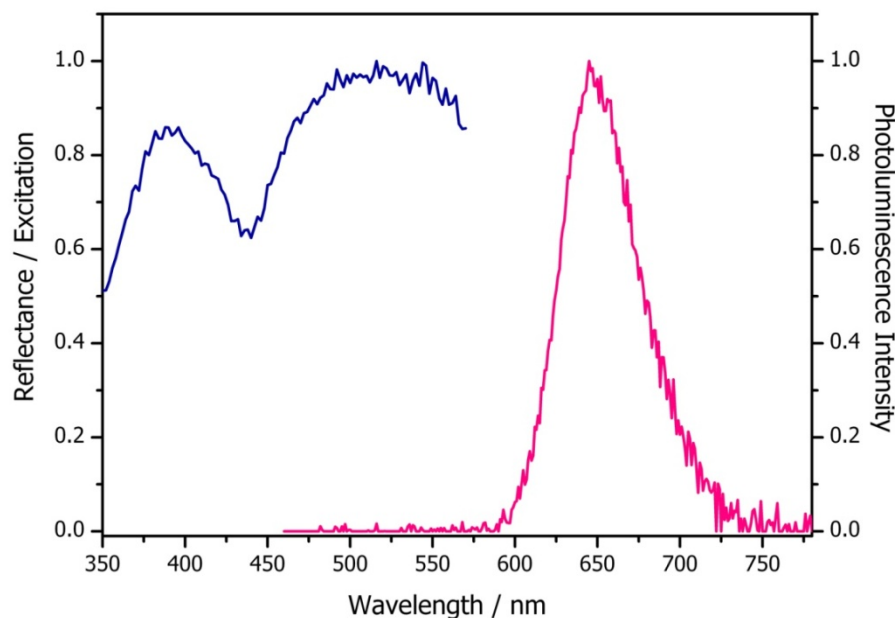


Figure 5. Excitation (blue, monitored at 650 nm) and emission (red, excited at 450 nm) spectra of $\text{Ca}_{18.75}\text{Li}_{10.5}\text{Al}_{39}\text{N}_{55}:\text{Eu}^{2+}$ bulk material with a dopant concentration of 0.5 mol% Eu (nominal composition).

Such a narrow band emission in an Eu^{2+} system is only obtained when different requirements for the host lattice are fulfilled. On the one hand the linked sphalerite type $\text{Al}_{35}\text{N}_{56}$ T5-supertetrahedra result in a framework with a degree of condensation of $\kappa = 0.71$. This relatively high degree of condensation is beneficial for suppressing phonons and thus for rigid, non-vibrating surroundings of the activator ions. On the other hand the highly symmetric coordination spheres (2x trigonal antiprismatic, 1x trigonal prismatic) of the three Ca^{2+} sites enable a small Stokes shift. This assumption is corroborated by other experimental observations, suggesting that a high activator site symmetry enables smaller Stokes shifts and, therefore, reduces emission bandwidth.^[22] This effect is also observed in other Eu^{2+} phosphors like $\text{M}[\text{LiAl}_3\text{N}_4]:\text{Eu}^{2+}$ ($\text{M} = \text{Ca}, \text{Sr}$) or $\text{BaSi}_2\text{O}_2\text{N}_2:\text{Eu}^{2+}$.^[12,13,23,24] As mentioned before, there are three crystallographically independent sites for Ca^{2+} or Eu^{2+} available here. This is not in good agreement with the observed narrow-band emission. Different crystal fields around the different activator sites usually cause inhomogeneous line broadening leading to broader emission bands. Due to the dense packing of the host network an occupation of interstitial positions by Eu^{2+} seems unlikely. We presume that Eu^{2+} favors the trigonal prismatically coordinated site of Ca2. The larger average Ca2-N distances (Ca2-N:

2.65 Å) are in better agreement with the sum of the ionic radii of Eu^{2+} and N^{3-} (2.68 Å) according to *Baur*,^[25] than the average distances of Ca1-N with 2.45 Å and Ca3-N with 2.42 Å. Obtaining facts in support of this assumption will be part of further work.

3.6.3.5 EELS

To confirm the presence of Li in the crystal structure, EELS measurements were performed in a TEM with an accelerating voltage of 300 kV. The Li-K edge in Figure 6 occurs at around 56.5 eV and has a maximum at 61.6 eV. The Al-L_{2,3} and Al-L₁ edges can be seen in the spectrum, but they overlap with the higher energy loss region of the Li-K edge. The onset values of the Al edges cannot be determined exactly because of overlapping. However, the Al-L_{2,3} edge shows a maximum peak at 82.6 eV. The value of Li-K shows a slight deviation compared to data obtained from the literature, for example Li_xTiP ($x = 2-11$), $\text{Li}_2\text{CaSi}_2\text{N}_4$ or $\text{Li}_2\text{SrSi}_2\text{N}_4$, which is entailed by different bonding types.^[26,27] Shape and maximum peak of the Al-L_{2,3} edge are in good accordance with data published in the literature.^[18,28] The EELS investigations clearly confirm the presence of Li and Al being integrated in the structure.

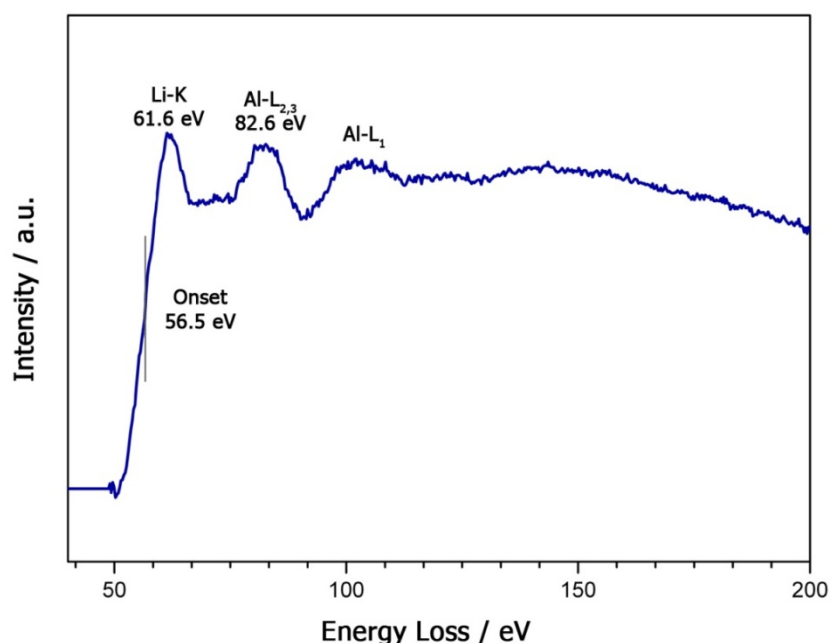


Figure 6. EELS spectrum of $\text{Ca}_{18.75}\text{Li}_{10.5}\text{Al}_{39}\text{N}_{55}:\text{Eu}^{2+}$. The energy loss region of the Li-K, Al-L_{2,3} and Al-L₁ edges is shown. The background left to the Li-K edge has been subtracted.

3.6.4 Conclusion

In this contribution we report on the new nitridolithoaluminate $\text{Ca}_{18.75}\text{Li}_{10.5}\text{Al}_{39}\text{N}_{55}:\text{Eu}^{2+}$ with an exceptional crystal structure and intriguing luminescence properties. The compound consists of a network of connected $\text{Al}_{35}\text{N}_{56}$ T5-supertetrahedra, each containing 35 AlN_4 tetrahedra. The structure itself is made up of two interpenetrating T5-tetrahedra networks of

opposite orientation which are bridged by AlN_4 tetrahedra. Ca^{2+} and Li^+ are filling the interstitial space between the T5-supertetrahedra network structure. The structural model was refined from single-crystal and powder XRD data. Furthermore, the presence of Li in the crystal structure was confirmed by EELS spectroscopy. Luminescence investigations on Eu doped samples of $\text{Ca}_{18.75}\text{Li}_{10.5}\text{Al}_{39}\text{N}_{55}$ show intense red emission peaking at 647 nm with an exceptionally narrow FWHM for Eu^{2+} phosphors of $\sim 1190 \text{ cm}^{-1}$ ($\sim 54 \text{ nm}$), when irradiated with UV to green light. These values are comparable to other recently published narrow band red-emitting materials like $\text{Sr}[\text{LiAl}_3\text{N}_4]:\text{Eu}^{2+}$ or $\text{Sr}[\text{Mg}_3\text{SiN}_4]:\text{Eu}^{2+}$ which are being discussed intensively as possible next-generation phosphors.^[12,14] However, the uncommon crystal structure of our material demonstrates that narrow band emission is not limited to derivatives of the UCr_4C_4 structure-type and a cubical coordination of the heavy atom. In fact, we could show that trigonal prismatic or octahedral coordination, respectively, are also suitable for narrow emission bands in Eu^{2+} doped materials. Consequently, we claim that $\text{Ca}_{18.75}\text{Li}_{10.5}\text{Al}_{39}\text{N}_{55}:\text{Eu}^{2+}$ widens the group of intriguing red-emitting materials and has the potential for application in high-power pc-LEDs. Due to the exceptional crystal structure and the regardless remarkably narrow red emission, we claim that $\text{Ca}_{18.75}\text{Li}_{10.5}\text{Al}_{39}\text{N}_{55}:\text{Eu}^{2+}$ is a key material to fully understand the principles behind narrow-band Eu^{2+} emission.

3.6.5 References

- [1] Office of Energy Analysis, U.S. Department of Energy, Washington, DC, **2013**.
- [2] http://ec.europa.eu/energy/lumen/professional/index_de.htm; follow link “FAQ für Fachleute”, visited on 12th August **2014**.
- [3] M. Born, T. Jüstel, *Chem. Unserer Zeit* **2006**, *40*, 294.
- [4] C. Feldmann, *Z. Anorg. Allg. Chem.* **2012**, *638*, 2169.
- [5] R. Mueller-Mach, G. Mueller, M. R. Krames, H. A. Höpfe, F. Stadler, W. Schnick, T. Juestel, P. Schmidt, *Phys. Status Solidi A* **2005**, *202*, 1727.
- [6] A. A. Setlur, *Electrochem. Soc. Interface* **2009**, *18*, 32.
- [7] M. Krames, G.O. Mueller, R.B. Mueller-Mach, H. Bechtel, P.J. Schmidt, *PCT Int. Appl.*, WO 2010131133, A1, **2010**.
- [8] H. A. Höpfe, H. Lutz, P. Morys, W. Schnick, A. Seilmeier, *J. Phys. Chem. Solids* **2000**, *61*, 2001.
- [9] K. Uheda, N. Hirosaki, H. Yamamoto, *Phys. Stat. Sol. A* **2006**, *11*, 2712.
- [10] K. Uheda, N. Hirosaki, Y. Yamamoto, A. Naita, T. Nakajima, H. Yamamoto, *Electrochem. Solid State Lett.* **2006**, *9*, H22.

- [11] R. K. Behrens, W. Jeitschko, *Monatsh. Chem.* **1987**, *118*, 43.
- [12] P. Pust, V. Weiler, C. Hecht, A. Tücks, A. S. Wochnik, A.-K. Henß, D. Wiechert, C. Scheu, P. J. Schmidt, W. Schnick, *Nat. Mater.* **2014**, *13*, 891.
- [13] P. Pust, A. S. Wochnik, E. Baumann, P. J. Schmidt, D. Wiechert, C. Scheu, W. Schnick, *Chem. Mater.* **2014**, *26*, 3544.
- [14] S. Schmiechen, H. Schneider, P. Wagatha, C. Hecht, P. J. Schmidt, W. Schnick, *Chem. Mater.* **2014**, *26*, 2712.
- [15] G. M. Sheldrick, *Acta Crystallogr., Sect. A: Found. Crystallogr.* **2008**, *64*, 112.
- [16] Stoe & Cie GmbH, *WINXPOW* - Program for powder data handling, **2007**, v2.21, Darmstadt, Germany.
- [17] A. Coelho, *TOPAS - Academic* **2007**, Brisbane: Coelho Software.
- [18] R. F. Egerton, *Electron Energy-Loss Spectroscopy in the Electron Microscope*, 3rd ed., Springer, New York, **2011**.
- [19] M. Ludwig, R. Niewa, R. Kniep, *Z. Naturforsch. B: Chem. Sci.* **1999**, *54*, 461.
- [20] J. C. Slater, *J. Chem. Phys.* **1964**, *41*, 3199.
- [21] A. Moeller, P. Amann, V. Kataev, N. Schittner, *Z. Anorg. Allg. Chem.* **2004**, *630*, 890.
- [22] G. J. Dirksen, G. Blasse, *J. Solid State Chem.* **1991**, *92*, 591.
- [23] J. A. Kechele, O. Oeckler, F. Stadler, W. Schnick, *Solid State Sci.* **2009**, *11*, 537.
- [24] M. Seibald, T. Rosenthal, O. Oeckler, W. Schnick, *Crit. Rev. Solid State Mater. Sci.* **2014**, *39*, 215.
- [25] W. H. Baur, *Crystallogr. Rev.* **1987**, *1*, 59.
- [26] V. Mauchamp, P. Moreau, L. Monconduit, M.-L. Doublet, F. Boucher, G. Ouvrard, *J. Phys. Chem. C* **2007**, *111*, 3996.
- [27] M. Zeuner, S. Pagano, S. Hug, P. Pust, S. Schmiechen, C. Scheu, W. Schnick, *Eur. J. Inorg. Chem.* **2010**, 4945.
- [28] C. Scheu, G. Dehm, H. Müllejans, R. Brydson, M. Rühle, *Microsc. Microanal. Microstruct.* **1995**, *6*, 19.

3.7 Narrow Red Emitters for Brighter White Light

published in: *Mater. Today* **2014**, Comment, 29.08.2014

authors: Philipp Pust, Sebastian Schmiechen and Wolfgang Schnick

Copyright © 2014 Elsevier

http://www.materialstoday.com/optical-materials/comment/narrow-red-emitters-for-brighter-white-light/#disqus_thread

3.7.1 Comment

More than two decades ago the lighting industry was one of the most stable, slow but steadily growing business sectors in the entire world. Well-established lighting systems like incandescent light bulbs based on glowing tungsten wires were superseded by the more energy efficient fluorescent lamps. These were mounted on standardized sockets, allowing easy exchanges of different products. However, both those systems have advantages and disadvantages. On the one hand, the color rendering index (CRI) of a classical light bulb reaches a maximum of 100, correlating with daylight, while on the other hand only about 5-10% of the consumed electrical energy is converted to light. Commercial fluorescent lamps show an increased efficiency, but with typical CRI values as low as 70-80, the emitted light is significantly lacking in color rendition. Furthermore, the use of toxic Hg is unavoidable in this type of device.

Nowadays, lighting business has changed dramatically. Environmental policy has driven a strong movement towards sustainability and “greener” products. Classical inefficient incandescent light bulbs have been nearly wiped out from the western market. This has enabled the breakthrough of another type of light source, namely light-emitting diodes (LEDs). Industry and science all over the world agree that LEDs will be the lighting technology of the future. LEDs are unbeaten in efficiency and environmental acceptability throughout their whole production and life cycle.

LEDs generate light by electron-transfer processes in semiconducting materials, whereby each emitter can only produce monochromic emission. Illumination-grade white light, however, requires covering the entire visible spectrum, ranging from blue to deep red. To achieve this, different approaches have been conceived. The easiest way is to combine three

semiconducting LEDs with blue, green and red emission. This approach, however, yields only very low quality white light. Instead, LEDs emitting high-energetic blue radiation are nowadays coated with different downconversion (or red-shifting) luminescent materials (so-called phosphors). To obtain a white-light phosphor-converted (pc-)LED, either a broadband yellow emitting (1-pc-LED) or a mixture of red and green phosphor materials (2-pc-LED) are used in addition to a blue LED die. The additive mixing of the initial blue light with the emission of different luminescent materials produces white light.

Most commercially available 1-pc-LEDs use garnet materials doped with Ce^{3+} like YAG:Ce ($\text{Y}_{3-x}\text{Gd}_x\text{Al}_{5-y}\text{Ga}_y\text{O}_{12}:\text{Ce}$) as the yellow broadband emitter. This material has excellent thermal and chemical stability. However, because of its lack of emission in the red spectral range, its application is limited to cool-white light (correlated color temperatures or CCT of 4000-8000 K) with low CRIs of typically <75 . To achieve illumination-grade light, CCT values ranging from 2700-4000 K and CRIs typically >80 are required, which only become accessible by using 2-pc-LEDs.

For this approach a huge number of materials, especially vred-emitters, have been investigated by the lighting industry but without fulfilling their demanding requirements, like chemical and thermal stability, quantum efficiencies close to 100%, and excellent thermal quenching behavior. However, through these investigations, (oxo)nitridosilicates have emerged as intriguing host lattices for doping with rare-earth ions and, therefore, as luminescent materials covering the whole spectral range from blue to red.^[1] Novel nitride-based pc-LEDs enable access to acceptable CRI values at CCTs in the desired range. With the state of the art phosphor materials, brilliant CRIs >90 can also easily be obtained, but only by accepting heavy losses in luminous efficacy (efficiency of light conversion relative to the human eye sensitivity in lm/W).

A current challenge for LED industry, therefore, is to further improve the color rendition of illumination-grade light sources without comprising energy efficiency or rather better adapting the pc-LED emission to the sensitivity of human vision to produce a high luminous efficacy. One promising approach is optimizing the spectral peak position and width of the red-emitting component.

The number of adequate red-emitting materials is rather small at present because of the challenging requirements like temperature stability up to 150°C on the LED chip surface. Eu^{2+} doped materials like $(\text{Ca,Sr})\text{SiAlN}_3:\text{Eu}^{2+}$ ($\lambda_{\text{em}} \sim 610\text{-}660\text{ nm}$, FWHM $\sim 2100\text{-}2500\text{ cm}^{-1}$)^[2,3] or $(\text{Ba,Sr})_2\text{Si}_5\text{N}_8:\text{Eu}^{2+}$ ($\lambda_{\text{em}} \sim 590\text{-}625\text{ nm}$, FWHM $\sim 2050\text{-}2600\text{ cm}^{-1}$)^[4-6] have found many applications in commercial white pc-LEDs as a result of the intense emission

caused by the $5d \rightarrow 4f$ transition. Thanks to rather broad emission bands of both materials, significant parts of the emitted light are above 700 nm and therefore outside the human eye's sensitivity. The width of the Eu^{2+} emission bands in these materials is strongly influenced by several factors. $(\text{Ca,Sr})\text{SiAlN}_3:\text{Eu}^{2+}$ is affected by the statistical distribution of Si and Al in the host lattice, leading to a broad variety of activator (Eu^{2+}) coordination spheres and, therefore, a rather broad emission band. $(\text{Ba,Sr})_2\text{Si}_5\text{N}_8:\text{Eu}^{2+}$ shows two crystallographic sites accessible for Eu^{2+} . The chemical difference between both sites leads to distinct emission maxima, which also resulting in a relatively broad composite emission.

The recently discovered group of narrow band red-emitting nitride materials like $\text{Sr}[\text{Mg}_3\text{SiN}_4]:\text{Eu}^{2+}$ ($\lambda_{\text{em}} = 615 \text{ nm}$, $\text{FWHM} \sim 1170 \text{ cm}^{-1}$)^[7] or $\text{Sr}[\text{LiAl}_3\text{N}_4]:\text{Eu}^{2+}$ ($\lambda_{\text{em}} = 650 \text{ nm}$, $\text{FWHM} \sim 1180 \text{ cm}^{-1}$)^[8] could be the basis for the next generation of illumination-grade pc-LEDs. In these materials the activator ion is situated in cuboid-like polyhedra with N as a counter ion, surrounded by a highly-condensed ordered network of edge- and corner-sharing tetrahedra. Phonons affecting the emission broadness and the thermal quenching are successfully reduced to a minimum thanks to the rigidity of the host lattice. The compound $\text{Sr}[\text{LiAl}_3\text{N}_4]:\text{Eu}^{2+}$ already demonstrates the high potential of such materials for industrial applications. The use of this material as a red-emitting component in a pc-LED helps to increase the luminous efficacy of a prototype device by 14% ($R_a8 = 91$, $R_9 = 57$) compared to a commercially available high-CRI LED, still keeping a brilliant CRI >90.

To further optimize the luminous efficacy of solid-state light sources for a variety of correlated color temperatures and color rendition requirements, tuning of the red emission spectrum towards shorter wavelengths ($\sim 600\text{--}630 \text{ nm}$) will be the next challenge for solid-state lighting industry to meet.

3.7.2 References

- [1] M. Zeuner, S. Pagano, W. Schnick, *Angew. Chem. Int. Ed.* **2011**, *50*, 7754.
- [2] K. Uheda, N. Hirosaki, H. Yamamoto, *Phys. Stat. Sol. A* **2006**, *11*, 2712.
- [3] K. Uheda, N. Hirosaki, Y. Yamamoto, A. Naita, T. Nakajima, H. Yamamoto, *Electrochem. Solid State Lett.* **2006**, *9*, H22.
- [4] M. Krames, G. O. Mueller, R. B. Mueller-Mach, H. Bechtel, P. J. Schmidt, *PCT Int. Appl.*, WO 2010131133, A1, **2010**.
- [5] H. A. Höpfe, H. Lutz, P. Morys, W. Schnick, A. Seilmeier, *J. Phys. Chem. Solids* **2000**, *61*, 2001.

-
- [6] R. Mueller-Mach, G. Mueller, M. R. Krames, H. A. Höpfe, F. Stadler, W. Schnick, T. Juestel, P. Schmidt, *Phys. Status Solidi A* **2005**, *202*, 1727.
- [7] S. Schmiechen, H. Schneider, P. Wagatha, C. Hecht, P. J. Schmidt, W. Schnick, *Chem. Mater.* **2014**, *26*, 2712.
- [8] P. Pust, V. Weiler, C. Hecht, A. Tücks, A. S. Wochnik, A.-K. Henß, D. Wiechert, C. Scheu, P. J. Schmidt, W. Schnick, *Nat. Mater.* **2014**, *13*, 891.

4 Conclusion and Outlook

Currently available illumination-grade pc-LEDs typically possess many advantages like superior energy efficiency and good color rendition compared to standard lighting systems. However, a major challenge in the LED industry is that excellent CRI values larger than 90 are only achievable by measures which significantly compromise energy efficiency. As already reported in literature, CRI values of pc-LEDs critically depend on the luminescence properties of the red-emitting components.^[1] Currently used phosphor materials such as $(\text{Ba,Sr})_2\text{Si}_5\text{N}_8:\text{Eu}^{2+}$ ($\lambda_{\text{em}} \sim 590\text{-}625$ nm, FWHM $\sim 2,050\text{-}2,600$ cm^{-1})^[2,3] or $(\text{Ca,Sr})\text{SiAlN}_3:\text{Eu}^{2+}$ ($\lambda_{\text{em}} \sim 610\text{-}660$ nm, FWHM $\sim 2,100\text{-}2,500$ cm^{-1})^[4,5] exhibit rather broad emission bands in the red spectral region. Significant parts of the emitted light therefore are outside the sensitivity range of the human eye at wavelengths exceeding 700 nm. This greatly limits the luminous efficacy of illumination-grade pc-LEDs. To reduce emission above 700 nm, inventing a red-emitting phosphor material with a very narrow FWHM would be the best option. Ideally, the values of such a material are $\lambda_{\text{em}} \sim 620\text{-}650$ nm with a FWHM of ~ 50 nm.

Within this thesis several new representatives of the nitridoaluminate compound class have been synthesized, characterized and investigated with respect to their luminescence properties.

DiSalvo et al. described the substitutability of Ga^{3+} and Ge^{4+} by Mg^{2+} in nitridogallates and –germanates, demonstrated by the two compounds $\text{Sr}[\text{Mg}_2\text{Ga}_2\text{N}_4]$ and $\text{Sr}[\text{Mg}_3\text{GeN}_4]$ both crystallizing in the UCr_4C_4 -structure type.^[6,7] This structure type was subsequently discussed as attractive host lattice for luminescent materials, due to the highly symmetric cuboidal coordination of the heavy atom site. A very similar substitutability was observed for Al^{3+} by Mg^{2+} in the compounds $M[\text{Mg}_2\text{Al}_2\text{N}_4]$ ($M = \text{Ca,Sr,Ba,Eu}$),^[8] also crystallizing in this structure type. Here, the first alkaline earth nitridoaluminates with a three dimensional network structure were synthesized. Furthermore, the degree of condensation in this structure type is $\kappa = 1$ (atomic ratio (Al,Mg):N). The κ value of 1 is comparable to the binary nitride AlN , predicting a high stability. Doped samples of $M[\text{Mg}_2\text{Al}_2\text{N}_4]:\text{Eu}^{2+}$ ($M = \text{Ca,Sr,Ba}$) show intense red luminescence with FWHM values between 80 and 100 nm. More thorough studies revealed anomalous luminescence phenomena like trapped exciton emission. These phenomena are possibly caused by the rather small band gaps of the investigated materials (3.6-3.8 eV) and the therefore small energy difference between the Eu(II) $5d$ levels and the conduction band of the host. It is also expected that the relatively broad emission bands result from the statistical distribution of the tetrahedrally coordinated cations Al and Mg. This leads

to constantly varying (Al,Mg)-N bond lengths in the tetrahedral spheres, accompanied by a wide variety of activator-N bond lengths and environments. Similar properties are also known from the nitridoalumosilicate $(\text{Ca,Sr})\text{SiAlN}_3:\text{Eu}^{2+}$.^[4,5] So far, it was demonstrated that nitridoaluminates are potential host lattices for Eu^{2+} doped phosphor materials. Intense red emission is observed, however, the UCr_4C_4 structure type is not suited for narrow-band red emission. This is due to the disordered network with the combination of Al^{3+} and Mg^{2+} as tetrahedral network cations leading to rather small band gaps.

Hoppe et al. demonstrated the large structural variety of the UCr_4C_4 structure type by characterizing various ordered oxidic structure types, e.g. $\text{Na}[\text{Li}_3\text{SiO}_4]$.^[9] Different substitutional variants were developed based on similar $\text{A}[\text{BC}_3\text{X}_4]$ structures with either Li/Al or Mg/Si occupying the tetrahedrally coordinated sites B and C. The novel nitridolithoaluminate $\text{Ca}[\text{LiAl}_3\text{N}_4]:\text{Eu}^{2+}$ was discovered during this research.^[10] $\text{Ca}[\text{LiAl}_3\text{N}_4]:\text{Eu}^{2+}$ crystallizes in the ordered $\text{Na}[\text{Li}_3\text{SiO}_4]$ structure type with very similar structural features to $\text{M}[\text{Mg}_2\text{Al}_2\text{N}_4]$ ($M = \text{Ca,Sr,Ba,Eu}$). The most important difference is that there are four crystallographically independent sites in tetrahedral coordination enabling an ordering of the $[\text{AlN}_4]$ and $[\text{LiN}_4]$ tetrahedra. This significantly influences the luminescence properties ($\lambda_{\text{em}} \sim 668 \text{ nm}$, $\text{FWHM} \sim 1333 \text{ cm}^{-1}$ ($\sim 60 \text{ nm}$)) and reduces the FWHM to values very close to the desired 50 nm. The recently published isotypic $\text{Sr}[\text{Mg}_3\text{SiN}_4]:\text{Eu}^{2+}$ ($\lambda_{\text{em}} \sim 615 \text{ nm}$, $\text{FWHM} \sim 1170 \text{ cm}^{-1}$ ($\sim 43 \text{ nm}$)) represents the world record for narrow-band Eu^{2+} emission in the red spectral region which can be considered as proof of concept.^[11] However, the luminescence properties of the latter compound are also affected by the rather small band gap ($\sim 3.9 \text{ eV}$), leading to distinct thermal quenching even at room temperature.

The nitridolithoaluminate $\text{Sr}[\text{LiAl}_3\text{N}_4]:\text{Eu}^{2+}$ which crystallizes in the $\text{Cs}[\text{Na}_3\text{PbO}_4]$ -structure type finally fulfilled industrial requirements.^[12,13] With $\lambda_{\text{em}} \sim 650 \text{ nm}$ and a FWHM of $\sim 1180 \text{ cm}^{-1}$ ($\sim 50 \text{ nm}$) an intense red emission is observed. The emission is not as narrow as by $\text{Sr}[\text{Mg}_3\text{SiN}_4]:\text{Eu}^{2+}$, but with a better thermal behavior. Due to an increased band gap ($\sim 4.7 \text{ eV}$), $\text{Sr}[\text{LiAl}_3\text{N}_4]:\text{Eu}^{2+}$ shows virtually no thermal quenching up to $200 \text{ }^\circ\text{C}$ ($>95\%$ relative quantum efficiency at $200 \text{ }^\circ\text{C}$) and external quantum efficiencies of currently up to $\text{QE}_{\text{ex}} = 52\%$ ($\text{QE}_{\text{int}} = 76\%$). A prototype pc-LED employing $\text{Sr}[\text{LiAl}_3\text{N}_4]:\text{Eu}^{2+}$ as red-emitting component, exhibited an increase of 14% in luminous efficacy compared to a commercially available high-CRI LED. Additionally, an excellent color rendition ($R_a8 = 91$, $R_9 = 57$) was achieved. The development towards an industrial product containing this material is currently in progress. To further understand the luminescence mechanisms, the electronic structure of

Sr[LiAl₃N₄]:Eu²⁺ was investigated by XAS and XES measurements and by theoretical calculations.

In general, the group of “UCr₄C₄-like” phosphor materials is an excellent example for systematic proceeding and tuning of luminescence properties regarding a narrow-band red emission. Furthermore, it is a nice model system for a stepwise understanding of the structural requirements for efficient luminescence. With the discovery of new and highly promising red-emitting phosphor materials and the investigation and description of their physical properties, a fundamental step toward the design on demand of new phosphor materials was achieved.

However, narrow-band red emission is not limited to materials with a cuboidal heavy atom site, which is partly occupied by the activator ion. The nitridolithoaluminate Ca_{18.75}Li_{10.5}Al₃₉N₅₅:Eu²⁺ is homeotypic to the manganate Na₂₆Mn₃₉O₅₅ forming a highly-condensed network of connected Al₃₅N₅₆ T5-supertetrahedra.^[14] This material also exhibits an intense red emission peaking at 647 nm with a FWHM of ~1190 cm⁻¹ (~54 nm). The structure comprises three different Ca²⁺ sites in octahedral and trigonal prismatic coordination by nitrogen. Due to the dense packing of the crystal structure Eu²⁺ is expected to be positioned on the Ca²⁺ sites and not on possible interstitial positions. The characterization of this luminophor demonstrated that there are still many facets in luminescence that are not yet totally understood.

In this thesis a firm foundation for many assumptions regarding structure-property-relations of luminescent materials could be established and several work hypotheses could be proved. However, some new questions arose, that will be the basis for subsequent research and further close collaboration between the lighting industry and universities.

References

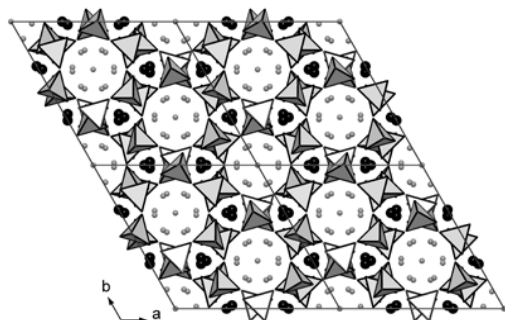
- [1] M. Krames, G.O. Mueller, R.B. Mueller-Mach, H. Bechtel, P.J. Schmidt, *PCT Int. Appl.*, WO 2010131133, A1, **2010**.
- [2] H. A. Höpfe, H. Lutz, P. Morys, W. Schnick, A. Seilmeier, *J. Phys. Chem. Solids* **2000**, *61*, 2001.
- [3] R. Mueller-Mach, G. Mueller, M. R. Krames, H. A. Höpfe, F. Stadler, W. Schnick, T. Juestel, P. Schmidt, *Phys. Status Solidi A* **2005**, *202*, 1727.
- [4] K. Uheda, N. Hirosaki, H. Yamamoto, *Phys. Stat. Sol. A* **2006**, *11*, 2712.
- [5] K. Uheda, N. Hirosaki, Y. Yamamoto, A. Naita, T. Nakajima, H. Yamamoto, *Electrochem. Solid State Lett.* **2006**, *9*, H22.
- [6] R. K. Behrens, W. Jeitschko, *Monatsh. Chem.* **1987**, *118*, 43.
- [7] D. G. Park, Y. Dong, F. J. DiSalvo, *Solid State Sci.* **2008**, *10*, 1846.

-
- [8] P. Pust, F. Hintze, C. Hecht, V. Weiler, A. Locher, D. Zitnanska, S. Harm, D. Wiechert, P. J. Schmidt, W. Schnick, *Chem. Mater.* **2014**, in press.
- [9] B. Nowitzki, R. Hoppe, *Rev. Chim. Min.* **1986**, *23*, 217.
- [10] P. Pust, A. S. Wochnik, E. Baumann, P. J. Schmidt, D. Wiechert, C. Scheu, W. Schnick, *Chem. Mater.* **2014**, *26*, 3544.
- [11] S. Schmiechen, H. Schneider, P. Wagatha, C. Hecht, P. J. Schmidt, W. Schnick, *Chem. Mater.* **2014**, *26*, 2712.
- [12] P. Pust, V. Weiler, C. Hecht, A. Tücks, A. S. Wochnik, A.-K. Henß, D. Wiechert, C. Scheu, P. J. Schmidt, W. Schnick, *Nat. Mater.* **2014**, *13*, 891.
- [13] H. Stoll, R. Hoppe, *Rev. Chim. Min.* **1987**, *24*, 96.
- [14] A. Moeller, P. Amann, V. Kataev, N. Schittner, *Z. Anorg. Allg. Chem.* **2004**, *630*, 890.

5 Summary

1. Ammonothermal Synthesis and Crystal Structure of $\text{BaAl}_2(\text{NH}_2)_8 \cdot 2\text{NH}_3$

The compound $\text{BaAl}_2(\text{NH}_2)_8 \cdot 2\text{NH}_3$ was synthesized under ammonothermal conditions in a stainless-steel autoclave at 823 K and 245 MPa. Single crystals of this material were grown on Al substrates and prepared and measured under low-temperature conditions. The crystal

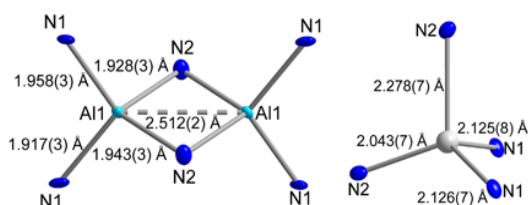


structure ($R\bar{3}c$ (no. 167), $a = 15.7370(17)$, $c = 28.804(6)$ Å, $Z = 18$, $wR_2 = 0.07$) was solved on the basis of single-crystal X-ray diffraction data and the structure shows tube like pores with a calculated volume of 1242.5 Å³. $\text{BaAl}_2(\text{NH}_2)_8 \cdot 2\text{NH}_3$ may be a suitable precursor material for nitridoaluminate synthesis since

constituting atoms are already arranged on an atomic level and a ternary compound in the system Ba-Al-N may be formed by thermal decomposition of the precursor.

2. $\text{Ca}[\text{LiAlN}_2]$: A Quaternary Nitridoaluminate

$\text{Ca}[\text{LiAlN}_2]$ was synthesized from LiAlH_4 , LiN_3 , calcium, and lithium metal as fluxing agent in welded-shut tantalum crucibles at 900 °C and crystallizes in the form of colorless platelets that undergo hydrolysis under moisture. The crystal structure of $\text{Ca}[\text{LiAlN}_2]$ ($P2_1/c$ (no. 14), $a = 5.7587(12)$ Å, $b = 6.8773(14)$ Å, $c = 5.7960(12)$ Å, $\beta = 90.28(3)^\circ$, $Z = 4$) was successfully solved by using single-crystal X-ray diffraction data and was confirmed with X-ray powder-diffraction data as well as lattice-energy calculations (MAPLE). $\text{Ca}[\text{LiAlN}_2]$ represents the first example of a quaternary calcium nitridolithoaluminate with tetrahedral AlN_4 and LiN_4

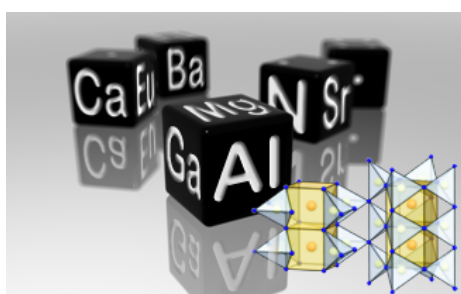


units forming layers of edge- and vertex-sharing AlN_4 tetrahedra. Li^+ ions are positioned in tetrahedral voids within the $[\text{Al}_2\text{N}_2\text{N}_{4/2}]$ layers resulting in a highly condensed structure of Al- and Li-centered polyhedra. Here we could show

that the Li-flux route combined with a hydride as precursor permits a convenient synthetic approach to new nitridoaluminates at moderate temperatures.

3. Group (III) Nitrides $M[\text{Mg}_2\text{Al}_2\text{N}_4]$ ($M = \text{Ca}, \text{Sr}, \text{Ba}, \text{Eu}$) and $\text{Ba}[\text{Mg}_2\text{Ga}_2\text{N}_4]$ - Structural Relation and Nontypical Luminescence Properties of Eu^{2+} Doped Samples

The isotopic nitridomagnesoaluminates $M[\text{Mg}_2\text{Al}_2\text{N}_4]$ ($M = \text{Ca}, \text{Sr}, \text{Ba}, \text{Eu}$) as well as a novel nitridomagnesogallate $\text{Ba}[\text{Mg}_2\text{Ga}_2\text{N}_4]$ have been synthesized by high-temperature reactions. All compounds crystallize in the UCr_4C_4 -structure type forming a highly condensed anionic network of disordered $(\text{Al}/\text{Mg})\text{N}_4$ and $(\text{Ga}/\text{Mg})\text{N}_4$ units, connected to each other by common edges and corners. There is only one heavy atom site centered in *vierer* ring channels along $[001]$ and coordinated in a cuboidal manner by N making this group of materials attractive candidates for luminescence. Doped with Eu^{2+} these compounds show intense luminescence

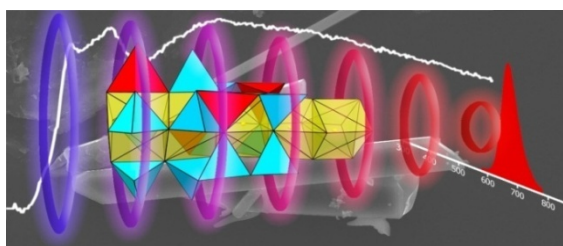


in the red spectral region. However, in the row of $M[\text{Mg}_2\text{Al}_2\text{N}_4]:\text{Eu}^{2+}$ ($M = \text{Ca}, \text{Sr}, \text{Ba}$) a nontypical emission red-shift is observed with increasing alkaline earth cation size and also untypical low-temperature luminescence properties. Regular Eu^{2+} emission is only observed for $M[\text{Mg}_2\text{Al}_2\text{N}_4]:\text{Eu}^{2+}$ ($M = \text{Ca}, \text{Sr}$) at

temperatures above 100 K. Below this temperature and also for $M = \text{Ba}$ emission from a trapped exciton state is observed.

4. $\text{Ca}[\text{LiAl}_3\text{N}_4]:\text{Eu}^{2+}$ - A Narrow Band Red-Emitting Nitridolithoaluminate

$\text{Ca}[\text{LiAl}_3\text{N}_4]:\text{Eu}^{2+}$ ($I4_1/a$ (no. 88), $a = 11.1600(16)$ Å, and $c = 12.865(3)$ Å, $Z = 16$) is an intriguing new narrow-band red-emitting phosphor material with potential for application in illumination-grade pc-LEDs and was synthesized by high-temperature reaction. The compound consists of a highly-condensed rigid framework of AlN_4 and LiN_4 tetrahedra with Ca atoms positioned in *vierer* ring channels along $[001]$ in eightfold coordination by nitrogen. The structural model was verified by lattice-energy calculations (MAPLE) and the



incorporation of Li ions in the structure was corroborated by EELS measurements. Single-crystal luminescence measurements yielded an emission maximum at 668 nm with a FWHM of only 1333 cm^{-1} ($\sim 60 \text{ nm}$). A highly-condensed,

rigid network structure like in $\text{Ca}[\text{LiAl}_3\text{N}_4]:\text{Eu}^{2+}$, which comprises a single, cuboidally coordinated alkaline earth atom position seems to be beneficial for narrow-band red emission.

5. Narrow-Band Red-Emitting Sr[LiAl₃N₄]:Eu²⁺ as a Next-Generation LED-Phosphor Material

To facilitate the next generation of high-power white pc-LEDs, the discovery of more efficient red-emitting phosphor materials is essential. Sr[LiAl₃N₄]:Eu²⁺ was synthesized by high-temperature reaction and structurally characterized by single-crystal and powder XRD

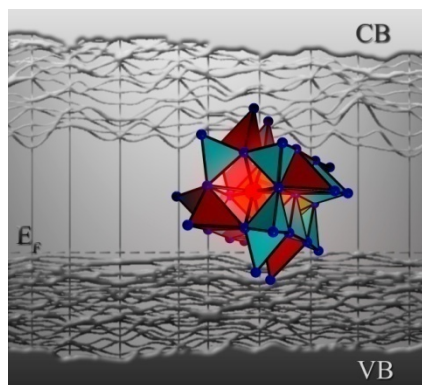


data (*P* $\bar{1}$ (no. 2), $a = 5.86631(12)$ Å, $b = 7.51099(15)$ Å, $c = 9.96545(17)$ Å, $\alpha = 83.6028(12)^\circ$, $\beta = 76.7720(13)^\circ$ and $\gamma = 79.5650(14)^\circ$, $Z = 4$). The incorporation of Li in the structure was corroborated by EELS measurements and by ⁷Li-MAS-NMR spectroscopy. Doped with Eu²⁺, Sr[LiAl₃N₄] emerged as a new high-performance narrow-band red-emitting phosphor material ($\lambda_{\text{max}} \sim 650$ nm, FWHM $\sim 1,180$ cm⁻¹ (~ 50 nm)) which exhibits only very low thermal quenching ($>95\%$ relative to the quantum efficiency at 200 °C). A prototype pc-LED, employing Sr[LiAl₃N₄]:Eu²⁺ as the red-emitting component, already

shows an increase of 14% in luminous efficacy compared to a commercially available high-CRI LED, keeping an excellent color rendition ($R_{a8} = 91$, $R_9 = 57$).

6. Investigations of the Electronic Structure and Band Gap of the Next-Generation LED-Phosphor Sr[LiAl₃N₄]:Eu²⁺ - Experiment and Calculations

To fully understand the complex structure-property relationships and to enable further optimization of the material properties of Sr[LiAl₃N₄]:Eu²⁺, an in-depth presentation of the electronic structure determined through experimental soft X-ray spectroscopy measurements

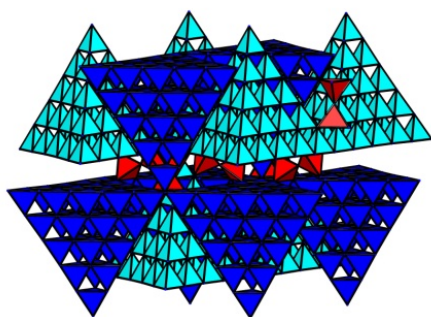


and density functional theory calculations is presented in this contribution. Sr[LiAl₃N₄]:Eu²⁺ is found to have an indirect band gap of (4.56 ± 0.25) eV, a highly similar local electronic structure of the two nonequivalent Sr sites, and the necessary characteristics for a uniform shift in the centroid of the Eu²⁺ 5d states. These investigations clarify why, such a narrow emission band is still observed

although there are two sites which can be occupied by the activator ion Eu²⁺, and re-enforce the importance of Sr[LiAl₃N₄]:Eu²⁺ as a phosphor for LED applications.

7. $\text{Ca}_{18.75}\text{Li}_{10.5}\text{Al}_{39}\text{N}_{55}:\text{Eu}^{2+}$ - Supertetrahedron Phosphors for Solid-State Lighting

Highly-efficient red-emitting phosphor materials deliver the basis for next-generation illumination-grade light-emitting diodes (LEDs). $\text{Ca}_{18.75}\text{Li}_{10.5}\text{Al}_{39}\text{N}_{55}:\text{Eu}^{2+}$ is a novel material, with efficient narrow-band red emission ($\lambda_{\text{em}} \sim 647 \text{ nm}$, FWHM $\sim 1190 \text{ cm}^{-1}$). This compound has been synthesized by high-temperature reaction in a hot isostatic press under nitrogen



pressure and characterized by single-crystal XRD data ($Fd\bar{3}m$ (no. 227) with $a = 22.415(3) \text{ \AA}$ and $Z = 8$). $\text{Ca}_{18.75}\text{Li}_{10.5}\text{Al}_{39}\text{N}_{55}:\text{Eu}^{2+}$ features a rather uncommon crystal structure, forming sphalerite-like T5-supertetrahedra of AlN_4 tetrahedra, which are interconnected by additional AlN_4 tetrahedra. The presence of Li in the crystal structure was confirmed by

EELS measurements. Luminescence investigations of doped samples show an intense red emission peaking at 647 nm with an exceptionally narrow FWHM of $\sim 1190 \text{ cm}^{-1}$ ($\sim 54 \text{ nm}$).

8. Narrow Red Emitters for Brighter White Light

The comment article summarizes the challenges for LED technology in the presence and the future. The strong movement towards sustainability by environmental policy enabled the breakthrough for illumination-grade pc-LEDs as energy-saving light sources of the future. Thereby, pc-LEDs are unbeaten in efficiency and environmental acceptability, during the whole production period and life cycle. With state of the art phosphor materials also brilliant CRIs >90 (like with common incandescent light bulbs) can easily be obtained, however, by accepting heavy losses in luminous efficacy. Therefore, the current challenge for LED industry is to further improve the color rendition without comprising energy efficiency. Most beneficial for this is optimizing the spectral peak position and width of the red-emitting component to eliminate emission losses in the infrared region. Narrow-band red emitting materials like $\text{Ca}[\text{LiAl}_3\text{N}_4]:\text{Eu}^{2+}$, $\text{Sr}[\text{LiAl}_3\text{N}_4]:\text{Eu}^{2+}$ or $\text{Sr}[\text{Mg}_3\text{SiN}_4]:\text{Eu}^{2+}$ convince with intriguing luminescence properties and point the way toward the next generation of white light LEDs.

6 Appendix

6.1 Supporting Information for Chapter 3.1

Philipp Pust, Sandro Pagano and Wolfgang Schnick, *Eur. J. Inorg. Chem.* **2013**, 1157-1160.

Table S1. Crystallographic data of Rietveld refinement of Ca[LiAlN₂].

Formula	Ca[LiAlN ₂]
Crystal system	monoclinic
Space group	<i>P</i> 2 ₁ / <i>c</i> (no. 14)
Lattice parameters (Å, °)	<i>a</i> = 5.76304(5), <i>b</i> = 6.88006(5), <i>c</i> = 5.80399(5), <i>β</i> = 90.256(7)
Cell volume (Å ³)	230.126(3)
Formula units per unit cell	4
Density (g·cm ⁻³)	2.952
T (K)	293(2)
Diffractometer	STOE STADI P
Radiation (Å)	Cu-Kα ₁ (λ = 1.54056 Å)
Profile range	5.0 ≤ θ ≤ 38.5
Data points	6720
Total number of reflections	403
Refined parameters	62
Background function	Shifted Chebyshev (36 parameters)
<i>R</i> values	<i>R</i> _P = 0.0497; <i>wR</i> _P = 0.0631; <i>R</i> (<i>F</i> ²) = 0.0392

6.2 Supporting Information for Chapter 3.2

Philipp Pust, Frauke Hintze, Cora Hecht, Volker Weiler, Andreas Locher, Daniela Zitnanska, Sascha Harm, Detlef Wiechert, Peter J. Schmidt and Wolfgang Schnick, *Chem. Mater.* **2014**, DOI 10.1021/cm502280p, (in press)

Ca[Mg₂Al₂N₄]

Table S1. Crystallographic data of Ca[Mg₂Al₂N₄].

Formula	Ca[Mg ₂ Al ₂ N ₄]
Crystal system	tetragonal
Space group	<i>I4/m</i> (no. 87)
Lattice parameters /Å	$a = b = 8.0655(11)$, $c = 3.2857(7)$
Cell volume /Å ³	213.74(6)
Formula units /cell	2
$\rho_{\text{calcd.}} / \text{g} \cdot \text{cm}^{-3}$	3.09
μ / mm^{-1}	2.018
T /K	293(2)
F(000)	196
Radiation /Å, monochromator	Mo-K α ($\lambda = 0.71073$), graphite
Absorption correction	none
θ range /°	3.6 - 29.4
Index ranges	$-11 \leq h \leq 11$ $-11 \leq k \leq 11$ $-4 \leq l \leq 4$
Independent reflections	176 ($R_{\text{int}} = 0.0436$)
Refined parameters	15
Goodness of fit	1.199
$R1$ (all data); $R1$ ($F^2 > 2\sigma(F^2)$)	0.0323; 0.0311
$wR2$ (all data); $wR2$ ($F^2 > 2\sigma(F^2)$)	0.0864; 0.0849
Max. / min. residual electron density /e·Å ⁻³	0.46 / -0.50

Table S2. Atomic coordinates and isotropic displacement parameters / \AA^2 of $\text{Ca}[\text{Mg}_2\text{Al}_2\text{N}_4]$, standard deviations in parentheses.

Atom (Wyck.)	x	y	z	U_{eq}
Ca (2a)	0	0	0	0.0199(4)
Al (8h)	0.18465(13)	0.36323(12)	0	0.0169(4)
Mg (8h)	0.18465(13)	0.36323(12)	0	0.0169(4)
N (8h)	0.4048(3)	0.2416(5)	0	0.0295(8)

Sr[Mg₂Al₂N₄]**Table S3.** Crystallographic data of Rietveld refinement of $\text{Sr}[\text{Mg}_2\text{Al}_2\text{N}_4]$.

Formula	$\text{Sr}[\text{Mg}_2\text{Al}_2\text{N}_4]$
Crystal system	tetragonal
Space group	$I4/m$ (no. 87)
Lattice parameters / \AA	$a = b = 8.16855(14)$, $c = 3.35391(6)$
Cell volume / \AA^3	223.790(9)
Formula units per unit cell	2
Density / $\text{g}\cdot\text{cm}^{-3}$	3.654
T /K	293(2)
Diffractometer	Huber G670
Radiation / \AA , monochromator	$\text{Cu-K}\alpha_1$ ($\lambda = 1.54056$), Ge(111)
Profile range	$5.0 \leq \theta \leq 41.0$
Data points	14384
Total number of reflections	44
Refined parameters	63
Background function	Shifted Chebyshev (18 parameters)
R values	$R_p = 0.0305$; $wR_p = 0.0407$; $R(F^2) = 0.0224$

Ba[Mg₂Al₂N₄]**Table S4.** Crystallographic data of Rietveld refinement of Ba[Mg₂Al₂N₄].

Formula	Ba[Mg ₂ Al ₂ N ₄]
Crystal system	tetragonal
Space group	<i>I4/m</i> (no. 87)
Lattice parameters /Å	$a = b = 8.2602(9)$, $c = 3.43198(19)$
Cell volume /Å ³	234.17(5)
Formula units per unit cell	2
Density /g·cm ⁻³	4.197
T /K	293(2)
Diffractometer	Huber G670
Radiation /Å, monochromator	Cu-Kα ₁ ($\lambda = 1.54056$), Ge(111)
Profile range	$5.0 \leq \theta \leq 41.0$
Data points	14384
Total number of reflections	46
Refined parameters	63
Background function	Shifted Chebyshev (18 parameters)
R values	$R_p = 0.0228$; $wR_p = 0.0306$; $R(F^2) = 0.0336$

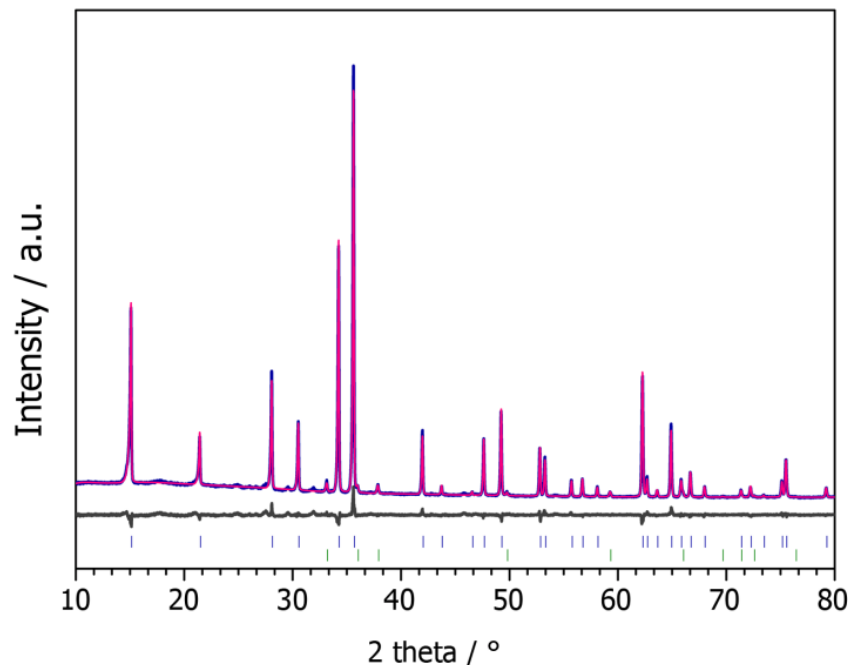


Figure S1. Rietveld refinement ($R_p = 0.0228$, $wR_p = 0.0306$; 14384 data points) of X-ray powder-diffraction pattern of Ba[Mg₂Al₂N₄] with measured histogram (blue line), calculated pattern (red line), difference curve (gray line) and positions of reflections (blue bars). Positions of AlN reflections (green bars).

Eu[Mg₂Al₂N₄]**Table S5.** Crystallographic data of Eu[Mg₂Al₂N₄].

Formula	Eu[Mg ₂ Al ₂ N ₄]
Crystal system	tetragonal
Space group	<i>I4/m</i> (no. 87)
Lattice parameters /Å	<i>a</i> = <i>b</i> = 8.1539(12), <i>c</i> = 3.3430(7)
Cell volume /Å ³	222.26(7)
Formula units /cell	2
$\rho_{\text{calcd.}}$ /g·cm ⁻³	4.64
μ /mm ⁻¹	14.637
T /K	293(2)
F(000)	282
Diffractometer	STOE IPDS I
Radiation /Å, monochromator	Mo-K α (λ = 0.71073), graphite
Absorption correction	multi scan
Max. / min. transmission	0.3894 / 0.3644
θ range /°	3.1 - 40.3
Index ranges	-11 ≤ <i>h</i> ≤ 11 -11 ≤ <i>k</i> ≤ 11 -4 ≤ <i>l</i> ≤ 4
Independent reflections	179 (<i>R</i> _{int} = 0.0415)
Refined parameters	16
Goodness of fit	1.105
<i>R</i> 1 (all data); <i>R</i> 1 (<i>F</i> ² > 2σ(<i>F</i> ²))	0.0152; 0.0152
<i>wR</i> 2 (all data); <i>wR</i> 2 (<i>F</i> ² > 2σ(<i>F</i> ²))	0.0333; 0.0333
Max. / min. residual electron density /e·Å ⁻³	2.06 / -0.94

Table S6. Atomic coordinates and isotropic displacement parameters / Å² of Eu[Mg₂Al₂N₄], standard deviations in parentheses.

Atom (Wyck.)	<i>x</i>	<i>y</i>	<i>z</i>	<i>U</i> _{eq}
Eu (2 <i>a</i>)	0	0	0	0.01207(18)
Al (8 <i>h</i>)	0.18343(14)	0.36371(13)	0	0.0105(2)
Mg (8 <i>h</i>)	0.18343(14)	0.36371(13)	0	0.0153(2)
N (8 <i>h</i>)	0.2365(5)	0.5973(4)	0	0.0207(6)

Table S7. Crystallographic data of Rietveld refinement of Eu[Mg₂Al₂N₄].

Formula	Eu[Mg ₂ Al ₂ N ₄]
Crystal system	tetragonal
Space group	<i>I4/m</i> (no. 87)
Lattice parameters /Å	$a = b = 8.16004(13)$, $c = 3.35036(7)$
Cell volume /Å ³	223.088(8)
Formula units per unit cell	2
Density /g·cm ⁻³	4.623
T /K	293(2)
Diffractometer	STOE STADI P
Radiation /Å, monochromator	Cu-Kα ₁ ($\lambda = 1.54056$), Ge(111)
Profile range	$5.0 \leq \theta \leq 35.0$
Data points	6000
Total number of reflections	33
Refined parameters	57
Background function	Shifted Chebyshev (36 parameters)
R values	$R_p = 0.0273$; $wR_p = 0.0345$; $R(F^2) = 0.0374$

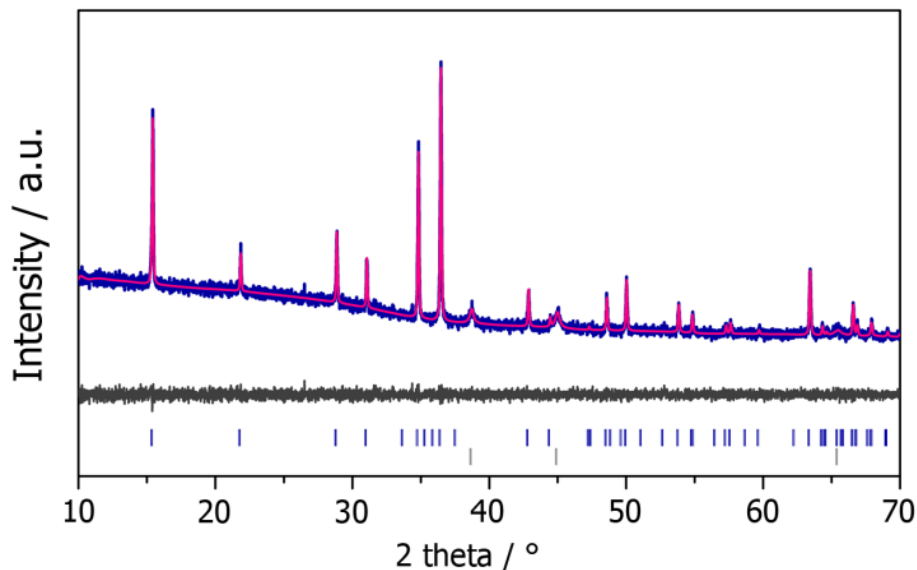


Figure S2. Rietveld refinement ($R_p = 0.0273$, $wR_p = 0.0345$; 6000 data points) of X-ray powder-diffraction pattern of Eu[Mg₂Al₂N₄] with measured histogram (blue line), calculated pattern (red line), difference curve (gray line) and positions of reflections (blue bars). Positions of LiF reflections (gray bars).

Ba[Mg₂Ga₂N₄]**Table S8.** Crystallographic data of Ba[Mg₂Ga₂N₄].

Formula	Ba[Mg ₂ Ga ₂ N ₄]
Crystal system	tetragonal
Space group	<i>I4/m</i> (no. 87)
Lattice parameters /Å	$a = b = 8.3654(12)$ $c = 3.4411(7)$
Cell volume /Å ³	240.81(7)
Formula units /cell	2
$\rho_{\text{calcd.}}$ /g·cm ⁻³	5.261
μ /mm ⁻¹	19.317
T /K	293(2)
F(000)	232
Radiation /Å, monochromator	Mo-K α ($\lambda = 0.71073$), graphite
Absorption correction	Multi-Scan
θ range /°	3.44 - 39.44
Index ranges	$-14 \leq h \leq 14$ $-14 \leq k \leq 14$ $-6 \leq l \leq 6$
Independent reflections	402 ($R_{\text{int}} = 0.0326$)
Refined parameters	16
Goodness of fit	1.101
$R1$ (all data); $R1$ ($F^2 > 2\sigma(F^2)$)	0.0155; 0.0146
$wR2$ (all data); $wR2$ ($F^2 > 2\sigma(F^2)$)	0.0309; 0.0305
Max. / min. residual electron density /e·Å ⁻³	1.266 / -1.004

Table S9. Atomic coordinates and isotropic displacement parameters / Å² of Ba[Mg₂Ga₂N₄], standard deviations in parentheses.

Atom (Wyck.)	x	y	z	Ueq
Ba (2a)	0	0	0	0.00887(6)
Ga (8h)	0.18296(4)	0.63525(4)	0	0.00592(7)
Mg (8h)	0.18296(4)	0.63525(4)	0	0.00592(7)
N (8h)	0.2328(2)	0.40145(19)	0	0.0103(3)

6.3 Supporting Information for Chapter 3.4

Philipp Pust, Volker Weiler, Cora Hecht, Andreas Tücks, Angela S. Wochnik, Ann-Kathrin Henß, Detlef Wiechert, Christina Scheu, Peter J. Schmidt and Wolfgang Schnick, *Nat. Mater.* **2014**, *13*, 891-896.

Colour Rendering Index

The Colour Rendering Index (CRI) is a dimensionless index which depicts a measure of the degree to which the perceived colours of objects illuminated by a light source conform to those of the same objects illuminated by a reference source for specified conditions.^[1,2] The reference illuminant is the Planckian radiation for test sources with a correlated colour temperature (CCT) of <5000 K, or a phase of daylight for test sources with CCT of <5000 K. CRI is a figure of merit of a light source which indicates how a light source renders the colours of illuminated people and objects.^[3] When CRI is calculated, it can be rated on a scale from 0 to 100. A CRI of 100 would represent that all colour samples illuminated by a light source in question would appear to have the same colour as those same samples illuminated by a reference source.

Luminous Efficacy

Luminous efficacy is a figure of merit for light sources. The luminous efficacy of a light source is defined as the ratio of the total luminous flux (lumens) to the power (usually watts).^[1,2] Depending on the context, the power can be either the radiant flux of the source output, or the total electric power consumed by the source. The lumen is defined as 1/683 W of monochromatic green light at a frequency of $540 \cdot 10^{12}$ Hz (corresponding to a wavelength of about 555 nm where the human eye is most sensitive). This means that the theoretically attainable maximum value assuming complete conversion of energy at 555 nm would be 683 lm/W. The luminous efficacy is always in contradiction with CRI, because a high CRI value requires proper spectral dispersion over all the visible range, which would make the luminous efficacy far below 683 lm/W. Thus, balanced values of these two parameters are adopted for different lighting occasions.

Table S1. Crystallographic data of Rietveld refinement of Sr[LiAl₃N₄]:Eu²⁺.

Formula	Sr[LiAl ₃ N ₄]:Eu ²⁺
Crystal system	Triclinic
Space group	<i>P</i> $\bar{1}$ (no. 2)
Lattice parameters (Å, °)	<i>a</i> = 5.86631(12), <i>b</i> = 7.51099(15), <i>c</i> = 9.96545(17), α = 83.6028(12), β = 76.7720(13) and γ = 79.5650(14)
Cell volume (Å ³)	419.25(1)
Formula units per unit cell	4
Density (g·cm ⁻³)	3.668
T (K)	297(2)
Diffractometer	STOE STADI P
Radiation (Å)	Cu-K α_1 (λ = 1.54056 Å)
Profile range	5.0 ≤ θ ≤ 60.0
Data points	11000
Total number of reflections	1259
Refined parameters	147
Background function	Shifted Chebyshev (18 parameters)
<i>R</i> values	<i>R</i> _P = 0.03589; <i>R</i> _P exp. = 0.03209, <i>wR</i> _P = 0.04825; <i>R</i> (<i>F</i> ²) = 0.01367
Goodness of fit	1.504

Table S2. Fractional atomic coordinates, isotropic thermal displacement parameters, and site occupancies for Sr[LiAl₃N₄]:Eu²⁺ with standard deviations in parentheses.

Atom	x	y	z	U _{eq} / Å ²	Occupancy
Sr1	0.0030(3)	0.1339(3)	0.1271(2)	0.0111(4)	1.0
Sr2	0.0220(2)	0.3824(3)	0.37203(19)	0.0052(4)	1.0
Al1	0.5493(8)	0.9556(7)	0.1241(5)	0.0041(4)	1.0
Al2	0.1798(8)	0.9432(7)	0.3966(5)	0.0041(4)	1.0
Al3	0.1670(9)	0.7066(7)	0.1532(5)	0.0041(4)	1.0
Al4	0.8247(9)	0.5563(6)	0.1035(5)	0.0041(4)	1.0
Al5	0.4711(8)	0.5580(8)	0.3741(6)	0.0041(4)	1.0
Al6	0.5645(9)	0.2044(7)	0.3665(6)	0.0041(4)	1.0
N1	0.3483(16)	0.8678(15)	0.0208(12)	0.0063(8)	1.0
N2	0.3721(18)	0.3465(16)	0.5086(12)	0.0063(8)	1.0
N3	0.3786(17)	0.0849(14)	0.2839(12)	0.0063(8)	1.0
N4	0.1479(18)	0.9372(16)	0.5954(12)	0.0063(8)	1.0
N5	0.8402(18)	0.7987(17)	0.1462(11)	0.0063(8)	1.0
N6	0.175(2)	0.4893(15)	0.0808(12)	0.0063(8)	1.0
N7	0.1918(16)	0.7027(16)	0.3404(12)	0.0063(8)	1.0
N8	0.6612(18)	0.4128(16)	0.2324(12)	0.0063(8)	1.0
Li1	0.450(5)	0.325(4)	0.116(3)	0.0089	1.0
Li2	0.208(5)	0.172(4)	0.636(3)	0.0089	1.0

Table S3. Selected interatomic distances / Å for Sr[LiAl₃N₄]:Eu²⁺ with standard deviations in parentheses.

Sr1-N5	2.690(10)	Al3-N6	1.846(13)
Sr1-N1	2.691(10)	Al3-N7	1.901(13)
Sr1-N4	2.727(11)	Al3-N5	1.931(12)
Sr1-N8	2.741(11)	Al3-N1	1.951(12)
Sr1-N1	2.797(12)	Al4-N8	1.798(12)
Sr1-N5	2.823(13)	Al4-N6	1.905(14)
Sr1-N3	2.930(12)	Al4-N5	1.938(14)
Sr1-N6	2.974(12)	Al4-N6	1.991(13)
Sr1-Sr2	3.266(3)	Al5-N7	1.872(11)
Sr2-N2	2.672(12)	Al5-N8	1.900(12)
Sr2-N4	2.721(13)	Al5-N2	1.909(15)
Sr2-N7	2.727(12)	Al5-N2	2.040(13)
Sr2-N8	2.751(12)	Al6-N2	1.894(12)
Sr2-N3	2.836(10)	Al6-N3	1.898(14)
Sr2-N6	2.902(11)	Al6-N4	1.917(12)
Sr2-N7	2.904(11)	Al6-N8	2.017(13)
Sr2-N2	2.912(10)	Li1-N6	1.92(3)
Al1-N1	1.916(12)	Li1-N1	2.11(3)
Al1-N5	1.933(11)	Li1-N8	2.11(4)
Al1-N3	1.935(12)	Li1-N3	2.35(3)
Al1-N1	1.968(14)	Li2-N2	1.95(3)
Al2-N3	1.827(11)	Li2-N4	1.96(4)
Al2-N7	1.935(14)	Li2-N5	2.15(3)
Al2-N4	1.943(13)	Li2-N7	2.33(3)
Al2-N4	1.957(11)		

Table S4. Selected bond angles / ° for Sr[LiAl₃N₄]:Eu²⁺ with standard deviations in parentheses.

N1-Sr1-N1	85.5(4)
N1-Sr1-N4	94.1(3)
N2-Sr2-N8	83.4(4)
N2-Sr2-N7	177.4(5)
N6-Al3-N6	112.4(6)
N2-Al5-N8	103.2(5)
N1-Li1-N1	101.1(9)
N5-Li2-N6	107.9(9)

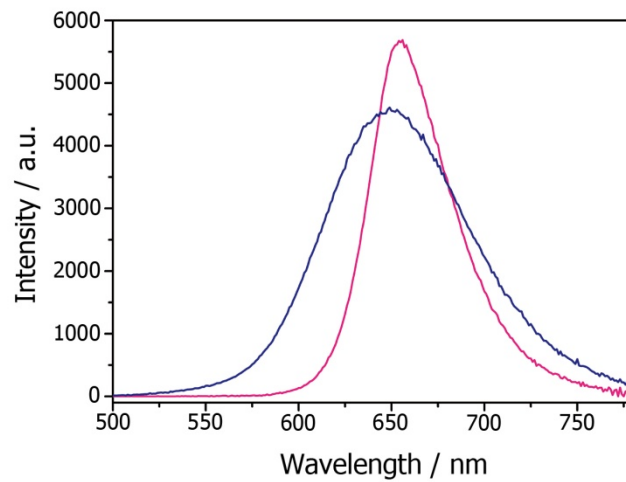


Figure S1. Emission spectra for $\lambda_{\text{exc}} = 440$ nm of optically infinite thick layers of SLA (red) and of commercially available CaAlSiN₃:Eu²⁺ with $QE_{\text{ex}} = 74\%$ (blue).

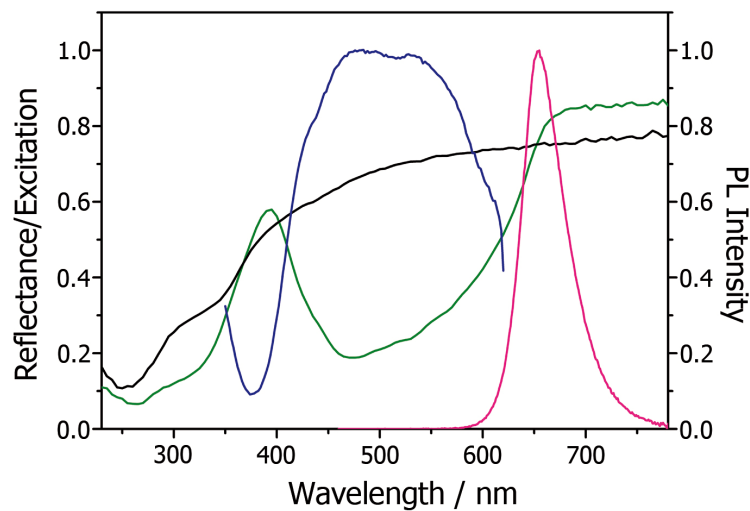


Figure S2. Excitation (blue) and emission (red, $\lambda_{\text{exc}} = 440$ nm) spectra for of SLA. Diffuse reflection spectra of SLA undoped sample (black) and with 0.4% Eu doping (green).

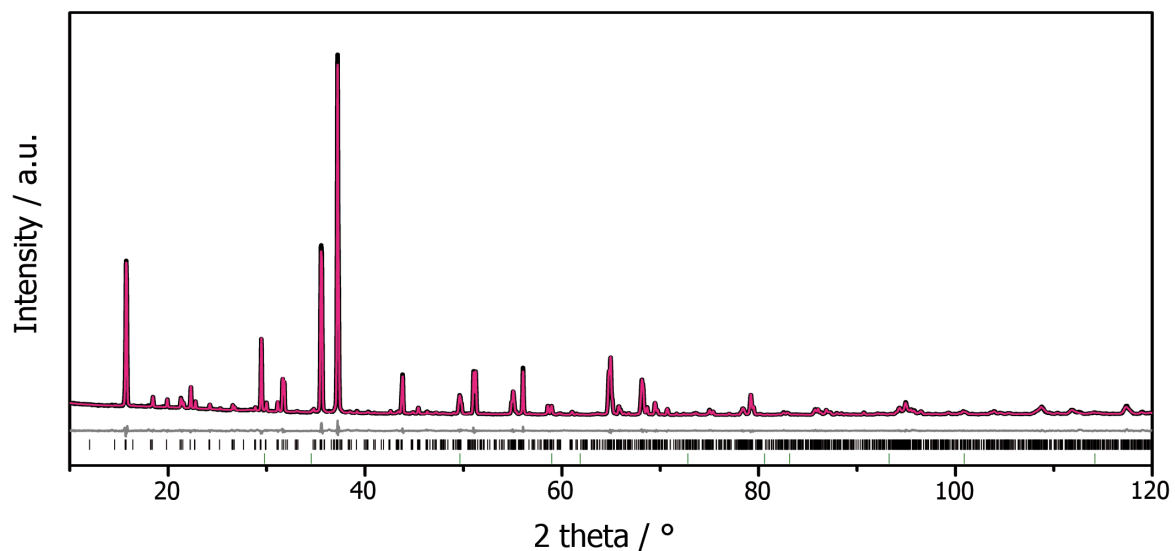


Figure S3. Rietveld refinement ($R_p = 0.036$, $wR_p = 0.048$; 11000 data points) of X-ray powder-diffraction pattern of SLA with measured histogram (black line), calculated pattern (red line), difference curve (gray line) and positions of reflections (black bars). Positions of SrO reflections (green bars).

References

- [1] J. E. Kaufman, J. F. Christensen, *Lighting Handbook*, Waverly Press, Maryland, **1972**.
- [2] S. Ye, et al., *Mater. Sci. Eng. R.* **2010**, *71*, 1.
- [3] R.-J. Xie, et al., *Nitride Phosphors and Solid-State Lighting*, CRC Press, Boca Raton, **2011**.

6.4 Supporting Information for Chapter 3.6

Philipp Pust, Volker Weiler, Angela S. Wochnik, Peter J. Schmidt, Christina Scheu and Wolfgang Schnick, *to be published*.

Table S1. Atomic coordinates, isotropic displacement parameters (\AA^2), Wyckoff positions and SOF of $\text{Ca}_{18.75}\text{Li}_{10.5}\text{Al}_{39}\text{N}_{55}$, with standard deviations in parentheses.

Atom	Wyckoff	Site	SOF	x	y	z	U_{eq}
Ca1	96h	.2	1	0	0.35133	0.64867	0.01111(14)
Ca2	48f	2.mm	1	0.2948	1/8	1/8	0.01019(16)
Ca3	16d	-.3m	0.375	1/2	1/2	1/2	0.0139(8)
Al1	96g	..m	1	0.27368	0.27368	0.17825	0.00701(17)
Al2	96g	..m	1	0.27747	0.27747	0.37409	0.00713(18)
Al3	48f	2.mm	1	0.43026	1/8	1/8	0.0075(2)
Al4	32e	.3m	1	0.04659	0.04659	0.04659	0.0071(3)
Al5	32e	.3m	1	0.17601	0.17601	0.17601	0.0071(3)
Al6	8b	-43m	1	3/8	3/8	3/8	0.0070(5)
N1	96g	..m	1	0.02341	0.02341	0.32571	0.0082(4)
N2	96g	..m	1	0.02561	0.02561	0.12678	0.0078(4)
N3	96g	..m	1	0.07474	0.07474	0.47744	0.0084(4)
N4	96g	..m	1	0.32478	0.32478	0.13032	0.0085(4)
N5	32e	.3m	1	0.32638	0.32638	0.32638	0.0068(7)
N6	16c	-.3m	1	0	0	0	0.0088(11)
N7	8a	-43m	1	1/8	1/8	1/8	0.0091(15)
Li1	192i	1	0.219	0.01804	0.206	0.32236	0.027(6)
Li2	96h	.2	0.438	0	0.43483	0.56517	0.027(6)

Table S2. Selected interatomic distances / Å for $\text{Ca}_{18.75}\text{Li}_{10.5}\text{Al}_{39}\text{N}_{55}$ with standard deviations in parentheses.

Ca1-N1	2.3922(16)	Al4-N4	1.889(2)
Ca1-N2	2.5057(17)	Al4-N7	1.9804(9)
Ca1-N3	2.4498(17)	Al5-N4	1.917(2)
Ca2-N1	2.491(2)	Al5-N6	1.8084(7)
Ca2-N4	2.731(2)	Al6-N5	1.888(2)
Ca3-N2	2.4229(16)	Li1-N1	1.95(3)
Al1-N2	1.9224(19)	Li1-N4	2.20(3)
Al1-N3	1.9442(19)	Li1-N6	1.94(3)
Al1-N5	1.884(2)	Li2-N1	2.233(9)
Al2-N1	1.9443(19)	Li2-N4	2.526(13)
Al2-N3	1.9098(19)	Li2-N6	2.067(14)
Al2-N4	1.9421(19)		
Al3-N1	1.9460(19)		
Al3-N2	1.9120(19)		

Table S3. Crystallographic data of Rietveld refinement of $\text{Ca}_{18.75}\text{Li}_{10.5}\text{Al}_{39}\text{N}_{55}$.

Formula	$\text{Ca}_{18.75}\text{Li}_{10.5}\text{Al}_{39}\text{N}_{55}$
Crystal system	cubic
Space group	$Fd\bar{3}m$ (no. 227)
Lattice parameters (Å)	$a = 22.37088(8)$
Cell volume (Å ³)	11195.65(12)
Formula units per unit cell	8
Density (g · cm ⁻³)	3.12(2)
T (K)	297(2)
Diffractometer	Huber G670
Radiation (Å), monochromator	Cu-K α_1 ($\lambda = 1.54056$ Å), Ge(111)
Profile range	$3.0 \leq \theta \leq 41.0$
Data points	15184
Total number of reflections	211
Refined parameters	90
Background function	Shifted Chebyshev (24 parameters)
R values	$R_p = 0.02445$; $R_p \text{ exp.} = 0.02066$, $wR_p = 0.03467$; $R(F^2) = 0.00825$
Goodness of fit	1.678

7 Publications

7.1 List of Publications Included in This Thesis

1. **Narrow-Band Red-Emitting Sr[LiAl₃N₄]:Eu²⁺ as Next-Generation LED-Phosphor Material**

Philipp Pust, Volker Weiler, Cora Hecht, Andreas Tücks, Angela S. Wochnik, Ann-Kathrin Henß, Detlef Wiechert, Christina Scheu, Peter J. Schmidt and Wolfgang Schnick

Nat. Mater. **2014**, *13*, 891-896.

In this contribution, writing the main part of the manuscript, screening of literature structure determination based on single-crystal and powder XRD data, interpretation of NMR measurements and image preparation were done by Philipp Pust. TEM investigations and interpretation of measured data were performed by Angela Wochnik and Christina Scheu. Sample preparation for TEM investigations were done by Philipp Pust in close collaboration with Angela Wochnik. Sample syntheses and synthesis optimization were done by Volker Weiler, Cora Hecht, Andreas Tücks, Ann-Kathrin Henß and Philipp Pust. Luminescence investigations and interpretation of measured values were done in the LDC Aachen by Detlef Wiechert and Peter J. Schmidt. Supervision of the research project was carried out by Wolfgang Schnick.

2. **Ca[LiAl₃N₄]:Eu²⁺ - A Narrow-Band Red-Emitting Nitridolithoaluminate**

Philipp Pust, Angela S. Wochnik, Elen Baumann, Peter J. Schmidt, Detlef Wiechert, Christina Scheu, Wolfgang Schnick

Chem. Mater. **2014**, *26*, 3544-3549.

For this publication, writing the manuscript main part, structure solution and refinement based on single-crystal XRD data, screening of literature and image preparation were done by Philipp Pust. TEM investigations and interpretation of measured data were performed by Angela Wochnik and Christina Scheu. In close collaboration Angela Wochnik and Philipp Pust prepared samples for TEM investigations. Sample synthesis was done by Elen Baumann under instruction of Philipp Pust. Luminescence investigations and interpretation of measured values were

done in the LDC Aachen by Detlef Wiechert and Peter J. Schmidt. Supervision of the research project was carried out by Wolfgang Schnick.

3. Group (III) Nitrides $M[\text{Mg}_2\text{Al}_2\text{N}_4]$ ($M = \text{Ca}, \text{Sr}, \text{Ba}, \text{Eu}$) and $\text{Ba}[\text{Mg}_2\text{Ga}_2\text{N}_4]$ - Structural Relation and Nontypical Luminescence Properties of Eu^{2+} Doped Samples

Philipp Pust, Frauke Hintze, Cora Hecht, Volker Weiler, Andreas Locher, Daniela Zitnanska, Sascha Harm, Detlef Wiechert, Peter J. Schmidt and Wolfgang Schnick
Chem. Mater. **2014**, 26, 6113-6119.

For this article, writing the main part of the Manuscript was done by Philipp Pust and Frauke Hintze. The image preparation was done by Philipp Pust. Structure solution and refinement of the nitridoaluminates were done by Philipp Pust, the nitridogallate was characterized by Frauke Hintze. Syntheses were performed and optimized by Philipp Pust, Frauke Hintze, Cora Hecht, Volker Weiler, Andreas Locher, Daniela Zitnanska and Sascha Harm. Luminescence investigations and interpretation of measured values were done in the LDC Aachen by Detlef Wiechert and Peter J. Schmidt. Supervision of the research project was carried out by Wolfgang Schnick.

4. Investigations of the Electronic Structure and Band Gap of the Next-generation LED-Phosphor $\text{Sr}[\text{LiAl}_3\text{N}_4]:\text{Eu}^{2+}$ - Experiment and Calculations

Thomas M. Tolhurst, Teak D. Boyko, Philipp Pust, Neil W. Johnson, Wolfgang Schnick and Alexander Moewes
Adv. Opt. Mater. **2015**, 3, 546-550.

For this publication, writing the manuscript main part and screening of literature was done by Thomas Tolhurst. Image preparation was done by Thomas Tolhurst, Teak Boyko and Philipp Pust. Samples were synthesized by Philipp Pust. The interpretation of measured and calculated results was done by Thomas Tolhurst, Teak Boyko Neil Johnson and Alexander Moewes. Supervision of the research project was carried out by Wolfgang Schnick and Alexander Moewes.

5. $\text{Ca}_{18.75}\text{Li}_{10.5}\text{Al}_{39}\text{N}_{55}:\text{Eu}^{2+}$ - Supertetrahedron phosphors for solid-state lighting

Philipp Pust, Volker Weiler, Angela S. Wochnik, Peter J. Schmidt, Christina Scheu and Wolfgang Schnick

to be submitted.

For this contribution, writing the manuscript main part, structure solution and refinement based on single-crystal XRD data and image preparation were done by Philipp Pust. Sample synthesis was performed by Volker Weiler. TEM investigations and the interpretation of obtained results were done by Angela Wochnik and Christina Scheu. Luminescence investigations and interpretation of measured values were done in the LDC Aachen by Detlef Wiechert and Peter J. Schmidt. Supervision of the research project was carried out by Wolfgang Schnick.

6. Narrow Red Emitters for Brighter White Light

Philipp Pust, Sebastian Schmiechen and Wolfgang Schnick

Mater. Today **2014**, Comment, 29.08.2014.

For this article, writing the manuscript was done by Philipp Pust and Sebastian Schmiechen. Literature screening was done by Philipp Pust. Supervision of the research project was carried out by Wolfgang Schnick.

7. $\text{Ca}[\text{LiAlN}_2]$: A Quaternary Nitridoaluminate

Philipp Pust, Sandro Pagano and Wolfgang Schnick

Eur. J. Inorg. Chem. **2013**, 1157-1160.

For this article, writing the manuscript was done by Philipp Pust. Synthesis of samples, single-crystal and Rietveld refinement and MAPLE calculations were performed by Sandro Pagano. Supervision of the research project was carried out by Wolfgang Schnick.

8. Ammonothermal Synthesis and Crystal Structure of $\text{BaAl}_2(\text{NH}_2)_8 \cdot 2\text{NH}_3$

Philipp Pust, Sebastian Schmiechen, Frauke Hintze and Wolfgang Schnick

Z. Anorg. Allg. Chem. **2013**, 639, 1185-1187.

In this contribution, synthesis of samples, construction of a low-temperature single-crystal preparation device, single-crystal structure refinement, literature screening and writing the main part of the manuscript were done by Philipp Pust. Frauke Hintze and Sebastian Schmiechen helped developing and installing the used autoclaves and the filling device. Supervision of the research project was carried out by Wolfgang Schnick.

7.2 Patent Applications

New Phosphors, such as New Narrow-Band Red Emitting Phosphors, for Solid State Lighting

Peter J. Schmidt, Frauke Hintze, Philipp A. H. Pust, Volker Weiler, Cora Hecht, Sebastian F. Schmiechen, Wolfgang Schnick and Detlef U. Wiechert
PCT Int. Appl. **2013**, WO 2013175336, A1, Koninklijke Philips Electronics NV, Philips Intellectual Property & Standards GmbH, Germany.

7.3 Other Publications

1. **Weißes Licht aus Nitriden**

Sebastian Schmiechen, Philipp Pust, Peter J. Schmidt and Wolfgang Schnick
Nachr. Chem. **2014**, 62, 847-851.

2. **Li₂Sr₄Al₂Ta₂N₈O - A Nitridoalumotantalate with BCT-Zeolite Type Structure**

Philipp Pust and Wolfgang Schnick
Z. Anorg. Allg. Chem. **2012**, 638, 352-356.

3. **LiSr₂[TaN₃]F - A Single Chain Nitridotantalate**

Philipp Pust and Wolfgang Schnick
Z. Anorg. Allg. Chem. **2011**, 637, 1486-1489.

4. **Li₂CaSi₂N₄ and Li₂SrSi₂N₄ - A Synthetic Approach to Three-Dimensional Lithium Nitridosilicates**

Martin Zeuner, Sandro Pagano, Stephan Hug, Philipp Pust, Sebastian Schmiechen, Christina Scheu and Wolfgang Schnick
Eur. J. Inorg. Chem. **2010**, 4945-4951.

5. **Trispyrazol-1-ylmethane**

T. Kerscher, P. Pust, R. Betz, P. Kluefers, P. Mayer
Acta Crystallographica, Section E: Structure Reports Online **2009**, 65, o108.

7.4 Conference Contributions

- 1. Narrow Band Red-Emitting Nitridoaluminates (poster)**
Philipp Pust, Sebastian Schmiechen and Wolfgang Schnick
8th International Symposium on Nitrides (ISNT), Wildbad Kreuth, 31. August – 05. September 2014.
- 2. Towards Novel Narrow Band Red-Emitting Phosphors: The Nitridomagnesosilicate $\text{Sr}[\text{Mg}_3\text{SiN}_4]:\text{Eu}^{2+}$ (poster)**
Sebastian Schmiechen, Philipp Pust and Wolfgang Schnick
8th International Symposium on Nitrides (ISNT), Wildbad Kreuth, 31. August – 05. September 2014.
- 3. The First Mg and Li containing Nitridoalumosilicate: $\text{Ba}[(\text{Mg}_{2-x}\text{Li}_x)(\text{Al}_{4-x}\text{Li}_x)\text{N}_6]$ (poster)**
Markus Siegert, Sebastian Schmiechen, Philipp Pust and Wolfgang Schnick
Undergraduate Research Conference on Molecular Sciences (URCUP), Wildbad Kreuth, 27. – 28. Juli 2014.
- 4. Ordnung leuchtet ein (talk)**
Philipp Pust and Wolfgang Schnick
Hemdsärmelkolloquium, Köln, 06. – 08. März 2014.
- 5. Rote Leuchtstoffe - Von der Theorie zur Anwendungsreife (talk)**
Philipp Pust and Wolfgang Schnick
Festkörperseminar Obergurgl, Obergurgl, 28. – 31. Januar 2014.
- 6. Carbothermal Reduction and Nitridation: From Bolgnian Stone to pc-LEDs (poster)**
Thomas Reith, Sebastian Schmiechen, Philipp Pust and Wolfgang Schnick
Undergraduate Research Conference on Molecular Sciences (URCUP), Wildbad Kreuth, 29. – 30. September 2013.
- 7. $\text{Ca}[\text{LiAlN}_2]$ - A Novel Quarternary Nitridoaluminate (poster)**
Philipp Pust and Wolfgang Schnick
European Conference on Solid State Chemistry ECSSC XIV, Bordeaux, 07. – 10. Juli 2013.

8. Synthesis and Analysis - Strategies for New Phosphor Materials (poster)

Frauke Hintze, Markus Seibald, Philipp Pust, Sebastian Schmiechen and Wolfgang Schnick

Phosphor Global Summit 2012, Scottsdale (AZ), 20. – 22. März 2012.

9. Nitride Phosphor Materials - Research, Application and Pertinence (poster)

Sebastian Schmiechen, Frauke Hintze, Markus Seibald, Philipp Pust and Wolfgang Schnick

Phosphor Global Summit 2012, Scottsdale (AZ), 20. – 22. März 2012.

10. Neues von Nitridotantalaten (talk)

Philipp Pust and W. Schnick

Festkörperchemie-Seminar, Hirschegg, 23. – 25. Juni 2011.

7.5 CSD Numbers

Crystallographic data (cif file) of investigated compounds can be obtained from the Fachinformationszentrum Karlsruhe, 76344 Eggenstein-Leopoldshafen, Germany (fax, (+49)7247-808-666; e-mail, crysdata@fiz-karlsruhe.de) by quoting the corresponding depository numbers.

Sr[LiAl ₃ N ₄]	CSD-427067
Ca[LiAl ₃ N ₄]	CSD-427066
Ca[Mg ₂ Al ₂ N ₄]	CSD-425319
Sr[Mg ₂ Al ₂ N ₄]	CSD-425321
Ba[Mg ₂ Al ₂ N ₄]	CSD-427065
Eu[Mg ₂ Al ₂ N ₄]	CSD-425320
Ba[Mg ₂ Ga ₂ N ₄]	CSD-425318
Ca[LiAlN ₂]	CSD-424911
Ca _{18.75} Li _{10.5} Al ₃₉ N ₅₅	CSD-428388
BaAl ₂ (NH ₂) ₈ ·2NH ₃	CSD-425323